

Role of the mitochondrial ATP-dependent Clp protease in mammalian metabolism

Inaugural-Dissertation

zur

Erlangung des Doktorgrades

der Mathematisch-Naturwissenschaftlichen Fakultät

der Universität zu Köln



vorgelegt von

Christina Becker

aus Werl

Köln, 2017

Berichtersteller: **Prof. Dr. Aleksandra Trifunovic**
Prof. Dr. Elena Rugarli

Tag der mündlichen Prüfung: 25.04.2017

To my family and Ludwig

Table of Contents

List of Figures	VII
List of Tables	IX
Abbreviations	X
Abstract	XIII
Zusammenfassung	XIV
1 Introduction	1
1.1 Mitochondria	1
1.1.1 Mitochondrial structure and function	1
1.1.2 Mitochondrial genetics	2
1.2 Mitochondrial quality control	3
1.3 ClpXP protease	4
1.3.1 ClpXP- structure and function	4
1.3.2 Physiological functions of ClpXP	6
1.4 Metabolism	8
1.4.1 Cellular metabolism	10
1.4.1.1 Cytosolic metabolism	10
1.4.1.2 Mitochondrial metabolism	13
1.4.2 Whole body metabolism	16
1.4.2.1 Endocrine regulation of metabolism	16
1.4.2.2 Organ interrelation in metabolism with regard to mitochondrial function	17
1.5 Mitochondrial dysfunction and metabolic diseases	19
1.6 Objectives	20
2 Materials and Methods	22
2.1 Animal care	22
2.2 Experimental mouse models	22
2.3 Phenotyping	23
2.3.1 Body weight	23
2.3.2 Body composition	23
2.3.3 Indirect calorimetry	23
2.3.4 Blood glucose measurement	23
2.3.5 Serum analyses	24
2.3.6 Glucose tolerance test and insulin tolerance test	24
2.3.7 Insulin signaling	24
2.3.8 Acute cold exposure and measurement of rectal body temperature	24
2.3.9 Femur length	25

2.3.10	Micro computed tomography.....	25
2.4	Molecular biology.....	25
2.4.1	Isolation of genomic DNA from mouse ear biopsies	25
2.4.2	Isolation of genomic DNA from mouse tissues	25
2.4.3	Isolation of total RNA.....	25
2.4.4	Quantification of nucleic acids.....	26
2.4.5	Polymerase chain reaction.....	26
2.4.6	Northern blot analysis for mitochondrial mRNA levels	27
2.4.7	Reverse transcription and quantitative real-time PCR.....	27
2.5	Biochemistry	29
2.5.1	Protein extraction from mouse tissues.....	29
2.5.2	Isolation of mitochondria from liver and brown adipose tissue	29
2.5.3	Isolation of mitochondria from skeletal muscle	29
2.5.4	Blue native polyacrylamide gel electrophoresis	30
2.5.5	SDS-PAGE and Western blot	30
2.5.6	Mitochondrial respiration.....	32
2.5.7	Palmitate oxidation rate <i>ex vivo</i>	32
2.5.8	Sucrose gradient fractionation of mitochondrial ribosomes	33
2.5.9	<i>In organello</i> translation	33
2.6	Histological analysis	33
2.6.1	Embedding of tissues in paraffin	33
2.6.2	Cryostat sections.....	34
2.6.3	Hematoxylin and Eosin staining	34
2.6.4	Periodic acid Schiff's reaction	34
2.6.5	Oil red O staining.....	34
2.6.6	COX-SDH staining.....	34
2.6.7	Transmission electron microscopy	35
2.7	Cell Culture.....	35
2.8	Label-free quantification of the liver proteome	35
2.8.1	In-solution digest	35
2.8.2	Liquid chromatography and mass spectrometry	36
2.9	Computer analyses.....	36
2.9.1	Software.....	36
2.9.2	Statistical analyses	36
2.10	Chemicals.....	36
3	Results.....	39
3.1	Phenotypic analysis of whole body CLPP deficient mice.....	39
3.1.1	Loss of CLPP does not affect lifespan.....	39
3.1.2	Clpp ^{-/-} mice have increased energy expenditure and improved glucose homeostasis despite lower locomotor activity	42
3.1.3	CLPP deficiency causes a fasting-like phenotype.....	45

3.1.4	Lack of CLPP decreases glycogen content in liver and skeletal muscle.....	48
3.1.5	Effect of CLPP deficiency on fatty acid β -oxidation.....	49
3.1.6	Loss of CLPP severely impairs cold tolerance.....	55
3.1.7	Loss of CLPP leads to enhanced browning of WAT	59
3.2	Phenotype of $Clpp^{-/-}$ mice is independent of FGF21	63
3.3	Tissue-specific disruption of <i>Clpp</i>	66
3.3.1	Liver restricted loss of CLPP does not affect body weight and glucose homeostasis	66
3.3.2	Liver restricted loss of CLPP alters FAO enzyme levels and leads to moderate mitochondrial dysfunction.....	67
3.3.3	CLPP ablation in skeletal muscle and heart does not alter body weight and glucose homeostasis	68
3.3.4	Muscle restricted loss of CLPP induces FAO oxidation profile and causes mitochondrial dysfunction	70
3.3.5	$Clpp^{MKO}$ mice exhibit functional shivering activity.....	71
3.4	High fat feeding impairs hepatic mitochondrial translation in the absence of CLPP	72
3.4.1	$Clpp^{-/-}$ mice maintain lean phenotype and enhanced glucose metabolism during HFD-feeding.....	72
3.4.2	Label-free quantitative proteomic profiling of liver reveals deregulated OXPHOS subunit levels due to HFD-feeding upon loss of CLPP.....	77
3.4.3	Loss of CLPP during HFD-feeding leads to strong decrease only in hepatic mitochondrial respiratory chain complexes.....	79
3.4.4	Decreased hepatic mitochondrial complex subunits in HFD fed $Clpp^{-/-}$ mice are not caused by increased turnover	84
3.4.5	Loss of CLPP causes increased mitochondrial mRNA levels and reduced <i>de novo</i> protein synthesis with an aggravating effect of HFD.....	88
3.4.6	Loss of CLPP does not impair hepatic mitoribosome assembly	92
3.4.7	Hepatic translation defect of CLPP deficient liver mitochondria is not caused by an increased association of ERAL1 with the 28S ribosomal subunit	93
4	Discussion	98
4.1	Loss of CLPP alters whole body metabolism	99
4.2	FGF21 is not a metabolic regulator of the CLPP phenotype	103
4.3	Tissue-specific CLPP deletion does not have systemic implications	105
4.4	CLPP is required for hepatic mitochondrial translation in metabolic stress conditions	106
4.5	Summary.....	109
	References	110
	Acknowledgments	125
	Erklärung	126
	Curriculum vitae.....	127

List of Figures

Figure 1.1 Mitochondrial DNA.....	3
Figure 1.2 Schematic presentation of the ClpXP degradation cycle.....	6
Figure 1.3 OXPHOS system.....	15
Figure 3.1 Validation of ubiquitous CLPP deletion.....	40
Figure 3.2 Phenotypic characterization of Clpp ^{-/-} mice.....	41
Figure 3.3 Clpp ^{-/-} mice exhibit growth defect.....	42
Figure 3.4 Loss of CLPP increases energy expenditure.....	43
Figure 3.5 Reduced locomotor and rearing activities in Clpp ^{-/-} mice.....	44
Figure 3.6 Improved glucose homeostasis in Clpp ^{-/-} mice due to increased peripheral glucose uptake.....	45
Figure 3.7 Serum parameters of control and CLPP deficient mice.....	47
Figure 3.8 AMPK activation in SkM of CLPP deficient mice.....	48
Figure 3.9 Loss of CLPP decreases glycogen content in liver and SkM.....	49
Figure 3.10 CLPP deficient mice exhibit decreased FAO in liver and SkM.....	50
Figure 3.11 Profile of FAO enzymes in Clpp ^{-/-} mice (1).....	52
Figure 3.12 Profile of FAO enzymes in Clpp ^{-/-} mice (2).....	53
Figure 3.13 VLCAD is a putative substrate of CLPP.....	55
Figure 3.14 Lipid accumulation in BAT of Clpp ^{-/-} mice.....	57
Figure 3.15 CLPP is essential for cold induced thermogenesis.....	59
Figure 3.16 Browning of WAT in Clpp ^{-/-} mice.....	61
Figure 3.17 Systemic induction of <i>Fgf21</i> and increased circulating levels in Clpp ^{-/-} mice.....	63
Figure 3.18 Loss of FGF21 in CLPP deficient mice does not normalize whole body physiology.....	65
Figure 3.19 FGF21 deletion in CLPP deficient liver alters LONP1 and TFAM abundance.....	66
Figure 3.20 Liver restricted loss of CLPP does not alter body weight and glucose homeostasis.....	67
Figure 3.21 Hepatic deficiency of CLPP causes mitochondrial dysfunction and similar FAO profile as observed for Clpp ^{-/-} mice.....	68
Figure 3.22 Skeletal muscle and heart restricted loss of CLPP does not alter body weight and glucose homeostasis.....	70
Figure 3.23 Muscle deficiency of CLPP causes mitochondrial dysfunction and similar FAO profile as observed for Clpp ^{-/-} mice.....	71
Figure 3.24 Cold induced adaptive thermogenesis is not impaired in Clpp ^{MKO} mice....	72
Figure 3.25 Loss of CLPP protects against HFD induced obesity.....	74
Figure 3.26 Serum parameters of control and CLPP deficient mice fed HFD.....	75

Figure 3.27 Clpp ^{-/-} mice are protected against HFD induced hypertrophy of EWAT....	76
Figure 3.28 CPT2 is upregulated upon HFD-feeding in Clpp ^{-/-} mice.....	77
Figure 3.29 Quantitative assessment of liver proteomes of CLPP deficient mice fed NCD or HFD.....	79
Figure 3.30 High dietary fat content causes mitochondrial dysfunction in liver.....	80
Figure 3.31 Decreased steady state levels of mitochondrial and nuclear-encoded complex I subunits in 5-week-old and HFD fed Clpp ^{-/-} mice.....	82
Figure 3.32 Complex composition is not affected by HFD-feeding in CLPP deficient SkM mitochondria.....	84
Figure 3.33 Decreased mitochondrial complex subunits in liver do not result from increased turnover or altered fusion events rather from increased biogenesis.....	87
Figure 3.34 Mitochondrial transcript levels are increased in liver of CLPP deficient mice.	89
Figure 3.35 High fat feeding exacerbates the mitochondrial translation defect in liver in the absence of CLPP.	90
Figure 3.36 Mitochondrial translation defect in 5-week-old CLPP deficient liver is comparable to HFD fed Clpp ^{-/-} mice.....	91
Figure 3.37 Loss of CLPP does not affect mitoribosomal protein levels of the small and large subunit and mitoribosome assembly in liver.....	93
Figure 3.38 Mild comigration of the CLPP substrate ERAL1 with the small ribosomal subunit in liver irrespective of diet.....	94
Figure 3.39 Difference in hepatic mitochondrial translation of NCD and HFD fed CLPP deficient mice might be affected by altered ratios of mitochondrial translation factors.....	97

List of Tables

Table 2.1 Oligonucleotides used for genotyping	26
Table 2.2 Primers used for quantitative real-time PCR	28
Table 2.3 Taqman Probes used for quantitative real-time PCR	28
Table 2.4 Primary antibodies used for Western blot analysis.....	31
Table 2.5 Chemicals.....	36

Abbreviations

°C	degree Celsius
3'	three prime end of DNA sequences
5'	five prime end of DNA sequences
A	adenosine
ADP	adenosine diphosphate
ATP	adenosine triphosphate
BAT	brown adipose tissue
bp	base pairs
BN	blue native
BSA	bovine serum albumin
C	cytosine
cDNA	complementary DNA
cAMP	cyclic AMP
Ci	Curie
Cre	bacteriophage P1 derived site-specific recombinase
Cyt	cytochrome
CHX	cycloheximide
Da	Dalton
ddH ₂ O	double distilled water
DKO	double knockout
DNA	deoxyribonucleic acid
dNTP	deoxyribonucleotide-triphosphate
ECL	enhanced chemiluminescence
EDTA	ethylenediaminetetraacetic acid
EGTA	ethylene glycol tetraacetic acid
ETC	electron transport chain
EtOH	ethanol
ETS	electron transfer system
EWAT	epididymal white adipose tissue
FADH ₂	flavin adenine dinucleotide, reduced
FAO	fatty acid β -oxidation
FCCP	carbonylcyanide p-trifluoromethoxyphenylhydrazone
Fe-S	iron-sulfur
g	gram
G	guanine

H ₂ O ₂	hydrogen peroxide
HCl	hydrochloric acid
HEPES	N-2-hydroxyethylpiperazine-N-2-ethansulfonic acid
HFD	high fat diet
HSP	heavy strand promoter
i.e.	<i>id est</i>
IMM	inner mitochondrial membrane
IMS	inter membrane space
IWAT	inguinal white adipose tissue
k	kilo
KCl	potassium chloride
KO	knockout
KOH	potassium hydroxide
l	liter
fl	loxP flanked
LSP	light strand promoter
m	milli
M	molar
MgCl ₂	magnesium chloride
mtDNA	mitochondrial DNA
mRNA	messenger RNA
NCD	normal chow diet
nDNA	nuclear DNA
NaCl	sodium chloride
NADH	nicotinamide adenine dinucleotide, reduced
NADP	nicotinamide adenine dinucleotide phosphate, reduced
NaF	sodium fluoride
NaH ₂ PO ₄	monosodium phosphate
NaHCO ₃	sodium bicarbonate
NaOH	sodium hydroxide
OMM	outer mitochondrial membrane
OXPHOS	oxidative phosphorylation
PAGE	polyacrylamide gel electrophoresis
PBS	phosphate buffered saline
PCR	polymerase chain reaction
Pi	Phosphates
RNA	ribonucleic acid

rRNA	ribosomal RNA
RNase	ribonuclease
ROS	reactive oxygen species
rpm	revolutions per minute
RT	room temperature
rtPCR	reverse transcription polymerase chain reaction
SD	standard deviation
SDS	sodium dodecyl sulfate
SkM	skeletal muscle
TBE	tris-borate-EDTA buffer
TE	tris-EDTA buffer
Tris	2-amino-2-(hydroxymethyl)-1,3-propanediol
tRNA	transfer RNA
TWEEN	polyoxyethylene-sorbitan-monolaurate
U	units
UPR ^{mt}	mitochondrial unfolded protein response
V	volt
v/v	volume per volume
w/v	weight per volume
WT	wildtype
β-me	β-mercaptoethanol
μ	micro

Abstract

Mitochondria are fundamental for cellular metabolism and take center stage in the regulation of systemic energy metabolism. They are origin and target of nutrient intermediates of converging metabolic pathways. Thus, it is essential to maintain mitochondrial homeostasis. Cells harbor a large set of mitochondrial proteases involved in quality control, including the ATP-dependent Clp protease (CLPP). However, CLPP not only degrades misfolded or damaged proteins, CLPP is also involved in highly regulated proteolytic activities. Many bacterial and mammalian ClpXP substrates have been identified in various metabolic pathways. This study analyzes the role of CLPP in mammalian metabolism using whole body and tissue-specific *Clpp* knockout mouse models.

The ubiquitous loss of CLPP under normal dietary conditions leads to a lean phenotype with enhanced glucose metabolism. The absence of CLPP further facilitates increased energy expenditure in part by WAT browning, despite decreased physical activity. Moreover, CLPP was shown to be involved in fatty acid oxidation by the regulation of its putative substrate VLCAD. In addition, CLPP has a critical role in BAT homeostasis and cold induced thermogenesis. The mild to moderate mitochondrial dysfunction caused by the loss of CLPP in various tissues, induced the expression of the mitokine FGF21. However, using *Clpp/Fgf21* double knockout mice, it could be shown that FGF21 is not mediating the metabolic changes observed in CLPP deficient mice.

The tissue-specific depletion of CLPP in liver or skeletal muscle and heart revealed a dispensable role for CLPP with regard to whole body metabolism, although tissue restricted mitochondrial dysfunction was present. Finally, ablation of CLPP was demonstrated to protect against HFD induced obesity and insulin resistance. Remarkably, HFD-feeding impaired hepatic mitochondrial translation in the absence of CLPP resulting in decreased complex subunits and decreased supercomplexes levels in an alternate mechanism as previously described for the heart. Thus, mitochondrial CLPP has a critical role in metabolic stress conditions in particular during cold exposure and high fat diet feeding. Therefore, by analyzing CLPP protease function and its link to metabolic stress this study may help to understand pathologies with deregulated *Clpp* expression.

Zusammenfassung

Mitochondrien sind für den Zellstoffwechsel von grundlegender Bedeutung und nehmen eine zentrale Rolle in der Regulierung des systemischen Energiestoffwechsels ein. Sie sind Ursprung und Zielort von Nährstoffzwischenprodukten konvergierender Stoffwechselwege. Daher ist es von besonderer Bedeutung, die mitochondriale Homöostase aufrechtzuerhalten. Zu diesem Zweck beherbergen Zellen eine Vielzahl von mitochondrialen Proteasen, die an der Qualitätskontrolle beteiligt sind, einschließlich der ATP-abhängigen Clp-Protease (CLPP). Allerdings ist CLPP nicht nur an der Degradierung fehlgefalteter oder beschädigter Proteine, sondern auch an regulierten proteolytischen Aktivitäten beteiligt. CLPP Substrate vieler Bakterien und Säugetiere spielen eine Rolle in verschiedenen Stoffwechselwegen. In dieser Studie sollte daher die Rolle von CLPP im Stoffwechsel mit Hilfe von Ganzkörper und Gewebespezifischen *Clpp* Knockout Mausmodellen analysiert werden.

Der ubiquitäre Verlust von CLPP unter Bedingungen einer Normaldiät führt zu einem schlankeren Phänotyp mit erhöhtem Glukosestoffwechsel. Weiterhin weisen CLPP-defiziente Mäuse, trotz einer verminderten körperlichen Aktivität, einen erhöhten Energieverbrauch auf, was teilweise bedingt ist durch die Bräunung des weißen Fettgewebes. Darüber hinaus wurde gezeigt, dass CLPP eine entscheidende Rolle in der Homöostase des braunen Fettgewebes und der Kälte induzierten Thermogenese spielt und durch die Regulierung seines potentiellen Substrats VLCAD an der Fettsäureoxidation beteiligt ist. Die leichte bis mäßige mitochondriale Dysfunktion, die durch den Verlust von CLPP in verschiedenen Geweben verursacht wird, induzierte dabei die Expression des Mitokins FGF21. Unter Verwendung eines *Clpp/Fgf21* Doppel Knockout Mausmodells konnte jedoch gezeigt werden, dass FGF21 nicht ursächlich für die metabolischen Veränderungen ist, die bei CLPP-defizienten Mäusen beobachtet wurden. Der spezifische Verlust von CLPP in der Leber oder dem Herz- und Skelettmuskel zeigte eine unbedeutende Rolle für CLPP im Hinblick auf den Ganzkörper-Stoffwechsel, obwohl eine mitochondriale Dysfunktion in den jeweiligen Geweben vorhanden war. Schließlich wurde gezeigt, dass die Ablation von CLPP gegen eine hochkalorische Diät induzierte Fettleibigkeit und Insulinresistenz schützt. Bemerkenswerterweise führte die Fütterung der fettreichen Diät in Abwesenheit von CLPP zu einer Beeinträchtigung der mitochondrialen Translation in der Leber. Allerdings liegt dem ein anderer Mechanismus zugrunde, als welcher zuvor für das Herz beschrieben wurde. Dabei konnte eine verminderte Anzahl von Untereinheiten der Atmungskette und Superkomplexen beobachtet werden. Die mitochondriale CLPP Protease hat daher eine entscheidende Rolle in metabolischen Stresskonditionen,

insbesondere bei Kälteexposition und der Fütterung mit hochkalorischer Diät. Die Analyse der Funktion von CLPP und deren Verknüpfung mit metabolischem Stress kann somit dazu beitragen, Pathologien mit deregulierter *C/pps* Expression besser zu verstehen.

1 Introduction

1.1 Mitochondria

Two billion years ago, when the oxygen levels in the earth's atmosphere were changing, an α -proteobacterium entered an ancestral host cell to start a symbiotic relationship (Kurland and Andersson, 2000). This is known as the endosymbiotic theory, which is suggesting the origin of eukaryotic cells from prokaryotes (Margulis, 1975). Mitochondria are thought to have evolved from these anaerobic bacterial endosymbionts, introducing the oxidative respiratory system into the host cell.

1.1.1 Mitochondrial structure and function

Mitochondria (Greek *mitos* "thread" and *chondrion* "granule") are found in almost all eukaryotic cells with the exception of erythrocytes. They form a highly dynamic network within the cell undergoing constant fusion and fission and occupying about 20% of its volume (McBride et al., 2006). Mitochondria are compartmentalized by two membranes composed of phospholipid bilayers, namely the outer (OMM) and the inner mitochondrial membrane (IMM) that are separated by the inter membrane space (IMS). The inner membrane has several invaginations referred to as cristae and encloses the matrix. The matrix harbors the mitochondrial DNA (mtDNA) a unique feature of mitochondria denoting its prokaryotic origin. The mtDNA has great similarity to the genome of the bacterium *Rickettsia prowazekii* (Kurland et al., 1998). During the course of evolution, the majority of the ancestral bacterial genes have been lost and transferred to the nuclear genome, through a process known as endosymbiotic gene transfer (Timmis et al., 2004). Mammalian mitochondria therefore maintain a genome encoding only for 13 core proteins of the respiratory chain complexes, 2 rRNA and 22 tRNAs (Chan, 2006; Wallace, 2005). Mitochondria harbor their own replication

machinery for the propagation of the mtDNA, as well as separate systems for the transcription and translation of the mitochondrial proteins. The vast majority of the mitochondrial proteome, roughly 1500 proteins, is encoded in the nucleus and needs to be imported into the mitochondria.

The hallmark ability of mitochondria is the generation of cellular energy, adenosine triphosphate (ATP), through the process of oxidative phosphorylation (OXPHOS) (see section 1.3.2.3). Moreover, mitochondria are involved in diverse other cellular processes, such as iron-sulfur (Fe-S) cluster biogenesis, lipid biosynthesis, Calcium homeostasis, apoptosis and generation of reactive oxygen species (ROS) (Chan, 2006; Lill and Mühlenhoff, 2005; Nunnari and Suomalainen, 2012; Wallace, 2005).

1.1.2 Mitochondrial genetics

Mitochondria contain their own genome (mtDNA), which is a closed circular, double-stranded DNA of approx. 16.6 kb in size. Despite the rather small genome size compared to the nuclear genome, point mutations or depletion of mtDNA can lead to severe pathologies. Mitochondrial DNA comprises a total of 37 genes of which 13 are encoding core subunits of the mitochondrial respiratory complexes I, III, IV and V. Additionally, mtDNA encompasses genes for 2 ribosomal RNAs (rRNA) and 22 transfer RNA (tRNA) that are essential for mitochondrial translation. Only a small portion of the mtDNA (about 1100 bp) comprises a non-coding control region encompassing the heavy and light strand promoter (HSP, LSP) for transcription and the origin of replication of the heavy strand (O_H), whereas the origin of replication for the light strand (O_L) is located in a distant position (Figure 1.1) (Wallace, 2007).

Transcription of polycistronic transcripts is initiated from the two promoters and they are further processed into mature mRNAs, tRNAs and rRNAs. Those transcripts also function as primer for mtDNA replication, which is accomplished by “strand displacement” (Holt and Reyes, 2012).

Unlike the nuclear genome, mitochondria contain between 2-10 copies of mtDNA as result of relaxed replication. Although mammalian mitochondria harbor a DNA repair system, mutations of mtDNA still occur and can lead to a heterogeneous population of mtDNA sequences (Boesch et al., 2009). This condition is termed heteroplasmy, whereas the presence of identical mtDNA copies in a cell is described as homoplasmy (Larsson, 2010).

The mtDNA underlies a non-Mendelian inheritance pattern. It is maternally transmitted, while the paternal mtDNA is degraded after fertilization and is not passed to the offspring (Al Rawi et al., 2011). This implies that also mtDNA molecules carrying mutations are transmitted maternally. When the load of mutated mtDNA molecules

exceeds a certain threshold in the cell, this can lead to mitochondrial dysfunction (Wong, 2007). The threshold effect is different for each mutation and tissue, and determines the manifestation and the outcome of a mitochondrial disease. This is also important during cell division, since mitochondria are randomly distributed to the daughter cells (Stewart and Chinnery, 2015).

Mitochondrial DNA mutations commonly affect the OXPHOS system, leading to diverse and multifactorial mitochondrial pathologies (Wallace, 2013).

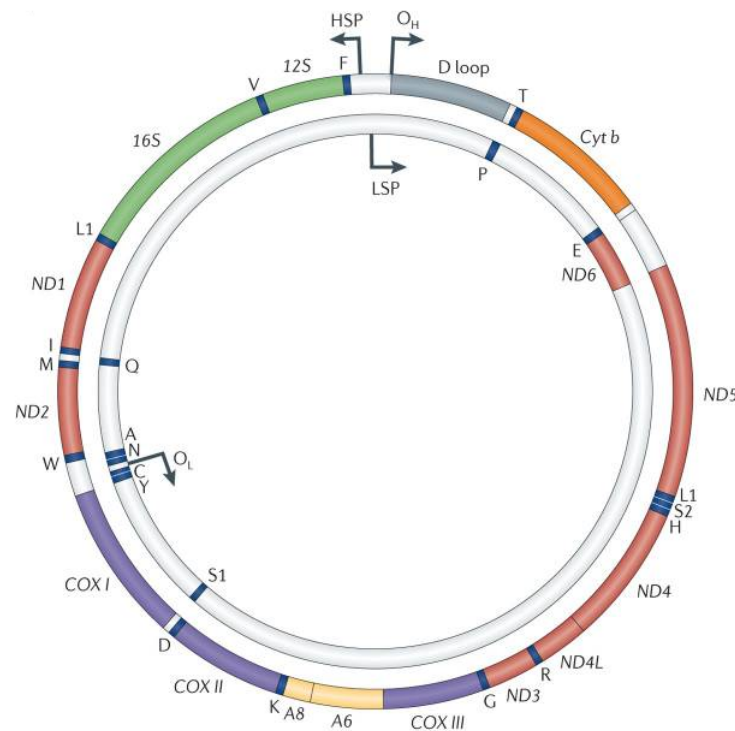


Figure 1.1 Mitochondrial DNA.

The mitochondrial DNA (mtDNA) encodes 37 genes, including 7 subunits of Complex I (red), 1 subunit of Complex III (orange), 3 subunits of Complex IV (purple), 2 subunits of F_0F_1 -ATP synthase (yellow), 2 ribosomal RNAs (rRNA, green) and 22 transfer RNAs (tRNA, blue) (Schon et al., 2012).

1.2 Mitochondrial quality control

The maintenance and surveillance of the mitochondrial proteome is crucial for mitochondrial function and cellular homeostasis. The dual origin of the mitochondrial proteins represents a particular challenge. Most mitochondrial proteins are encoded in the nucleus and have to be translocated across one or two membranes, sorted into one of the four compartments and properly folded (Neupert and Herrmann, 2007). In addition, the mitochondrial-encoded proteins are synthesized in the matrix and are subsequently assembled into respiratory chain complex. The timed coordination of the two genomes and the arrangement of all proteins and complexes into the respective

compartments requires a stringent quality control system. Additionally, mitochondrial protein homeostasis can be perturbed during different stress conditions like nutrient starvation or excess, oxidative stress or age dependent pathologies. A hierarchical system of quality control mechanisms allows the surveillance of mitochondrial proteostasis and the selective removal of proteins or entire organelles (Rugarli and Langer, 2012).

During the import of nuclear-encoded proteins, the mitochondrial targeting sequence is cleaved by the mitochondrial processing peptidase (MPP). The translocation and folding of the newly imported proteins is facilitated by the molecular chaperone mtHSP70. In addition, mtHSP70 prevents the aggregation of misfolded proteins to allow proteolysis (Liu et al., 2001; Wagner et al., 1994). Another matrix chaperone, HSP60, is also involved in folding activity of unfolded proteins after import and is further needed during mitochondrial stress conditions (Bender et al., 2011; Ostermann et al., 1989). The proteolytic removal of proteins is required for terminally damaged, misfolded and non-assembled proteins to prevent proteotoxic stress. There are four different ATP-dependent proteases performing quality control surveillance within the mitochondria. The metalloproteases i-AAA and m-AAA are localized in the IMM with their catalytic site oriented towards the IMS or the matrix, respectively and they execute quality control for the mitochondrial respiratory system (Gerdes et al., 2012). The mitochondrial matrix harbors two proteases LONP1 and ClpXP. Whereas LONP1 is important for the degradation of oxidized proteins, besides other cellular functions (Ngo and Davies, 2007), the function of ClpXP is less clear and implicated in the degradation of misfolded proteins (Zhao et al., 2002). At the organelle level, sustained stress may lead to mitochondrial hyperfusion or fragmentation, depending on the degree of mitochondrial dysfunction (Rugarli and Langer, 2012). Hyperfusion allows mitochondria to exchange genetic material and increase ATP production to alleviate stress. Mitochondrial fragmentation facilitates the segregation of damaged mitochondria and their subsequent degradation through mitophagy (Kusminski et al., 2014). The failure of this quality control system results in dysfunctional mitochondria and ultimately in cell death, which might trigger pathological processes.

1.3 ClpXP protease

1.3.1 ClpXP- structure and function

ClpXP is a AAA+ protease (ATPases associated with various cellular activities) that utilizes energy of ATP binding and hydrolysis to catalyze the unfolding and degradation of proteins and thereby regulate many mitochondrial processes. The ClpXP complex consists of two distinct proteins, the AAA+ ATPase CLPX and the peptidase CLPP and

is localized within the mitochondrial matrix. Both proteins are highly conserved and are found in almost all bacteria, chloroplast and mitochondria of eukaryotic cells, yet *S.cerevisiae* and *S.pombe* are lacking a ClpXP homolog (Yu and Houry, 2007).

Most of what is known today about ClpXP structure, substrates and functions was revealed from prokaryotic studies, especially *E.coli* and much less is known about the mammalian protease. The crystal structure of ClpXP has been solved in different organisms including humans (Glynn et al., 2009; Kang et al., 2004; Wang et al., 1997). Bacterial CLPP consist of two homoheptameric rings that are stacked to form a spherical degradation chamber with an axial channel. Human CLPP was shown to exist as a single heptameric ring and only upon binding CLPX the double ring is formed (Kang et al., 2005). Each CLPP subunit harbors a serine-histidine-aspartate catalytic triad, a hallmark of serine proteases. The 14 proteolytic active sites are facing the inside of the chamber. This allows to control the proteolytic activity of CLPP, since the opening of the channel is restricting the access of native proteins resulting in a low peptidase activity of CLPP, being able to degrade peptides less than 15 amino acids long (Thompson et al., 1994). To obtain proteolytic activity CLPP assembles on one or both ends with a hexameric ring of CLPX to form a holoenzyme complex (Kang et al., 2005). In bacteria, in addition to CLPX, the ATPases CLPA and CLPC associate with CLPP (Sauer and Baker, 2011). The CLPX chaperone functions in substrate recognition, ATP-dependent protein unfolding and translocation of the substrate into the proteolytic chamber of CLPP (Baker and Sauer, 2012). The targeting of substrates for degradation and the recognition by CLPX is mediated by recognition motifs called degrons at the N- or C-terminus of the target protein (Flynn et al., 2003). Upon binding of such a peptide sequence to the axial opening, CLPX is denaturing and translocating the native protein into CLPP in a process requiring numerous cycles of ATP hydrolysis to catalyze the conformational change of CLPX to excerpt the mechanical pulling (Ortega et al., 2000). The actual function of CLPP is to cleave the translocated protein, typically resulting in peptides of 3-7 amino acids in length (Choi and Licht, 2005) that exit the chamber and are further degraded by exopeptidases (Figure 1.2).

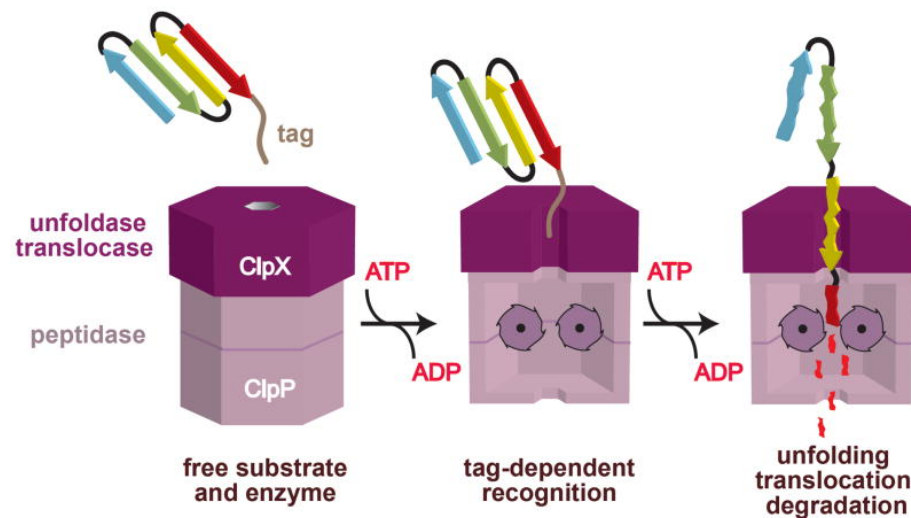


Figure 1.2 Schematic presentation of the ClpXP degradation cycle.

The CLPX hexamer recognizes the substrate upon binding of the recognition tag to axial pore. The protein substrate is then unfolded and translocated into the CLPP chamber for proteolysis (Baker and Sauer, 2012).

1.3.2 Physiological functions of ClpXP

Protein degradation by ClpXP is a vital process contributing to protein quality control by limiting misfolded or damaged proteins, however, ClpXP is also involved in highly regulated proteolytic activities thereby sustaining cellular homeostasis. The selective degradation of substrates based on substrate recognition represents an important mechanism of proteolytic regulation.

In *E.coli* several recognition motifs have been identified. In general these peptide sequences contain 3-10 amino acids and are located at the N- or C-terminal end of the target protein (Flynn et al., 2003; Gottesman et al., 1998). The best-studied recognition motif in *E.coli* is the *ssrA* tag. When ribosomes stall during protein synthesis, the 11 amino acid residue is cotranslationally added to the nascent polypeptides by the tmRNA system (Keiler et al., 1996). This allows termination of translation and the recycling of the ribosome machinery. The *ssrA* tagged peptide is then degraded by ClpXP. Mutagenesis experiments have shown that the last three residues (Leu-Ala-Ala) are sufficient for CLPX recognition (Flynn et al., 2001), while the other residues are bound by the SspB adaptor protein to enhance ClpXP mediated degradation (Flynn et al., 2004). So far the recognition motifs of the mammalian CLPX are unknown.

ClpXP is not only involved in the quality of *de novo* protein synthesis but also in the regulation of specific stress responses of in *E.coli*. The DNA repair protein RecN genetically encodes a ClpXP recognition motif (Leu-Ala-Ala), which constantly targets it for degradation by ClpXP. Upon DNA damage RecN is highly induced as part of the SOS regulon and accumulates within the cell irrespective of the ClpXP degradation (Neher et al., 2006). As soon as the stress condition is solved the transcription slows

down and RecN is efficiently degraded by ClpXP. Similarly, the general stress response regulatory protein σ^S is regulated by ClpXP degradation together with the adapter protein RssB (Hengge, 2009; Zhou et al., 2001). During exponential growth RssB binds to σ^S and targets it for degradation, however, in the stationary phase or other stress conditions the σ^S is stabilized due to decreased binding of RssB (Becker et al., 2000). Furthermore, CLPP was demonstrated to be important for the stress tolerance of many prokaryotes, including *Staphylococcus aureus*, *Streptococcus mutants* and *Haemophilus parasuis* (Frees et al., 2003; Hou et al., 2014; Huang et al., 2016). CLPP also plays an important role in the virulence of the mammalian pathogens *Salmonella typhimurium* and *Listeria monocytogenes* (Gaillot et al., 2000; Yamamoto et al., 2001). Different than in bacteria, in the fungus *Podospora anserine* ablation of CLPP leads to an increase in lifespan and this it is not accompanied by decreased health, which is commonly observed for life expanding interventions (Fischer et al., 2013).

Moreover, ClpXP dependent degradation of CtrA is required for the cell cycle progression in *Caulobacter crescentus* (Brown et al., 2009). In HEK293 cells, ClpXP was suggested to be involved in the regulation of mitophagy through the degradation of PINK1 together with MPP, m-AAA protease and LONP1 (Greene et al., 2012).

In *C.elegans*, CLPP-1 was implicated in the retrograde signaling of the mitochondrial unfolded protein response (UPR^{mt}) (Haynes et al., 2007). In response to an increased accumulation of unfolded or unassembled proteins or a mitonuclear imbalance that is exceeding the folding capacity of chaperones, the nuclear expression of mitochondrial chaperones and proteases is induced (Houtkoper et al., 2013). CLPP-1 has been proposed to degrade unfolded proteins to small peptides, which are exported by the ABC transporter HAF (Haynes et al., 2010). The efflux of those peptides might serve as an initial signal for the activation and nuclear translocation of the bZIP transcription factor ATFS-1, which activates expression of hsp-60 and hsp-6 (HSP60 and mtHSP70) (Nargund et al., 2012). In mammals far less is known about the signaling of the UPR^{mt}. In response to unfolded mitochondrial protein stress, the transcription factor CHOP (C/EBP homology protein), the chaperones HSP60 and mtDNAJ, as well as CLPP as a protease were shown to be specifically induced in mammalian cells (Zhao et al., 2002). However, unlike in *C.elegans*, in mammals the induction of those UPR responsive genes is not dependent on CLPP (Seiferling et al., 2016), suggesting a different signaling mechanism or the involvement of another protease for the UPR^{mt} in mammals.

Recently, a novel role for ClpXP in the regulation of mitochondrial translation through the degradation of ERAL1 has been proposed (Szczepanowska et al., 2016). ERAL1

binds to the small ribosomal subunit and acts as a chaperone for the mitochondrial 12S rRNA during ribosome assembly (Dennerlein et al., 2010). In the absence of CLPP, ERAL1 cannot be degraded and is not removed from the small ribosomal subunit, which leads to an impaired mitoribosomal assembly and in turn impairs mitochondrial translation (Szczepanowska et al., 2016).

In humans, recessive mutations in CLPP were found to cause Perrault Syndrome, which is characterized by premature ovarian failure, sensorineural hearing loss and growth retardation besides some other symptoms described for the patients with *Clpp* mutations (Jenkinson et al., 2013; Mytinger et al., 2016). The mouse model lacking *Clpp* expression represents a faithful model of the disease with similar pathologies (Gispert et al., 2013).

Although ClpXP has been extensively characterized in prokaryotes, including a comprehensive description of ClpXP substrates, the role of mammalian ClpXP is far less understood. A recent study identified 48 potential CLPP interaction proteins using a proximity based labeling technique in human cells (Cole et al., 2015). Most of these proteins were subunits of the mitochondrial respiratory chain and enzymes involved in mitochondrial metabolism. Intriguingly, another study reported overlapping candidates of ClpXP interaction partners and substrates in mouse heart, using a more sophisticated method to distinguish interactors from near neighbors and to additionally identify putative substrates (Szczepanowska et al., 2016). Hence, ClpXP seems to be involved in the regulation of mitochondrial metabolism and thereby also cellular and whole body metabolism.

1.4 Metabolism

Metabolism is the entity of all essential biochemical reactions taking place in a cell of living organisms. These reactions are organized into metabolic pathways, which begin with a particular molecule that is altered and converted into another molecule or molecules in a series of defined steps. Metabolic pathways can be divided into catabolic and anabolic processes. Catabolic pathways produce chemical energy through the degradation of organic molecules, whereas anabolic pathways require energy for biosynthetic reactions. Depending on the energy condition within the cell, some pathways can be either anabolic or catabolic (Berg et al., 2002). The generation of energy is essential for all types of cells. However, the metabolic requirement of each cell type is determined by the tissue function (see section 1.4.2.1) and environmental factors, like the type and availability of nutrients.

Due to the interconnection and interdependence of all metabolic pathways, their activity requires a fine coordination and tight regulation to ensure metabolic

homeostasis in a dynamically changing environment. The metabolic regulation is taking place at different levels (Metallo and Vander Heiden, 2013). The communication between tissues is mediated through hormone signaling and other extracellular factors (see section 1.4.2.2). At the cellular level, the abundance of enzymes or regulatory factors is regulated tissue- or context-specifically by mRNA transcription, splicing, stability or translation (Cairns et al., 2011). Transcriptional regulation for example involves transcription factors such as PPAR α or PPAR γ or transcription coregulators like PGC1 α . The nuclear receptor peroxisome proliferator-activated receptors (PPARs) are activated by ligand binding and control the expression of gene networks involved in lipid metabolism, adipogenesis and inflammation (Ahmadian et al., 2013). Additionally, these transcription factors are modulated by the peroxisome-proliferator-activated receptor coactivator 1 α (PGC1 α), the master regulator of mitochondrial biogenesis.

Another means to regulate enzyme activities and functions are posttranslational modifications through the covalent addition of a chemical moiety, such as acetate or phosphate to amino acid residues, proteolytic cleavage or degradation of the whole protein (Zhao et al., 2010). Enzyme activities can be further modulated by allosteric effects in the presence of small molecules, which alter the conformation of an enzyme either increasing or decreasing the affinity for its substrate (Phillips and Ainsworth, 1977). Finally, feedback regulation is a mechanism known to modulate the flux through the pathway. When a metabolite reaches a certain concentration, the upstream enzyme activity is regulated.

These mechanisms controlling enzyme activities and therefore metabolic flux can act separately or in conjunction. An important example for the interplay of two regulatory processes is the control of AMP-activated kinase (AMPK) activity. AMPK functions as an energy sensor and master regulator of metabolism (Yuan et al., 2013). Cellular energy levels are sensed by AMPK through the direct binding of AMP or ADP (allosteric regulation), which leads to a conformational change of AMPK. This conformational change allows AMPK to be phosphorylated by upstream kinases leading to its activation. In turn AMPK coordinates diverse metabolic responses through the phosphorylation of its downstream targets to increase catabolic pathways for the rapid modulation of ATP production and consumption.

All these processes aim to regulate metabolic flux according to the requirements of the individual cells.

1.4.1 Cellular metabolism

Metabolic pathways in the cell are compartmentalized to the cytosol, nucleus, mitochondria, peroxisomes, endoplasmatic reticulum and lysosomes. Here, we focus on the main metabolic reactions allocated to the cytosol and the mitochondria.

1.4.1.1 Cytosolic metabolism

Cytosol is the liquid component of the cytoplasm surrounding the nucleus and the cytoplasmic organelles. The biochemical reactions taking place in the cytosol are glycolysis, pentose phosphate pathway, fatty acid synthesis, amino acid metabolism and glycogen synthesis. The nutrient derived carbohydrates, lipids and proteins are taken up by the cell in the form of glucose, fatty acids and amino acids, which is facilitated by specialized membrane proteins. Glucose enters the cell through glucose transporters (GLUT1-4) and fatty acid uptake is mediated by fatty acid transporters, like the fatty acid translocase (FAT/CD36), tissue-specific fatty acid transport proteins (FATP) and plasma membrane fatty acid binding protein (FABPpm) (Fillmore et al., 2014).

Glycolysis

Glycolysis (Greek *glykos* „sweet“ and *lysis* “degradation”) is an ancient catabolic pathway derived from times when there was less oxygen in the atmosphere. It is conserved in almost all aerobe and anaerobe living organisms (Fothergill-Gilmore, 1986). In a series of 9 enzymatic steps one molecule of glucose is converted to two molecules of pyruvate. The glycolytic pathway can be divided into three stages. In the initial three reactions, glucose is converted to fructose-1-6-biphosphate, requiring two molecules of ATP. This first stage facilitates the trapping of glucose within the cell and its destabilization for the following reactions. The second stage is the cleavage of the six-carbon molecule fructose-1-6-biphosphate into two three-carbon molecules glyceraldehyde 3-phosphate and dihydroxyacetone phosphate. In the last stage ATP is harvested when the two three-carbon molecules are oxidized to pyruvate. This reaction sequence yields two molecules of ATP and two molecules of NADH (reduced nicotinamide adenine dinucleotide) (Hue and Hers, 1983). NADH is transported into mitochondria through the malate-aspartate and glycerol-3-phosphate shuttles for subsequent oxidation reactions (Stein and Imai, 2012). The fate of pyruvate depends on the cellular conditions. In the absence of oxygen, pyruvate can be reduced to lactate by the lactate dehydrogenase, while regenerating NAD⁺ (oxidized NAD) required for upstream reactions of glycolysis, which is important in skeletal muscle when the energy demands exceed the oxygen supply or in erythrocytes due to the lack

of mitochondria. Although this reaction is energetically unfavorable as compared to the entire oxidation of glucose via glycolysis, the tricarboxylic acid cycle (TCA) and oxidative phosphorylation, which is strictly dependent on the availability of oxygen. Increased blood lactate concentrations can be also evident for mitochondrial dysfunction due to an increased reliance on glycolysis and reduced oxidation of pyruvate within the mitochondria.

Glycolysis is regulated at three distinct steps, through feedback inhibition of the hexokinase catalyzing the initial step of glucose to glucose-6-phosphate conversion and the allosteric regulation of phosphofructokinase and pyruvate kinase by AMP, ADP, ATP or citrate depending on the energy state of the cell.

Gluconeogenesis

Gluconeogenesis is an anabolic pathway generating glucose from non-carbohydrate precursors. During prolonged fasting and starvation conditions gluconeogenesis is required to prevent hypoglycemia. The major precursors are pyruvate, lactate, gluconeogenic amino acids and glycerol. They are either first converted to pyruvate or enter the pathway through later intermediates. Gluconeogenesis is often considered the reverse reaction of glycolysis, however, the irreversible reactions of glycolysis have to be bypassed during gluconeogenesis by four different enzymes. The first reaction of gluconeogenesis is located in the mitochondria and requires a distinct enzyme pyruvate carboxylase (PC), the second reaction can be carried out within mitochondria or the cytosol by phosphoenolpyruvate carboxykinase (PEPCK) for the conversion of pyruvate in the cytosol and in the ER. The other distinctive enzymes required for gluconeogenesis are fructose 1,6-biphosphatase and glucose 6-phosphatase, which catalyze the hydrolysis reactions (Jitrapakdee, 2012). Gluconeogenesis is reciprocally regulated with glycolysis, therefore the same key steps are regulated (Berg et al., 2002).

Glycogen metabolism

Glycogen is a multi-branched polymer of glucose and functions as storage form of glucose within tissues, especially in liver and skeletal muscle. However, glycogen serves different functions in both tissues. Hepatic glycogen is required to maintain blood glucose levels during fasting conditions, whereas muscle glycogen is expended only for muscular activity as during intense exercise. The synthesis of glycogen (glycogenesis) requires a primer consisting of a glycogenin protein attached to α -1,4 linked glucose oligosaccharide. This primer is used by the glycogen synthase for the elongation with UDP-glucose molecules, an activated form of glucose generated from

glucose-1-phosphate. Additionally, a branching enzyme is required for the formation of α -1,6 linked glucose branches to obtain the polysaccharide glycogen.

The degradation of glycogen (glycogenolysis) is controlled by the glycogen phosphorylase. Together with a bifunctional debranching enzyme, the phosphorylase mediates the shortening of the oligosaccharide chains to release glucose-1-phosphate. The synthesis and degradation of glycogen are reciprocally regulated through the activity of glycogen synthase and phosphorylase. Hormone stimulated cyclic AMP (cAMP) cascade acting through protein kinase A is facilitating the switch between the active and inactive forms of glycogen synthase and phosphorylase (Bollen et al., 1998).

Fatty acid synthesis

In a high-energy state, when glycogen stores are already filled, a surplus of glucose results in the synthesis of fatty acids and the formation of triglycerides. Fatty acids are synthesized from acetyl-CoA, which is exported from the mitochondria as citrate and reconverted to acetyl-CoA in the cytosol. Acetyl-CoA is carboxylated by the acetyl-CoA carboxylase (ACC) to malonyl CoA. This reaction is the rate-limiting step during fatty acid synthesis and is highly regulated at the level of ACC (Hillgartner et al., 1995; Kim, 1997). The subsequent reaction steps of the *de novo* lipogenesis are catalyzed by the multifunctional enzyme fatty acid synthase (FAS) (Wakil, 1989). Malonyl CoA functions as a two-carbon donor for the elongation of acetyl-CoA. This step is repeated six times in a cyclic manner resulting in C16.0 palmitic acid. During the reaction nicotinamide adenine dinucleotide phosphate (NADPH), derived from the pentose phosphate pathway, functions as a reducing agent. The palmitic acid produced by the FAS can be further modulated by elongation or desaturation. In order to be stored in the liver or adipose tissue, three fatty acids are esterified with glycerol-3-phosphate resulting in the formation of triacylglycerol.

As mentioned earlier fatty acid synthesis and in parallel also fatty acid β -oxidation is regulated by ACC activity. Malonyl CoA generated by ACC, acts as an inhibitor of CPT1 and is thus controlling fatty acid uptake into mitochondria for β -oxidation. The activity of ACC is modulated by phosphorylation, dephosphorylation and also allosterically activated by citrate (Brownsey et al., 2006). The upstream kinase AMPK is mediating the inhibiting phosphorylation of ACC in low energy conditions. Hence, AMPK and ACC are stringently regulating fatty acid metabolism according to physiological needs.

1.4.1.2 Mitochondrial metabolism

Fatty acid β -oxidation

During fatty acid β -oxidation (FAO) fatty acids originating from the diet or the hydrolysis of triglycerides during fasting conditions are degraded to generate energy in the form of ATP. Most of the dietary fats are composed of long chain fatty acids, in particular palmitic acid (C16:0) (Rustan, 2009). Long chain fatty acids in the cytosol are converted and thereby activated in a two-step process with an acyl adenylate intermediate to acyl-CoA by acyl-CoA synthases (ACS) (Grevengoed et al., 2014). Long chain acyl-CoAs are unable to diffuse through the IMM and are esterified to acylcarnitines by the carnitine palmitoyltransferase 1 (CPT1). This permits the transport of the acylcarnitines across the IMM by the carnitine acylcarnitine translocase (CACT) in exchange for carnitine. Once inside the mitochondria, CPT2 reconverts the acylcarnitines to acyl-CoAs, which can finally undergo FAO (Eaton et al., 1996). Medium and short chain fatty acids diffuse through the mitochondrial membrane and are activated in an ATP-dependent reaction *in situ* before undergoing FAO.

The β -oxidation cycle comprises a series of four enzymatic reactions, in which a two-carbon acetyl-CoA is released from the acyl-CoA ester per cycle. In the first reaction acyl-CoAs are oxidized to enoyl-CoA by chain length specific acyl-CoA dehydrogenases: short-chain (C4-C6) acyl-CoA dehydrogenase (SCAD), medium-chain (C6-C12) acyl-CoA dehydrogenase (MCAD), long-chain (C12-C16) acyl-CoA dehydrogenase (LCAD) and very long-chain (C14-C20) acyl-CoA dehydrogenase (VLCAD) (Ojuka et al., 2016). The three subsequent reactions are a hydration, oxidation and thiolation that are catalyzed either by the mitochondrial trifunctional protein (MTP) for very long chain fatty acyl-CoAs or three separate enzymes (crotase, medium/short-chain hydroxyacyl-CoA dehydrogenase and medium-chain ketoacyl-CoA thiolase) for short-, medium- and long-chain fatty acids. Each cycle results in the formation of one FADH₂, one NADH, one acetyl-CoA and a 2-carbon shortened acyl-CoA, which re-enters the cycle until two acetyl-CoA molecules are produced. The reducing equivalents NADH and FADH₂ transfer their electrons either directly to complex I of the respiratory chain or via the electron transfer flavoprotein (ETF) to ubiquinone, respectively. Acetyl-CoA can be further oxidized in the TCA cycle or exported from the mitochondria for *de novo* lipogenesis. Furthermore, it can also be converted into ketone bodies during starvation conditions.

TCA cycle

The TCA cycle, also referred to as citric acid cycle or Krebs cycle, constitutes a central metabolic hub. It represents the final oxidation pathway for metabolic fuels derived

from carbohydrates, fats and proteins. Under aerobic conditions pyruvate derived from glycolysis in the cytosol is converted to acetyl-CoA by the pyruvate dehydrogenase, a reaction yielding one molecule of NADH. The acetyl-CoA is then utilized in the TCA cycle for its complete oxidation to CO₂ thereby producing three NADH, one FADH₂ and GTP. The electrons of NADH and FADH₂ are again allocated to the respiratory chain. The enzyme generating the FADH₂, succinate dehydrogenase (complex II) takes not only part in the TCA cycle, it is also part of the respiratory chain therefore electrons from the oxidation of succinate directly reduce FAD⁺, a prosthetic group of complex II (Akram, 2014).

The TCA cycle additionally provides many precursors and metabolites for biosynthetic pathways including gluconeogenesis, amino acid metabolism or porphyrin synthesis (Owen et al., 2002). Many of the TCA cycle intermediates are taken from the cycle by cataplerotic reactions, like α -ketoglutarate or oxaloacetate to form amino acids. However, they can also be placed back by anaplerotic reactions. Oxaloacetate can be redirected for gluconeogenesis or replenished by the pyruvate carboxylase converting pyruvate to oxaloacetate. Citrate represents an important source of acetyl CoA when exported from the mitochondria for fatty acid synthesis and ketone body formation. The TCA cycle is also important in providing succinyl-CoA for the initial reaction of the heme biosynthesis (Atamna, 2004).

Oxidative phosphorylation

The oxidative phosphorylation (OXPHOS) is the final biochemical pathway for the generation of the largest proportion of the cellular energy. The mitochondrial OXPHOS system consists of four electron transferring protein complexes namely complex I (NADH: ubiquinone oxidoreductase), complex II (succinate dehydrogenase), complex III (ubiquinol:cytochrome c oxidoreductase), complex IV (cytochrome c oxidase, also referred to as COX) and the F₀F₁-ATP synthase, which are embedded in the inner mitochondrial membrane (Figure 1.3) (Barrientos et al., 2002; Fontanesi et al., 2006; Lazarou et al., 2007; Rutter et al., 2010). The mobile redox carriers ubiquinone (coenzyme Q) and cytochrome c transfer electrons between the individual complexes (Figure 1.3). Additionally, ubiquinone is an entry point for electrons derived from FAO, which are transferred by the ETF.

In the beginning, electrons are transferred via redox reactions from the electron carrier NADH to complex I and from succinate (via FADH₂) to complex II and are passed down the respiratory chain to the terminal electron acceptor oxygen. These redox reactions drive the proton translocation from the matrix to the IMS by complex I, complex III and complex IV and are thereby generating an electrochemical proton gradient. The energy

stored within this gradient drives the F_0F_1 -ATP synthase to synthesize ATP from ADP and inorganic phosphate (Jonckheere et al., 2012). The protons that flow back to the matrix through F_0F_1 -ATP synthase are combined with the reduced oxygen to form H_2O .

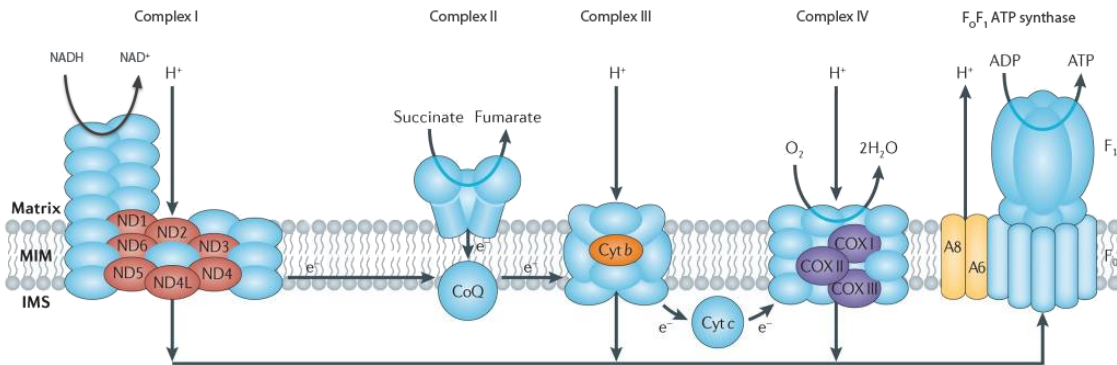


Figure 1.3 OXPHOS system.

The mitochondrial respiratory chain complexes generate an electrochemical gradient across the inner mitochondrial membrane. NADH and succinate are oxidized to NAD⁺ and fumarate by Complex I and Complex II, respectively. The electrons (e⁻) are transferred via coenzyme Q (CoQ) to Complex III and further to Complex IV via cytochrome c (Cyt c). At Complex IV electrons are transferred to the final electron acceptor oxygen that forms H₂O. The proton gradient produced by Complex I, Complex III and Complex IV is used by the F_0F_1 -ATP synthase for ATP synthesis. The nuclear-encoded proteins are colored in blue and the mitochondrial-encoded subunits in other colors. Reprinted with modifications from Schon et al., 2012.

The mitochondrial OXPHOS complexes are not simply arranged in sequence, however, they have a supramolecular organization (Chaban et al., 2014; Schägger and Pfeiffer, 2000). Complexes I, III and IV assemble into supercomplexes with different stoichiometry $CoI_{0-1}+CoIII_2+CoIV_{0-4}$ (Dudkina et al., 2010; Genova et al., 2008). Supercomplexes comprising all three complexes ($CoI+CoIII_2+CoIV_2$) are referred to as respirasomes (Marques et al., 2007; Wittig and Schägger, 2009). These supramolecular structures are proposed to facilitate channeling of the substrates ubiquinone and cytochrome c or to catalytically enhance the reactions due to shorter diffusion times. These assumptions are strengthened by the finding that OXPHOS complexes are predominantly localized to the protein rich mitochondrial cristae, which are structurally separated from the inner boundary membrane by cristae junctions (Frey et al., 2002; Gilkerson et al., 2003; Lippe et al., 1988; Schägger and Pfeiffer, 2000; Vogel et al., 2006). Another crucial function of the supercomplex formation is the stabilization of complex I by complex III and complex IV (Diaz et al., 2006; Schägger et al., 2004). The ATP synthase dimerizes and forms oligomeric chains, which is suggested to impose a curvature of the IMM and thereby increasing the local proton concentration (Strauss et al., 2008). Complex II is the only complex that has not been detected in higher order structures, which might be due to its dual function in the TCA cycle and OXPHOS. Noteworthy, it was shown that supercomplex formation is

important for mitochondrial function and cell physiology (Ikeda et al., 2013; Wittig and Schägger, 2009).

1.4.2 Whole body metabolism

1.4.2.1 Endocrine regulation of metabolism

Metabolism is tightly regulated through the concerted actions of endocrine hormones (Randle, 1963). It involves an extensive interrelation of metabolites and hormones to control and direct metabolic pathways. Here the endocrine actions of insulin, glucagon, leptin, ghrelin and incretins in the regulation of glucose and lipid metabolism and whole body energy expenditure are considered.

Blood glucose levels are maintained in a narrow range despite alternate fasting and feeding cycles. The glucose concentration in the blood is balanced by the absorption from the intestine, glucose production and secretion from the liver and to a lesser extent from the kidneys and the clearance by peripheral organs (Saltiel and Kahn, 2001).

Cellular responses to endocrine hormones are mediated through receptors on the cell surface. Hormone binding induces signaling via G protein coupled receptors and second messengers like cAMP (glucagon, ghrelin), tyrosine kinase receptors and a direct phosphorylation of downstream substrates (insulin) or cytokine receptors with bound Janus kinase (JAK) (leptin) (Schwartz et al., 2000).

Insulin is one of the most important anabolic peptide hormones. In response to increased blood glucose levels, insulin is secreted from pancreatic β -cells (Saltiel and Kahn, 2001). Insulin is mainly responsible for reducing blood glucose levels by increasing peripheral glucose uptake and reducing glucose production in the liver, by reducing gluconeogenesis and glycogenolysis (Rizza et al., 1981). Specifically it modulates enzyme levels by decreasing transcription of phosphoenolpyruvate carboxykinase (PEPCK), glucose-6-phosphatase, and fructose-1,6-biphosphatase and increasing transcription of glucokinase and pyruvate kinase (S J Pilkis and Granner, 1992). The peripheral insulin dependent glucose disposal is stimulated by membrane translocation of GLUT4 in skeletal muscle and adipose tissue, whereas skeletal muscle is clearing about 75% (Klip and Pâquet, 1990). Moreover, insulin facilitates storage of metabolic fuels in liver, skeletal muscle and adipose tissue by stimulating glycogenesis and lipogenesis.

Glucagon is secreted from pancreatic α -cells in order to increase blood glucose concentration. It dominates hepatic metabolism during fasting, by increasing glycogenolysis and gluconeogenesis (Campbell and Drucker, 2015). Additionally,

glucagon induces lipolysis in adipose tissue to provide more substrates for gluconeogenesis (glycerol) and FAO (fatty acids) (Slavin et al., 1994).

Two important hormones implicated in the regulation of whole body energy expenditure are leptin and ghrelin. Leptin is commonly known as the satiety hormone. It is secreted from adipocytes and acts on the hypothalamus in the central nervous system thereby regulating food intake, energy expenditure and body weight (Schwartz et al., 2000). Furthermore, leptin stimulates FAO through AMPK activation and is thus regulating lipid metabolism (Minokoshi et al., 2002). The loss of leptin leads to obesity and insulin resistance in mice (*ob/ob*) (Pelleymounter et al., 1995). However, circulating leptin levels are increased in obesity, since leptin secretion is proportional to adipose tissue weight, a condition often referred to as leptin resistance.

Ghrelin functions as the counter regulatory hormone to leptin. Its circulating levels are alternating and peaking pre-prandial, which was suggesting the function as hunger signal (Yin et al., 2009). It is secreted from the stomach and acts like leptin on the central nervous system (Abizaid et al., 2006). Ghrelin stimulates appetite and thus regulates body weight (Tschöp et al., 2000). Additional physiological functions are the stimulation of GH secretion and promotion of gastric motility (Yang et al., 2014).

The incretin hormones GLP-1 and GIP are secreted from the intestinal cells rapidly after food ingestion. They facilitate quick disposal of nutrients by facilitating insulin secretion from pancreatic β -cells (Baggio and Drucker, 2007). GLP-1 was also shown to promote satiety.

1.4.2.2 Organ interrelation in metabolism with regard to mitochondrial function

Each organ has specific functions in the body and varies widely in energy needs. The functional requirements of the mitochondria are reflected in the tissue-specific variations of the mitochondrial proteome, mitochondrial morphology, as well as differences in mitochondrial number, ranging from a few hundred to a few thousand per cell (Pagliarini et al., 2008; Thor Johnson et al., 2007). These differences are even apparent within one tissue, as for example in the different skeletal muscle fiber types.

The liver is the key metabolic organ governing whole body energy metabolism. It represents the metabolic hub providing fuels to other tissues and is the central organ in the regulation of glucose metabolism. During fasting conditions the liver increases glycogenolysis and gluconeogenesis in response to glucagon signaling in order to increase blood glucose levels. Additionally, the liver is the main organ generating ketone bodies from fatty acids during starvation, which serve as fuel for the brain. In the postprandial state, insulin stimulates glycogenesis and *de novo* lipogenesis in the liver (Rui, 2014). Hepatocytes harbor some distinctive enzymes in order to perform

these specialized functions. The glucose transporter GLUT2 allows unlimited uptake and release of glucose from and to the circulation. Moreover, liver cells possess glucokinase instead of hexokinase, which is mediating the first step in glycolysis, but the glucokinase is not allosterically inhibited by its product. Pyruvate derived from glycolysis in the liver mainly serves catabolic processes as mentioned above.

Therefore, hepatic mitochondria primarily have biosynthetic functions. This is reflected in the hepatic mitochondrial respiratory function, which has a large spare capacity, measurable after uncoupling with the proton ionophore FCCP, indicating that liver mitochondria respire at a low range for ATP production.

Skeletal muscle represents the largest organ in the body. The main fuel for muscle cells is glucose, fatty acids and ketone bodies. Skeletal muscle has the largest glycogen store for direct use within muscle cells. When immediate energy is required during muscle contraction, skeletal muscle cells rely almost entirely on glycolysis. A distinct feature of muscle cells is the anaerobic metabolism to generate ATP, when glucose is oxidized to lactate during intense exercise. In an exchange with the liver, lactate is converted to glucose and provided again to the muscle, this exchange is known as the Cori cycle (Berg et al., 2002). The resting muscle relies almost entirely on FAO for ATP generation. The presence of GLUT4 in skeletal muscle cells allows the insulin-stimulated uptake of glucose and the clearance of the largest proportion of blood glucose in the fed state. The alternate functions of skeletal muscle are evident in the different muscle fiber types harboring morphologically different mitochondria. Type 1 fibers contain many mitochondria and rely on OXPHOS for ATP generation, yet they are able to oxidize fatty acids and ketone bodies. In contrast, type 2a fibers possess many small mitochondria with high capacity for ATP generation. Finally, type 2b fibers contain only very few mitochondria since they rely on anaerobic glycolysis and contain high amounts of glycogen (Forner et al., 2006). Muscle mitochondria have a high ATP synthesis capacity and ATP synthesis is tightly coupled to oxygen consumption (Marcinek et al., 2004).

The heart, unlike the skeletal muscle exclusively functions aerobically. This is evident by the large density of mitochondria in the heart. Moreover, the heart relies entirely on fatty acids for energy generation (Doenst et al., 2013). Thus, heart mitochondria are primarily ATP generating and mitochondrial respiration is functioning to almost full capacity in the coupled state. The fatty acids required for heart functioning are in part provided by adipose tissue.

Adipose tissue can be divided into two subtypes depending on the morphology and thermogenic function: white adipose tissue (WAT) and brown adipose tissue (BAT). WAT contains unilocular adipocytes serving as energy storage in the form of

triglycerides also named triacylglycerol. Triacylglycerol is hydrolyzed upon fasting into fatty acids and glycerol and released for the oxidation by the liver, heart or skeletal muscle, whereas insulin stimulates triglyceride storage. Besides the WAT, the liver is the major site of *de novo* lipogenesis and triglycerides are transported to the WAT for storage. Next to skeletal muscles cells, white adipocytes harbor GLUT4 for the insulin stimulated glucose uptake. Glucose is required for the generation of glycerol-3-phosphate, which is needed for the esterification of fatty acids to triacylglycerol. Although WAT contains very few mitochondria, dysfunction of white adipose tissue mitochondria is associated with decreased lipogenesis and increased lipolysis (Kusminski and Scherer, 2012).

BAT contains multilocular adipocytes rich in mitochondria. The main function of BAT is the generation of heat via non-shivering thermogenesis. Cold induced β -adrenergic stimulation of BAT by norepinephrine, leads to the transcriptional activation of the uncoupling protein 1 (UCP1). UCP1 uncouples the mitochondrial proton gradient from ATP synthesis and thereby allows robust oxidation of fatty acids to generate heat without generating large amounts of ATP (Cannon and Nedergaard, 2004). Thus, BAT has a rather catabolic role in metabolism in contrast to WAT.

1.5 Mitochondrial dysfunction and metabolic diseases

Mitochondrial dysfunction has been reported in various chronic diseases ranging from metabolic diseases, including type 2 diabetes mellitus and obesity to cardiovascular diseases, cancer and neurodegeneration (Patti and Corvera, 2010). Although these pathologies are not directly caused by mutations in mitochondrial proteins, they do affect mitochondrial function.

The metabolic alteration in tumor cells, involving mitochondrial function, is the shift from OXPHOS to glycolysis. This metabolic switch has been assigned to mutations in mitochondrial proteins to inactivate OXPHOS or alter different metabolic pathways (Yan et al., 2009; Zhang et al., 2012a). Accordingly, increased expression or abundance of mitochondrial quality control proteins, including *Lonp1*, *Trap1* and CLPP have been associated with cancer (Chae et al., 2012; Cheng et al., 2013; Cole et al., 2015).

Type 2 diabetes is characterized by increased blood glucose levels due to impaired insulin secretion from pancreatic β -cells and insulin resistance in peripheral tissues. The decline in mitochondrial function in skeletal muscle has been attributed to contribute to development of diabetes with age (Petersen et al., 2003). Moreover, the electron transport chain (ETC) capacity in particular complex I was shown to be impaired in type 2 diabetic skeletal muscle (Kelley et al., 2002). A proposed

mechanism for the development of impaired insulin signaling and reduced glucose oxidation related to mitochondrial function is the accumulation of intermediates of fatty acid metabolism resulting from incomplete FAO (Koves et al., 2008). Another contributing factor to dysfunctional mitochondria during diabetes or obesity are reactive oxygen species (ROS) resulting from nutrient excess. High fat high sucrose diet feeding results in increased ROS production that caused oxidative damage to the mitochondria and their dysfunction, however, insulin resistance was preceding the latter one (Bonnard et al., 2008). Therefore, it seems reasonable that the reduction in mitochondrial respiratory function might be a protective mechanism counteracting ROS induced insulin resistance. Two studies reported an increased insulin sensitivity and a protection from diet induced obesity of mice with reduced mitochondrial respiratory activity (Wredenberg et al., 2006). While there are no reports about mutations in the mitochondrial quality control proteins associated with metabolic diseases, defects in this system has a profound influence on metabolism owing to the loss of mitochondrial homeostasis. Impaired proteostasis affects the OXPHOS system as well as other mitochondrial proteins, triggering alterations in cellular metabolism that might contribute to physiological deregulation and metabolic disease. Hence, defects in proteins facilitating mitochondrial biogenesis like PGC1 α , mitochondrial dynamics (MFN2 and OPA1) and the protease PARL have been linked to metabolic diseases and obesity (Civitarese et al., 2010; Lin et al., 2004; Quiró S et al., 2012; Sebastián et al., 2012).

1.6 Objectives

Mitochondrial proteases are essential for maintaining mitochondrial function and therefore cell homeostasis. This does not only involve protein quality control by degrading misfolded or damaged proteins, mitochondrial proteases also take part in highly regulated proteolytic activities and thereby influence several metabolic pathways. Due to the large complexity of the proteolytic landscape the physiological relevance of several proteases remains unknown. Therefore, this study aims to decipher the role of the mitochondrial protease CLPP in mammalian metabolism using different mouse models.

Whole body CLPP deficient mice were analyzed when fed normal chow diet (NCD) or high fat diet (HFD) to elucidate the function of CLPP under normal and metabolic stress conditions and to determine the relevance of CLPP for whole body physiology. Furthermore, tissue-specific CLPP deficient mice were exploited to investigate the impact of local impaired proteostasis on whole body metabolism.

In addition, a mouse model modulating the mitokine stress response induced by the absence of CLPP was developed. In order to dissect the contribution of the FGF21 mitokine induced response to the whole body phenotype of CLPP deficient mice, *Clpp/Fgf21* double knockout mice were generated.

The work outlined here will contribute to the understanding of the CLPP protease and its possible relevance in different physiological and pathological conditions.

2 Materials and Methods

2.1 Animal care

Animals were housed in groups of 3-5 mice per cage at ambient temperature (22-24°C) and maintained on a 12 hour light/dark cycle with lights on at 6 am. Mice had ad libitum access to either normal chow diet (R/M-H-V1554, ssniff Spezialdiäten GmbH) containing 55.1% carbohydrates, 19.3% proteins and 3.3% fat (9% calories from fat) or high fat diet (ssniff EF acc. D12492 (I) mod., ssniff Spezialdiäten GmbH) containing 27.1% carbohydrates, 24.1% protein and 34.0% fat (60% calories from fat) and drinking water. Mice were killed by cervical dislocation at the end of the study. The high fat diet was fed starting from 8 weeks of age until the termination of the experiment with 15 weeks. All experimental procedures were conducted in compliance with protocols approved by local government authorities (Bezirksregierung Köln) and were in accordance with NIH guidelines.

2.2 Experimental mouse models

The conditional targeting for the mitochondrial ATP-dependent Clp protease proteolytic subunit (*Clpp*) gene was conducted by Taconic Artemis, Germany in Art B6/3.5 stem cell line on a C56BL/6 TacN background. LoxP sites were introduced flanking exons 3 and 5 and in addition, an Frt flanked puromycin selection marker was inserted into intron 5. Upon successful germline transmission, the $Clpp^{+/PuroR-fl}$ mice were mated with Flp deleter mice to remove the PuroR selection cassette. Finally, floxed mice ($Clpp^{fl/fl}$) were intercrossed with transgenic mice expressing Cre recombinase. To generate full body CLPP knockout mice, $Clpp^{fl/fl}$ were mated with transgenic mice ubiquitously expressing Cre recombinase under control of the β -actin promoter, resulting in $Clpp^{+/-}$ mice. Heterozygous $Clpp^{+/-}$ mice were further intercrossed to obtain homozygous

Clpp^{-/-} mice. Liver-specific knockout animals were generated by mating *Clpp*^{fl/fl} animals with transgenic mice expressing Cre recombinase under control of the albumin enhancer and promoter and the α -fetoprotein enhancer (Afp-Cre) (Kellendonk et al., 2000). Heart and skeletal muscle-specific knockout animals were generated by mating *Clpp*^{fl/fl} animals with transgenic mice expressing Cre recombinase under control of the muscle creatine kinase promoter (Ckmm-Cre) (Larsson et al., 1998).

The fibroblast growth factor 21 (*Fgf21*) gene targeting was carried out in the lab of Prof. David Mangelsdorf that was described earlier (Potthoff et al., 2009). For the generation of double deficient *Clpp* and *Fgf21* knockout animals, *Clpp*^{fl/fl} *Fgf21*^{fl/fl} mice were mated with transgenic mice ubiquitously expressing Cre recombinase (β -actin Cre).

2.3 Phenotyping

2.3.1 Body weight

Body weight was assessed weekly of individual mice in the age from 4-16 weeks fed either NCD or HFD.

2.3.2 Body composition

The body fat content and lean mass was measured using the nuclear magnetic resonance (NMR) analyzer minispec mq7.5 (Bruker Optik).

2.3.3 Indirect calorimetry

Energy expenditure and respiratory exchange ratio (RER) were determined with indirect calorimetry using the PhenoMaster (TSE systems). Animals were acclimated in metabolic chambers (7.1 liter) for three days prior to data acquisition to adapt them to single housing, food and water dispensers. During this time animals were monitored daily and the body weight was determined to ensure proper adaption. Calorimetric measurements were conducted at 22°C for 72 h assessing oxygen consumption, carbon dioxide production and locomotor activity (infrared light beam frame, TSE systems). In addition, food and water intake was assessed with automated measuring devices (TSE systems).

2.3.4 Blood glucose measurement

Blood glucose levels were determined from whole venous tail blood using an automatic glucose monitor (Contour Next, Bayer) from either random fed or 6 h fasted animals.

2.3.5 Serum analyses

Serum was obtained by collecting blood from the submandibular vein. Blood samples were then incubated at room temperature (RT) for 45 min and centrifuged at 1500 g for 15 min. Resulting serum was stored at -80°C for subsequent analysis.

Serum hormone levels were measured using the Bio-Plex Pro Mouse Diabetes 8-Plex Assay (Bio-Rad) with the Bio-Plex™ 200 system (Bio-Rad). This system allows the simultaneous quantification of eight hormones based on antibody-coupled magnetic beads.

Serum non-esterified fatty acids were quantified using an acyl CoA synthase/ acyl-CoA oxidase based calorimetric kit (NEFA-HR2, WAKO Chemicals GmbH).

Serum Fgf21 levels were determined by an enzyme linked immunosorbent assay according to manufacturer's instructions (Mouse/Rat FGF-21 Quantikine ELISA Kit, R&D Systems).

2.3.6 Glucose tolerance test and insulin tolerance test

Glucose tolerance tests were carried out in 15-week-old animals following a 6 h fast. After measuring fasted blood glucose levels, mice were injected intraperitoneally (i.p.) with 2 mg g⁻¹ body weight glucose (20% glucose solution, Sigma Aldrich). Blood glucose levels were determined 15 min, 30 min, 60 min and 90 min post glucose injection.

Insulin tolerance tests were performed with ad libitum fed 16-week-old animals. After recording baseline glucose levels each animal was administered i.p. with 0.6 U kg⁻¹ body weight insulin (Insuman Rapid, Sanofi-Aventis) and blood glucose levels were monitored at 15 min, 30 min, 60 min and 90 min after injection.

2.3.7 Insulin signaling

Following a 2 h fast, mice were injected with 0.6 U kg⁻¹ body weight insulin (Insuman Rapid, Sanofi-Aventis) or saline. Mice were then sacrificed 30 min past injection and tissues were collected and frozen in liquid nitrogen.

2.3.8 Acute cold exposure and measurement of rectal body temperature

For acute cold exposure Clpp^{-/-} and control animals were individually housed in home cages with bedding material, however, without nesting material and exposed to 5°C. Rectal body temperature was measured using a rectal thermometer (Bioseb) prior to the experiment at ambient temperature. Afterwards body temperature was measured every hour for 7 h or until core body temperature dropped below 26°C.

2.3.9 Femur length

The mouse hind leg was carefully removed and then muscle and ligaments were trimmed away to dissect the femur. The femur was cleaned from connective tissue with paper cloth. In the end, the length of the femur was measured between femur head and the lateral condyle with a sliding caliper.

2.3.10 Micro computed tomography

The measurement of the bone mineral density was performed with the LaTheta microCT Scanner (Aloka) in anaesthetized mice using 2.5% Isoflurane in oxygen. The sections were set to 0.6 μm and analysis was done with the LaTheta software.

2.4 Molecular biology

2.4.1 Isolation of genomic DNA from mouse ear biopsies

Mouse ear biopsies were taken at weaning age and subsequently incubated in lysis buffer containing 100 mM Tris-HCl, pH 8.5, 5 mM EDTA, pH 8.0, 0,2% (w/v) SDS, 200 mM NaCl and 10 mg/mL Proteinase K (Sigma Aldrich) in a thermoshaker (Eppendorf) at 55°C overnight or until dissolved. DNA was precipitated by adding 1x volume of Isopropanol and subsequent centrifugation at 13.000 rpm for 30 min at 4°C in a bench top centrifuge (Eppendorf). After decanting the supernatant, the DNA pellet was washed with 70% (v/v) Ethanol and centrifuged again at 13,000 rpm for 20 min. Hereafter, the DNA pellet was dried and dissolved in 75 μL ddH₂O.

2.4.2 Isolation of genomic DNA from mouse tissues

Liver tissue was incubated overnight in lysis buffer (50 mM Tris-HCl pH 8.0, 2.5 mM EDTA, 0.5% (w/v) SDS, 0.1 M NaCl, 10 mg/mL Proteinase K) at 55°C. Contaminants were removed by adding 75 μL of 8 M Potassium Acetate and 500 μL chloroform and centrifuging at 13,000 rpm for 15 min. Resulting upper aqueous phase was transferred to a new tube and DNA was precipitated by adding 2x volume of ice-cold 100% Ethanol and centrifuging at 13,000 rpm for 15 min. The resulting DNA pellet was washed with 70% (v/v) Ethanol and resuspended in 200 μL ddH₂O.

2.4.3 Isolation of total RNA

Total RNA was isolated from mouse tissues using TRIzol reagent (Life Technologies). Initially 50-100 mg of fresh or snap frozen tissue was placed in 2 mL tubes (Peqlab) together with ceramic beads (Mobio, Dianova GmbH) and 1 mL TRIzol. The tissue was homogenized using a Precellys 24 fast-prep machine (Bertin) at 5500 rpm for 2x 20 sec. For tissues with high fat content (EWAT and IWAT), an additional

centrifugation step following homogenization was performed at 12.000 g for 10 min at 4°C. Homogenates were then transferred to a new tube and it was proceeded with the addition chloroform and subsequent phase separation according to the manufacturer's instruction. RNA pellet was resuspended in RNase/DNase free H₂O (Gibco).

2.4.4 Quantification of nucleic acids

Nucleic acid concentration (DNA and RNA) was determined by measuring sample absorption with a NanoDrop 8000 Spectrophotometer (Thermo Scientific). The absorbance ratio of 260/280 nm was used to assess nucleic acid quality. A ratio of 1.8 or 2 was considered as pure DNA or RNA, respectively.

2.4.5 Polymerase chain reaction

Polymerase chain reactions (PCR) (Mullis and Faloona, 1987; Saiki et al., 1988) were performed for the determination of mice genotypes with customized primers (Sigma Aldrich) listed in Table 2.1. Amplification reactions were carried out in a Veriti Thermocycler (Applied Biosystems, Life Technologies). Each PCR reaction was performed in a total volume of 20 µL containing approximately 50 ng DNA template, 1x DreamTaq Buffer (Thermo Scientific), 62.5 µM dNTP mix (Promega), 0.4 µM of each primer and 1U DreamTaq Polymerase (Thermo Scientific). PCR products were resolved by gel electrophoresis on 2% (w/v) agarose (Sigma Aldrich) gels (0.5x TBE, 1:50.000 GelRed (Biotium)).

Table 2.1 Oligonucleotides used for genotyping

Primer sequences are displayed in 5'-3' order.

Primer	Primer sequence 5'-3'	T _{Annealing} [°C]
Clpp WT forward	GTGGATGATGGTCAGTAGAATCC	61
Clpp WT reverse	CCCAGACATGATTCCCTAGCAC	61
Clpp KO forward	TGTGCATTCTTACCATAGTCTGC	61
Cre forward	CACGACCAAGTGACAGCAAT	53
Cre reverse	AGAGACGGAAATCCATCGCT	53
Fgf21 WT forward	GGGCTCTGATAAAGCATTCC	gradient (65°C -60°C)
Fgf21 WT reverse	CAGCACTAAGGGAGGCAGAG	gradient (65°C -60°C)
Fgf21 KO forward	CCTCCAGATTTAGGAGTGCAGA	56
Fgf21 KO reverse	AGGGAGGCAGAGGCAAGTGATT	56

PCR cycling conditions for *Ctpp*, *Cre* and *Fgf21* knockout allele

1. Initial denaturation at 95°C for 5 min
 2. Denaturation at 95°C for 30 sec
 3. Annealing at 61°C *Ctpp*, 53°C *Cre*, 56°C *Fgf21* KO 30 sec
 4. Elongation at 72°C for 1 min
 5. Final extension at 72°C for 10 min
- } 30x

PCR cycling conditions for *Fgf21* wildtype allele

1. Initial denaturation at 94°C for 2 min
 2. Denaturation at 94°C for 20 sec
 3. Annealing at 65°C for 15 sec
 4. Elongation at 68°C for 10 sec
 5. Denaturation at 94°C for 15 sec
 6. Annealing at 60°C for 15 sec
 7. Elongation at 72°C for 10 sec
 1. Final extension at 72°C for 2 min
- } 10x
- } 28x

In Step 3 the annealing temperature was decreased by 0.5°C per cycle.

2.4.6 Northern blot analysis for mitochondrial mRNA levels

RNA (2 µg) was mixed with RNA Sample Loading Buffer (Sigma-Aldrich) in a ratio of 1:3 and heated at 65°C for 10 min prior to running it on a 1.2% agarose-formaldehyde gel at 130V for 2.5 h. The gel was then washed three times with RNase free water and soaked in 20x SSC. Next, RNA was transferred by alkaline capillary transfer to Hybond N+ membrane (GE Healthcare) overnight. The membrane was then cross-linked at 80°C for 1.5 h.

Radioactive labeling with 50 µCi $\alpha^{32}\text{P}$ -dCTP of 70 ng mitochondrial probes or 18S nuclear probe was performed with the Random Primer DNA labeling kit (Invitrogen). The membrane was pre-hybridized with ravid-hyb buffer (GE healthcare) for 1 h at 65°C before adding the labeled probe to hybridize for 2 h. The membrane was then washed with increasingly stringent washing solution (2x SSC, 0.1% SDS, 1x SSC, 0.1% SDS, 0.5x SSC, 0.1% SDS) for 20 min each at 65°C. Radioactive signals were detected with Amersham Hyperfilms. Mitochondrial transcript levels were normalized to 18S rRNA levels.

2.4.7 Reverse transcription and quantitative real-time PCR

Total RNA was isolated from tissues as described previously. Next, RNA was subjected to DNase digestion by incubating 10 µg RNA in 1x DNase buffer and 2U DNaseI (NEB) at 37°C for 10 min. Followed by the addition of 10 mM EDTA and heat inactivation of the DNase at 75°C for 10 min. RNA (100 ng µL⁻¹ per sample) was

reverse transcribed using the High capacity reverse transcription kit (Applied Biosystems, Life Technologies). Resulting cDNA was amplified with Brilliant III Ultra-Fast SYBR QPCR Master Mix (Agilent Technologies, see Table 2.2) with the exception of *Atf5*, which was amplified using Taqman Assay-on-demand kit (Applied Biosystems, Life Technologies) (Table 2.3). Real-time PCR was performed on QuantStudio K Flex System (Applied Biosystems, Life Technologies). The target gene expression was adjusted for total mRNA content of hypoxanthine-guanine phosphoribosyltransferase 1 (*Hprt1*) or TATA box binding protein (*Tbp*). Calculations were performed using a comparative method ($2^{-\Delta\Delta CT}$).

Table 2.2 Primer used for quantitative real-time PCR

Gene	Forward Primer 5'-3'	Reverse Primer 5'-3'
<i>Acadvl</i>	CTACTGTGCTTCAGGGACAAC	CAAAGGACTTCGATTCTGCC
<i>Atf4</i>	GCAAGGAGGATGCCTTTTC	GTTTCCAGGTCATCCATTG
<i>Chop</i>	CTGGAAGCCTGGTATGAGGAT	CAGGGTCAAGAGTAGTGAAGGT
<i>Cidea</i>	TGACATTCATGGGATTGCAGAC	GGCCAGTTGTGATGACTAAGAC
<i>Cpt2</i>	CAGCACAGCATCGTACCCA	TCCCAATGCCGTTCTCAAAAT
<i>Dio2</i>	CAGCTTCCTCCTAGATGCCTA	CTGATTCAGGATTGGAGACGTG
<i>Hprt</i>	TCAGTCAACGGGGGACATAAA	GGGGCTGTACTGCTTAACCAG
<i>Igf1</i>	AAATCAGCAGCCTTCCAACCTC	GCACTTCCTCTACTTGTGTTCTT
<i>Fgf21</i>	GTGTCAAAGCCTCTAGGTTTCTT	GGTACACATTGTAACCGTCCTC
<i>Ndufa9</i>	GGCCAGCTTACCTTTCTGGAA	GCCCAATAAGATTGATGACCACG
<i>Ndufb6</i>	TGGAAGAACATGGTCTTTAAGGC	TTCGAGCTAACAATGGTGTATGG
<i>Ndufs2</i>	TCGTGCTGGAAGTGGTGGGA	GGCCTGTTTATTACACATCATGG
<i>Ndufs3</i>	CTGTGGCAGCACGTAAGAAG	GCTTGTGGGTCACATCACTCC
<i>Ndufv2</i>	GGCTACCTATCTCCGCTATGA	TCCCAACTGGCTTTTCGATTATAC
<i>Pgc1α</i>	TATGGAGTGACATAGAGTGTGCT	CCACTTCAATCCACCCAGAAAG
<i>Ppara</i>	AACATCGAGTGTGCAATATGTGG	CCGAATAGTTCGCCGAAAGAA
<i>Pparγ</i>	CCTGAAGCTCCAAGAATACCA	GCCTGATGCTTTATCCCCACA
<i>Sdha</i>	GAACACTCCAAAAACAGACCTGC	TCCACCACTGGGTATTGAGTAG
<i>Tbp</i>	GGGAGAATCATGGACCAGAA	TTGCTGCTGCTGTCTTTGTT
<i>Ucp1</i>	AGCCATCTGCATGGGATCAAA	GGGTCGTCCCTTTCCAAAGTG
<i>Uqcrc1</i>	AGACCCAGGTCAGCATCTTG	GCCGATTCTTTGTTCCCTTGA

Table 2.3 Taqman Probes used for quantitative real-time PCR

Probe	Catalog Number
<i>Atf5</i>	MM00459515_m1
<i>Hprt</i>	Mm00446968_m1

2.5 Biochemistry

2.5.1 Protein extraction from mouse tissues

For protein extraction, 30-50 mg tissue were disrupted in organ lysis buffer (50 mM HEPES, pH 7.4, 50 mM NaCl, 1% (v/v) Triton X-100, 0.1 M NaF, 10 mM EDTA, 0.1% (w/v) SDS, 10 mM Na-orthovanadat, 2 mM PMSF, 1x protease inhibitor cocktail (Sigma Aldrich) and if necessary 1x PhosSTOP phosphatase inhibitor (Roche)) by using a Precellys 24 fast-prep machine (Bertin) at 5500 rpm two times for 20 sec. Particulate matter was removed by centrifugation at 13.000 rpm for 45 min at 4°C. Afterwards, supernatants were transferred to fresh tubes and protein concentration was determined using Bradford reagent (Sigma Aldrich) according to the manufacturer's instructions. Protein extracts were either used directly or stored at -80°C until further use.

2.5.2 Isolation of mitochondria from liver and brown adipose tissue

Mice were sacrificed by cervical dislocation and tissues were dissected and rinsed with ice-cold mitochondria isolation buffer (MIB, 100 mM Sucrose, 50 mM KCl, 1 mM EDTA, 20 mM TES, 0.2% BSA fatty acid free, pH 7.2). Afterwards tissues were homogenized in 15 mL or 5 mL MIB for liver or brown adipose tissue (BAT), respectively with a Potter S homogenizer (Sartorius) at 1200 rpm with 10 strokes (liver) or 20 strokes (BAT). All subsequent procedures were carried out on ice or 4°C. Homogenates were transferred to 50 mL falcon tubes (liver) or 2 mL tubes (BAT) and centrifuged at 8400 g for 5 min. The supernatant with floating fat was discarded and the pellet containing mitochondria was resuspended in 30 mL (liver) or 1 mL (BAT) MIB. Next, cellular debris and cell nuclei were removed from homogenates by centrifugation at 800 g for 5 min. Then the supernatant comprising the mitochondria was transferred to a new 50 mL tube (liver) or 2 mL tube (BAT) and mitochondria were pelleted by centrifugation at 8200 g for 5 min. After the supernatant was discarded, the mitochondrial pellet was resuspended in 400 μ L (liver) or 50 μ L (BAT) MIB without BSA. Protein concentrations were determined by Bradford assay (Sigma Aldrich). Mitochondria were subsequently used for respiration analysis or snap frozen in liquid nitrogen.

2.5.3 Isolation of mitochondria from skeletal muscle

Mice were sacrificed by cervical dislocation and skeletal muscle (SkM) was dissected and placed in ice-cold PBS containing 10 mM EDTA. Following the removal of fat and ligaments, skeletal muscle tissues were cut into small pieces and incubated on ice for 30 min in PBS containing 10 mM EDTA and 0.05% trypsin. Next, the samples were centrifuged at 200 g for 2 min. The supernatant was discarded and the tissue pieces

were resuspended in 5 mL MIB1 (67 mM Sucrose, 50 mM Tris-HCl pH 7.4, 50 mM KCl, 10 mM EDTA pH 8.0, 0.02% BSA fatty acid free). After the homogenization using a Potter S homogenizer at 1200 rpm with 10 strokes, the homogenates were centrifuged at 700 g for 5 min at 4°C. The supernatant comprising the mitochondria was transferred to a new 50 mL tube and subsequently centrifuged at 8000 g for 5 min at 4°C to pellet mitochondria. The resulting cytosolic supernatant was discarded and the mitochondrial pellet was resuspended in MIB2 (250 mM Sucrose, 10 mM Tris-HCl pH 7.4, 0.3 mM EGTA-Tris). Proteins were quantified using Bradford reagent (Sigma Aldrich) according to manufacturer's instructions.

2.5.4 Blue native polyacrylamide gel electrophoresis

Blue native polyacrylamide gel electrophoresis (BN-PAGE) was conducted using the NativePAGE Novex Bis-Tris Gel System (Life Technologies) according to manufacturer's instructions. Briefly, 20-40 µg mitochondria were lysed with 4% digitonin for the analysis of mitochondrial supercomplexes or 1% DDM for the analysis of mitochondrial complexes. After incubation on ice for 15 min, mitochondrial debris were removed by centrifugation at 13.000 rpm for 30 min. The resulting supernatant was run on 4-16% Bis-Tris gradient gels. Proteins were then transferred onto PVDF membranes by wet transfer that was followed by immunodetection of mitochondrial complexes and supercomplexes.

2.5.5 SDS-PAGE and Western blot

For Western blot analysis, protein extracts were boiled for 5 min at 95°C in SDS-PAGE loading buffer (50 mM Tris-HCl, pH 6.8, 2% SDS, 10% Glycerol, 1% β-mercaptoethanol, 12.5 mM EDTA, 0.02% Bromophenol Blue). Proteins were resolved on 8-13% SDS polyacrylamide gels (Laemmli, 1970) together with protein marker (PageRuler™ Prestained Protein Ladder) and transferred to nitrocellulose membranes using wet transfer system (Bio-Rad). Membranes were then incubated for 1 h at RT in 5% nonfat dried milk in PBS-T or 5% BSA in TBS-T according to the antibodies used. Subsequently, membranes were incubated with primary antibodies (Table 2.4) for 2 h at RT or overnight at 4°C. After washing the membrane three times in PBS-T or TBS-T for 5 min each, membranes were incubated for 1 h at RT with the respective secondary antibody (diluted 1:2000, Sigma Aldrich). Again membranes were washed three times in PBS-T or TBS-T and signals were visualized using ECL solution (GE Healthcare) and exposition to X-ray films (Fujifilms). Films were developed in an automatic developer (Kodak). Western blots were quantified relative to levels of loading control proteins using the ImageJ software as intensity per mm².

Table 2.4 Primary antibodies used for Western blot analysis

Antigen	Cat. No.	Company	Dilution
ACADS	sc-365953	Santa Cruz	1:2000
ACADVL	sc-98338	Santa Cruz	1:2000
ACTIN	A5441	Sigma Aldrich	1:5000
AFG3L2	-	Polyclonal antisera made by Prof. Dr. Elena I. Rugarli	1:1000
AKT	9272	Cell Signaling	1:2000
AMPK	2532	Cell Signaling	1:1000
ATP5A1	MS507	Mitosciences	1:1000
CLPP	WH0008192-M1	Sigma Aldrich	1:1000
CLPX	HPA040262	Sigma Aldrich	1:1000
COX1	459600	Invitrogen	1:2000
COX4I1	A21348	Invitrogen	1:2000
CPT1	sc-31128	Santa Cruz	1:1000
CPT1M	CPT1M11-A	Alpha Diagnostic	1:1000
CPT2	ab181114	Abcam	1:1000
EFTU	-	Polyclonal antisera made by Prof. Dr. Nono Tomita-Takeuchi	1:1000
ERAL1	18881	IBL	1:1000
GFM1	ab6107496	Abcam	1:1000
GLUT1	sc-7903	Santa Cruz	1:300
GLUT4	07-1404	Millipore	1:1000
HADHA	ab54477	Abcam	1:1000
HSC70	sc-7298	Santa Cruz	1:5000
HSP60	611562	BD	1:10000
MTIF2	-	Polyclonal antisera made by Prof. Dr. Aleksandra Filipovska	1:1000
MTIF3	-	Polyclonal antisera made by Prof. Dr. Aleksandra Filipovska	1:1000
LONP1	ab103809	Abcam	1:400
MCAD	sc-49047	Santa Cruz	1:2000
MFN1	LSC154487	LSBio	1:1000
MFN2	ab50838	Abcam	1:1000
MnSOD	06-984	Millipore	1:500
MRPL37	HPA025826	Sigma	1:1000
MRPS18B	16139-1-AP	Proteintech	1:1000
MRPS35	16457-1-AP	Proteintech	1:1000
mtHSP70	ab82591	Abcam	1:1000
NDUFA9	459100	Invitrogen	1:5000
NDUFB6	A21359	Invitrogen	1:5000
NDUFS2	ab96160	Abcam	1:2000
NDUFS3	MS112	Mitosciences	1:1000
NDUFV2	15301-1-AP	Proteintech	1:2000
OPA1	BD612606	BD	1:500
pAKT (Ser473)	4060	Cell Signaling	1:1000
pAMPK (Thr172)	2535	Cell Signaling	1:1000

Antigen	Cat. No.	Company	Dilution
PGC-1 α	sc-13067	Santa Cruz	1:1000
SDHA	459200	Invitrogen	1:10000
TFAM	-	Polyclonal antisera made by Prof. Dr. Nils-Göran Larsson	1:1000
TOMM20	sc-11415	Santa Cruz Biotechnology	1:1000
UCP1	-	Polyclonal antisera made by Prof. Dr. Nils-Göran Larsson	1:1000
UQCRC1	459140	Invitrogen	1:5000
UQCRFS1	MS305	Mitosciences	1:1000
VDAC	4661	Cell Signaling	1:1000

2.5.6 Mitochondrial respiration

Oxygen consumption of isolated liver mitochondria was assessed with high-resolution respirometry (Oxygraph-2k, OROBOROS Instruments). Two different substrate uncoupler inhibitor titration (SUIT) protocols were applied. After air equilibration of the mitochondrial respiration buffer (120 mM Sucrose, 50 mM KCl, 20 mM Tris-HCl, 1 mM EGTA, 4 mM potassium dihydrogen phosphate, 2 mM magnesium chloride, 0.1% BSA) 200 μ g liver mitochondria were added. For the carbohydrate SUIT protocol, first the OXPHOS state for complex I was determined by adding 5 mM pyruvate, 2 mM malate, 20 mM glutamate and 2 mM ADP. The convergent electron flow through complex I and II was measured by adding 10 mM succinate. Next, LEAK respiration was assessed by the inhibition of the ATP synthase with oligomycin (1.5 μ g/mL). Titration of carbonylcyanide p-trifluoromethoxyphenylhydrazone (FCCP, 0.5 μ M) was performed to determine the maximal electron transfer system (ETS) capacity. Subsequently, complex I was inhibited by 0.5 μ L Rotenone to determine the maximal ETS capacity with electron flow through complex II only. Finally, residual oxygen consumption (ROX) was measured upon inhibition of complex III by 2.5 μ M Antimycin A.

For the fatty acid SUIT protocol, respiration was measured with 50 μ M palmitoylcarnitine, 5 mM malate and 2 mM ADP (OXPHOS state), proceeding with the addition of atractyloside (LEAK state) to inhibit the ATP synthase. Next, respiration was uncoupled by titrations of FCCP to determine maximal ETS capacity.

2.5.7 Palmitate oxidation rate *ex vivo*

Fatty acid β -oxidation in isolated mitochondria was performed as described previously (Huynh et al., 2014). Briefly, crude mitochondria were isolated from 200 μ g liver, 100 μ g SkM and 80 μ g BAT in STE buffer (0.25 M sucrose, 10 mM Tris-HCl pH 7.4, 1 mM EDTA). Isolated mitochondria were then incubated in oxidation reaction mixture containing 0.4 μ Ci BSA conjugated [1 - 14 C]-palmitate for 1 h at 37°C. After the

incubation, the reaction mixture is transferred to a tube with 200 μL of 1 M perchloric acid and piece of Whatman paper disc in the cap soaked with 20 μL 1 M NaOH. After 1 h incubation at RT the paper disc was transferred to a scintillation vial for the determination of $^{14}\text{CO}_2$. The acid solution was centrifuged and the supernatant afterwards transferred to a scintillation vial for the measurement of the acid soluble metabolites using a liquid scintillation counter (Beckmann Coulter).

2.5.8 Sucrose gradient fractionation of mitochondrial ribosomes

The analysis of mitoribosomes via sucrose gradient fractionation was performed as described elsewhere (Szczepanowska et al., 2016).

2.5.9 *In organello* translation

For the analysis of *de novo* mitochondrial translation, 2 mg of isolated mitochondria were incubated in 'hot' translation buffer (100 mM mannitol, 10 mM sodium succinate, 80 mM KCl, 5 mM MgCl_2 , 1 mM KPi, 25 mM HEPES, pH 7.4 supplemented with ^{35}S -methionine, all other amino acids (60 $\mu\text{g}/\text{mL}$), 5 mM ATP, 20 μM GTP, 6 mM creatine phosphate and 60 $\mu\text{g}/\text{mL}$ creatine kinase) at 37°C with constant rotation (pulse). Following the 1 h incubation, half of the mitochondria were lysed in SDS-PAGE loading buffer, while the other half was washed and incubated for additional 3 h in 'cold' translation buffer containing non-radioactive methionine (chase). Afterwards mitochondria were also lysed and both pulse and chase labeled fractions were separated by SDS-PAGE. Subsequently, gels were stained with Coomassie staining solution, dried at 80°C for 2 h and newly synthesized proteins were detected by autoradiography.

2.6 Histological analysis

2.6.1 Embedding of tissues in paraffin

After dissection tissues were placed in tissue cassettes (Roth) and immersed in 5% (w/v) paraformaldehyde overnight at 4°C for fixation. Next day tissues were dehydrated by passing them through increasing concentrations of ethanol for 2 h each (30% (v/v), 50% (v/v), 70% (v/v), 96% (v/v) and two times in 100% (v/v) ethanol). Afterwards they were incubated in xylol for two times 2 h and then transferred to paraffin, for the embedding in paraffin blocks. The fixed tissues (liver, SkM, BAT, EWAT and IWAT) were sectioned with a microtome (Leica) at 5 μm thickness and transferred onto poly-L-lysine glass slides (VWR).

2.6.2 Cryostat sections

For cryostat sections, liver tissues were embedded in Tissue-Tek (Sakura) and tissue trays were placed on dry ice until the complete hardening of the Tissue-Tek. The embedded tissues were then stored at -80°C. Using a Cryostat (Leica) liver or BAT tissue was sectioned at a thickness of 7 µm (COX SDH staining) or 12 µm (Oil red O staining) and transferred onto poly-L-lysine glass slides. For short term storage, slides were kept at -20°C until use.

2.6.3 Hematoxylin and Eosin staining

Deparaffinized (20 min xylol) and rehydrated tissue sections (2 min each in 100% (v/v) EtOH, 96% (v/v) EtOH, 75% (v/v) EtOH and 1 min tap water) were stained with Mayer's Hematoxylin for 4 min and blued in tepid tap water for 1 min. Afterwards sections were washed for 15 min in tap water and shortly rinsed with ddH₂O. For counterstaining, the samples were stained with Eosin for 1 min and then washed with tap water six times. Next, the sections were dehydrated for 1 min each in 75% (v/v), 95% (v/v) and 100% (v/v) EtOH and cleared with xylol. Coverslips were mounted using Entellan.

2.6.4 Periodic acid Schiff's reaction

Deparaffinization and rehydration of tissue slides was done as described above. Next, slides were incubated in periodic acid for 5 min and washed with ddH₂O two times for 5 min. The staining time with Schiff's reagent is tissue dependent and accounted for liver 1:20 min and for SkM 10 min. After washing the slides under running tap water for 10 min, sections were dehydrated for 1 min each in 75% (v/v), 95% (v/v) and 100% (v/v) EtOH and cleared with xylol. Finally, they were mounted with Entellan.

2.6.5 Oil red O staining

Oil red O (ORO) staining was performed on cryosections. The sections were air dried for 10 min and surrounded with a PAP pen (Sigma-Aldrich). Subsequently, sections were covered with ORO solution for 5 min and counterstained with Mayer's Hematoxylin for 30 sec. The slides were then rinsed under running tap water before they were mounted with FluorSave Reagent (Calbiochem).

2.6.6 COX-SDH staining

Enzyme histochemical staining for COX-SDH was performed on cryosections, after drying them for 10 min at RT. Next sections were surrounded with a PAP pen and incubated in COX solution (0.8 ml 3,3 diaminobenzidine tetrahydrochloride, 0.2 ml 500 µM cytochrome c, a few grains of catalase) at 37 °C for 40 min in a humidified

chamber to prevent drying of the sections. After a washing step in PBS, the sections were incubated in SDH solution 0.8 ml 1.875 mM nitroblue tetrazolium, 0.1 ml 1.3 M sodium succinate, 0.1 ml 2 mM phenazine methosulphate, 0.01 ml 100 mM sodium azide) for 60 min at 37 °C. Subsequently slides were washed in PBS and dehydrated for 1 min each in 75% (v/v), 95% (v/v) and 100% (v/v) EtOH before mounting the slides with Entellan.

2.6.7 Transmission electron microscopy

For ultrastructural analysis, very thin liver tissue slices were fixed for 24 h in 2% paraformaldehyde and 2% glutaraldehyde in 0.1 M cacodylat buffer. Tissues were then embedded in epoxy resin and ultrathin sections (70 nm) were cut and transferred to 100 mesh copper grids. Next, sections were stained with 1.5% uranyl acetate solution and lead nitrate. Electron micrographs were taken with the Zeiss 109. All consecutive steps after tissue fixation were performed by Beatrix Martiny (CECAD imaging facility).

2.7 Cell Culture

Mouse embryonic fibroblasts (MEFs) were cultured in Dulbecco's modified Eagle's medium (DMEM) (4.5 g L⁻¹ glucose, with L-Glutamine and sodium pyruvate; Gibco, Thermo Fisher Scientific) supplemented with 10% FBS (Biochrom AG) and 100 units ml⁻¹ penicillin and 100 µg of Streptomycin.

For protein extraction cells were trypsinized and the cell pellet was subsequently lysed in RIPA buffer containing 50 mM Tris-HCl pH 7.4, 150 mM NaCl, 0.5% Na-deoxycholate, 0.1% SDS, 2 mM EDTA, 10 mM NaF and 1x protease inhibitor cocktail (Sigma Aldrich). Following 30 min incubation on ice, suspensions were sonified in a water bath for 3 min. Afterwards cell lysates were centrifuged at full speed for 20 min to remove cellular debris. The cleared lysates were then directly used or kept at -80°C for later use.

2.8 Label-free quantification of the liver proteome

2.8.1 In-solution digest

Liver tissue was disrupted in Urea buffer (8 M Urea, 50 mM Triethylammonium-bicarbonate, 1x protease inhibitor cocktail) using a Precellys 24 fast-prep machine (Bertin) at 5500 rpm two times for 20 sec. Cell debris were then removed by centrifugation at 20.000 g for 15 min. Thereafter, proteins were reduced by incubation with 5 mM dithiothreitol at 37°C for 1 h and thiols were carboxymethylated with 10 mM iodoacetamide for 30 min. This step was followed by the protein digestion with endoproteinase Lys-C at 37°C for 4h and trypsin at 37°C overnight. Next day, the

digestion was terminated by acidification of the solution with formic acid (final concentration 1%). Purification of peptides was achieved using the StageTip technique before LC-MS/MS analysis was conducted (Rappsilber et al., 2002)

2.8.2 Liquid chromatography and mass spectrometry

The liquid chromatography and mass spectrometry (LC-MS/MS) device was made up of an EASY n-LC1000 (Thermo Scientific) linked via a nano-electrospray ionization source (Thermo Scientific) to an ion-trap based bench top Q-Executive Plus (Thermo Scientific). The experiment and data analysis was performed by the CECAD proteomics facility.

2.9 Computer analyses

2.9.1 Software

Statistical analysis was conducted using Microsoft Excel and Graphpad Prism 6 (Graphpad Software). Figures and Illustrations were prepared with Adobe Illustrator CS4 (Adobe Systems).

2.9.2 Statistical analyses

Data sets with two independent groups were analyzed for statistical significance using two-tailed unpaired Student's t-test. With one exception, respirometry data were analyzed using two-tailed paired Student's t-test. Data sets with more than two groups were analyzed using one way analysis of variance (ANOVA) followed by Tukey's post hoc test. All p-values below 0.05 were considered statistically significant; *p <0.05, ** p< 0.01, ***p< 0.001. All data are presented as mean ± SD.

2.10 Chemicals

Table 2.5 Chemicals

Name	Supplier
[1- ¹⁴ C]-palmitic acid	Hartmann Analytic
³² P-dCTP	Hartmann Analytic
³⁵ S-methionine	Hartmann Analytic
β-mercaptoethanol	Sigma Aldrich
Acetic acid	AppliChem
Catalase, bovine liver	Sigma Aldrich
Acetonitrile	Sigma Aldrich
Acryamide-Bisacrylamide 40	Carl Roth
Adenosine 5'-diphosphate sodium salt	Sigma Aldrich

Name	Supplier
Adenosine 5'-triphosphate disodium salt (ATP)	Sigma Aldrich
Agarose LE	Ambion
Albumin from bovine serum fatty acid free (BSA)	Sigma Aldrich
Ammonium bicarbonate	Sigma Aldrich
Ammonium persulfate (APS)	Sigma Aldrich
Antimycin A	Sigma Aldrich
Boric Acid	Sigma Aldrich
Bromophenol blue	Merck
carbonylcyanide p-trifluoromethoxyphenylhydrazone (FCCP)	Sigma Aldrich
Creatine Phosphokinase Type III, bovine	Sigma Aldrich
Chloramphenicol	Sigma Aldrich
Coenzyme A	Sigma Aldrich
Coomassie Brilliant Blue R-250	Merck
Cytochrome C, bovine heart	Sigma Aldrich
Diaminobenzidine tetrahydrochloride (DAB)	Sigma Aldrich
Diethyl Malate	Sigma Aldrich
Dimethylsulfoxide (DMSO)	Sigma Aldrich
Disodium phosphate (Na ₂ HPO ₄)	Sigma Aldrich
Dithiothreitol (DTT)	Sigma Aldrich
Doxycycline monohydrate	Sigma Aldrich
Ethanol	AppliChem
Ethylenediaminetetraacetic acid (EDTA)	Sigma Aldrich
Ethylene glycol-bis(β-aminoethyl ether)- N,N,N',N'-tetraacetic acid (EGTA)	Sigma Aldrich
Glucose	Merck
Glycerol	Sigma Aldrich
Glycine	AppliChem
Guanosine 5'triphosphate sodium salt hydra	Sigma Aldrich
HEPES	AppliChem
Hydrochloric acid (HCl)	VWR
Isopropanol	AppliChem
L-Carnitine	Sigma Aldrich
L-Glutamic Acid	Sigma Aldrich
Magnesium chloride hexahydrate	Sigma Aldrich
Magnesium sulfate (MgSO ₄)	Merck
Mannitol	AppliChem
Methanol	AppliChem
Milk powder	AppliChem
Monopotassium phosphate (KH ₂ PO ₄)	Sigma Aldrich
Nicotinamide adenine dinucleotide reduced sodium salt (NADH)	Sigma Aldrich

Name	Supplier
Nitrotetrazolium blue (NTB)	Sigma Aldrich
Oligomycin	Sigma Aldrich
Paraformaldehyde	Sigma Aldrich
Phenazine methosulphate (PMS)	Sigma Aldrich
Perchloric acid	Sigma Aldrich
Periodic acid	Sigma Aldrich
Phosphocreatine disodium salt hydrate enzymatic	Sigma Aldrich
Polyethylenglycol	Sigma Aldrich
PonceauS	Sigma Aldrich
Potassium chloride (KCl)	AppliChem
Potassium hydroxide (KOH)	AppliChem
Rotenone	Sigma Aldrich
Sodium azide	Sigma Aldrich
Sodium chloride (NaCl)	Sigma Aldrich
Sodium deoxycholate	Sigma Aldrich
Sodium dodecyl sulfate (SDS)	AppliChem
Sodium fluoride (NaF)	AppliChem
Sodium hydroxide (NaOH)	Sigma Aldrich
Sodium orthovanadat	AppliChem
Sodium pyruvate	Sigma Aldrich
Sodium succinate dibasic hexahydrate	Sigma Aldrich
Sucrose	Sigma Aldrich
Tetramethylethylenediamine (TEMED)	Sigma Aldrich
Tris	Sigma Aldrich
Triton X-100	Sigma Aldrich
Trizma Base	Sigma Aldrich
Tween-20	VWR

3 Results

3.1 Phenotypic analysis of whole body CLPP deficient mice

3.1.1 Loss of CLPP does not affect lifespan

To unravel the *in vivo* function of mitochondrial CLPP and elucidate the consequences of CLPP deficiency on whole body metabolism, CLPP was ubiquitously deleted using a β -actin promoter driven Cre recombinase. Deletion of the loxP flanked exon 3 to 5 results in the loss of the protease domain as well as a frame shift from exon 2 to 6, causing a premature translational stop signal (Szczepanowska et al., 2016). The remaining *Clpp* mRNA is likely to be degraded via nonsense-mediated decay mechanisms. To verify the loss of CLPP, Western blot analysis was performed in liver, skeletal muscle (quadriceps, SkM), brown adipose tissue (BAT), epididymal white adipose tissue (EWAT) and inguinal white adipose tissue (IWAT). CLPP protein was completely absent in all analyzed tissues, thus confirming efficient targeting of the *Clpp* gene (Figure 3.1). To decipher the metabolic phenotype of *Clpp*^{-/-} mice all experiments were performed with male mice at the age of 15 weeks unless otherwise indicated.

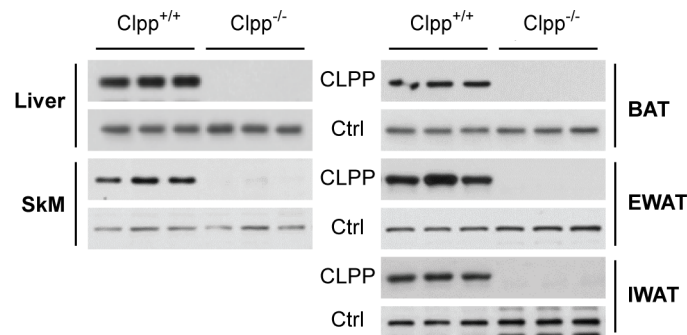


Figure 3.1 Validation of ubiquitous CLPP deletion.

Western blot analysis of CLPP levels in liver, skeletal muscle, heart, brown adipose tissue, epididymal white adipose tissue and inguinal white adipose tissue in control (Clpp^{+/+}) and CLPP deficient mice (Clpp^{-/-}). CALNEXIN, SDHA or VDAC serve as loading control (Ctrl).

Interestingly, CLPP deficiency did not result in embryonic lethality as it was observed for other mitochondrial proteases, such as LONP1, YME1L (Quirós et al., 2014; Wai et al., 2015). However, CLPP deficient mice (Clpp^{-/-}) were not born in Mendelian ratios. Only about 60% of Clpp^{-/-} mice were born, whereas the other genotypes (Clpp^{+/+}, Clpp^{+/-}) were recovered at the expected Mendelian ratios (Szczepanowska et al., 2016). Although CLPP seems to be essential during embryonic development under certain conditions, the lack of CLPP does not have an impact on the postnatal lifespan. No significant differences were observed for the median and maximal survival for both males and females (Figure 3.2 A, B).

To determine the effect of CLPP deficiency on body weight, control and Clpp^{-/-} mice fed normal chow diet (NCD) were monitored upon weaning for a period of 12 weeks. Already at three weeks of age CLPP deficient animals displayed a reduced body weight as compared to control mice. The weight reduction of approximately 25-30% persisted throughout the analyzed time period in both genders (Figure 3.2 C, D). Whether CLPP deficient mice are already born with a reduced body weight or if they develop differently upon birth, still needs to be investigated.

Furthermore, body composition was analyzed using magnetic resonance imaging. The fat mass of Clpp^{-/-} mice was significantly reduced by 51% and 53% in males and females as compared to control (Figure 3.2 E). Although the lean mass was also reduced in these animals, it was affected to a lesser extent than the fat mass, i.e. 33% and 25% in males and females, respectively (Figure 3.2 F). Thus, it can be concluded that the body weight of CLPP deficient mice is mainly reduced due to decreased fat mass.

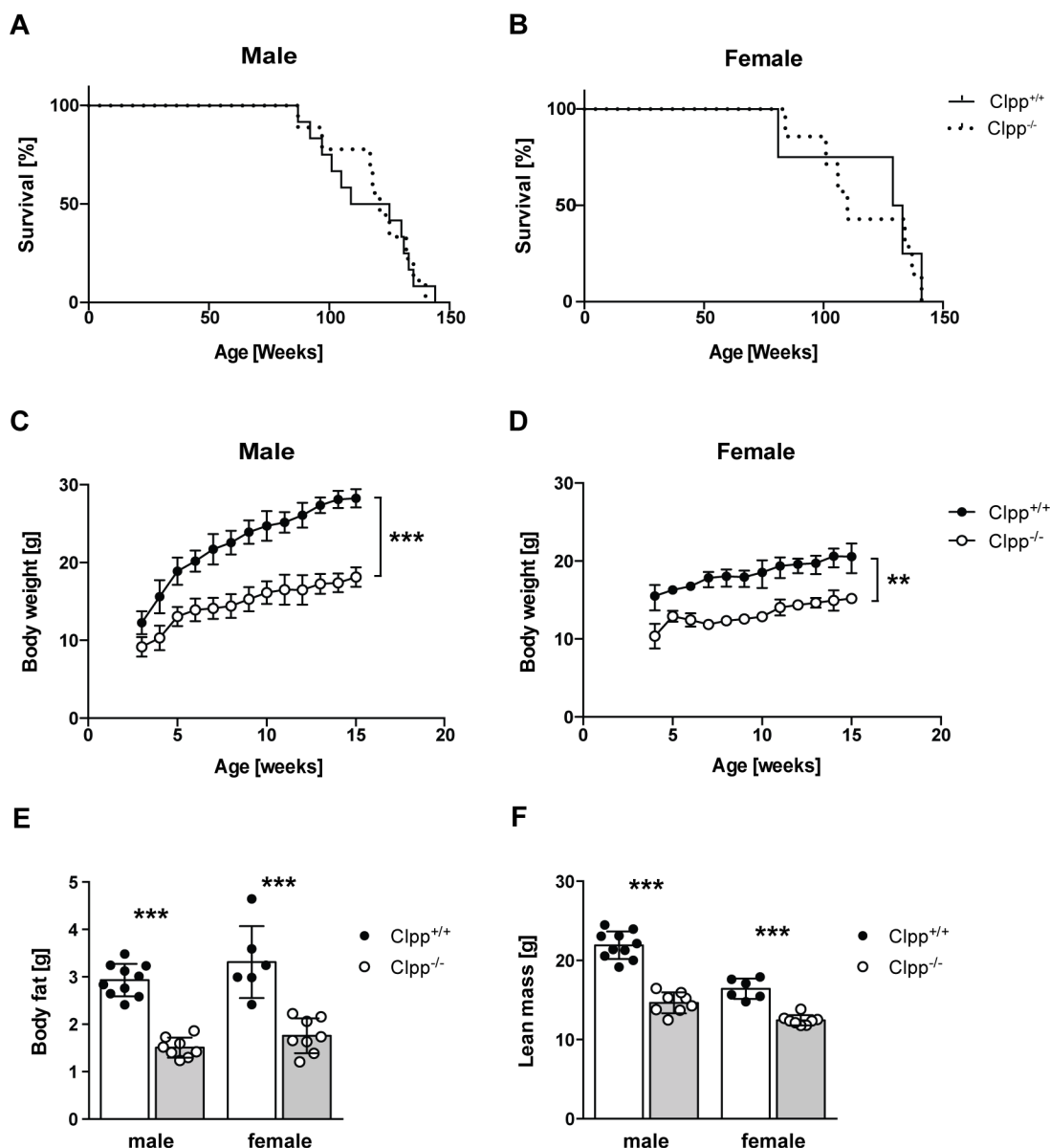


Figure 3.2 Phenotypic characterization of *Clpp*^{-/-} mice.

(A) Kaplan-Meier survival curves for male *Clpp*^{-/-} mice (n=14) and control mice (n=9). (B) Lifespan analysis of female *Clpp*^{-/-} mice (n=4) and control mice (n=7). (C) Body weight of male *Clpp*^{-/-} mice (n=10) and control mice (n=9) was monitored till 15 weeks of age on normal chow diet (NCD). (D) Body weight of female *Clpp*^{-/-} mice (n=8) and control mice (n=9) was monitored till 15 weeks of age on normal chow diet (NCD). (E) Body fat mass of *Clpp*^{-/-} mice and control mice fed NCD determined by NMR at 15 weeks of age (male n=8 and female n=7). (F) Lean body mass of *Clpp*^{-/-} mice and control mice fed NCD determined by NMR at 15 weeks of age (male n=8 and female n=7). Data are presented as mean \pm SD (*P<0.05, **P<0.01, ***P<0.001; unpaired two-tailed t-test).

As well as a significant reduction in body weight, also reduced body length was observed for *Clpp*^{-/-} mice (Figure 3.3 A). The overall decrease in body length correlated with a decrease of femur length in these mice at 15 weeks of age (Figure 3.3 B). Moreover, the bone morphology was altered due to the lack of CLPP. Micro computed tomography (microCT) analysis revealed a significant decrease of total bone mineral density (BMD) by 8% in males and 14% in females (Figure 3.3 C).

To determine whether alterations in the growth hormone (GH)/ insulin like growth factor 1 (IGF1) axis are contributing to the growth defect in *Clpp*^{-/-} mice, *Igf1* transcript levels were analyzed in liver of 5- and 15-week-old mice. The liver is the main source of circulating IGF1, which is acting as an endocrine hormone and promoting the linear growth effect of pituitary GH (Laron, 2001; Yakar et al., 2002). However, no change in *Igf1* transcript levels was observed in *Clpp*^{-/-} mice at 5 and 15 weeks of age (Figure 3.3 D). One reason for this unexpected result could be the selected time points, since the growth defect is already present at an earlier age or the experimental assessment.

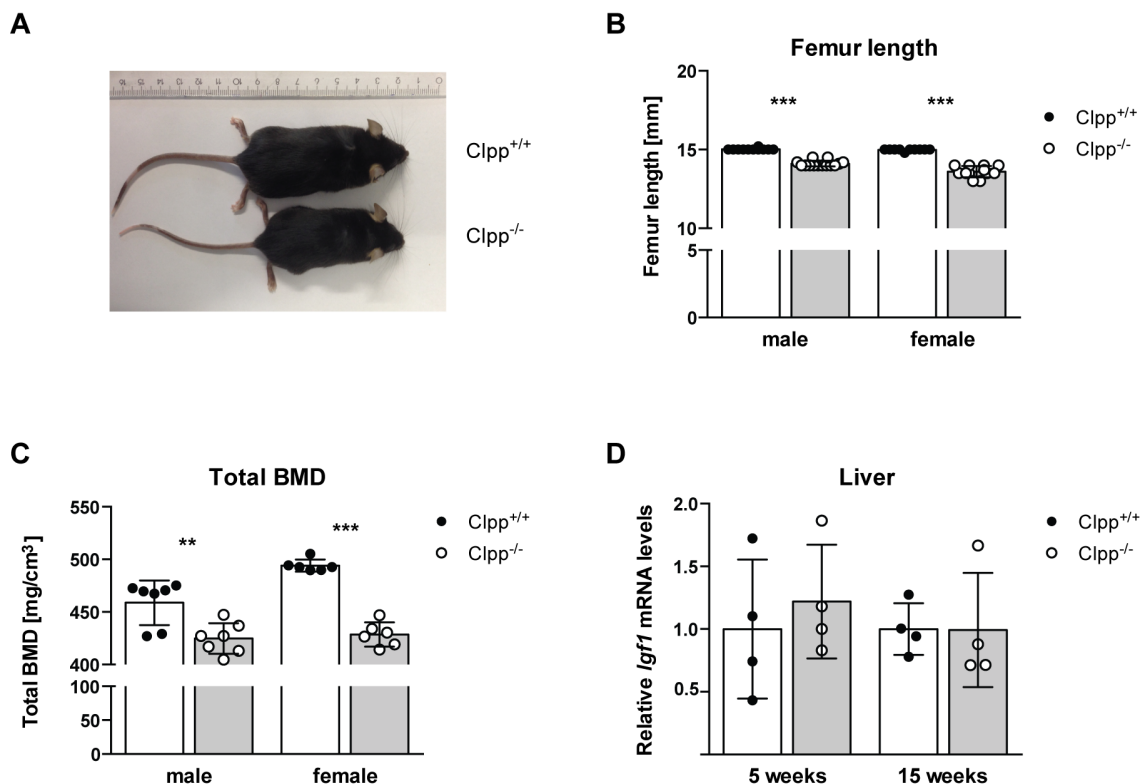


Figure 3.3 *Clpp*^{-/-} mice exhibit growth defect.

(A) Representative image of male control and *Clpp*^{-/-} mouse revealing the difference in body size. (B) Femur length of *Clpp*^{-/-} mice and control mice measured between femur head and lateral condyle (male n=6-7, female n=6). (C) Total bone marrow density of control and CLPP deficient animals (n=6-7). (D) *Igf1* transcript levels in liver of *Clpp*^{-/-} mice and control mice at 5 and 15 weeks (n=4). Data are presented as mean \pm SD (* P <0.05, ** P <0.01, *** P <0.001; unpaired two-tailed t-test).

3.1.2 *Clpp*^{-/-} mice have increased energy expenditure and improved glucose homeostasis despite lower locomotor activity

To further investigate the energy homeostasis of *Clpp*^{-/-} mice, indirect calorimetry was performed in metabolic cages. The results of all parameters represent mean values obtained during the light (6:00 am to 6:00 pm) and the dark phase (6:00 pm to 6:00 am) and clearly show the diurnal rhythm in all groups. The highest values were obtained in the dark phase, corresponding to the period with the major activity of the

animals. No significant difference in food and water intake was observed between control mice and $Clpp^{-/-}$ mice (Figure 3.4 A, B), ruling out decreased caloric intake as reason for the lean phenotype of $Clpp^{-/-}$ mice. The respiratory exchange ratio (RER) is the ratio of CO_2 produced / O_2 consumed and indicates the primary type of fuel utilization. An RER of 1.0 indicates use of carbohydrates and a value of 0.7 is indicative for fat as primary fuel source. No significant difference in the RER during the light and the dark phase was observed between control and $Clpp^{-/-}$ mice (Figure 3.4 C), indicating no major alteration in metabolic fuel preference. However, consistent with the lean phenotype, energy expenditure in the dark phase, normalized for the lean body weight, was increased in $Clpp^{-/-}$ mice (Figure 3.4 D).

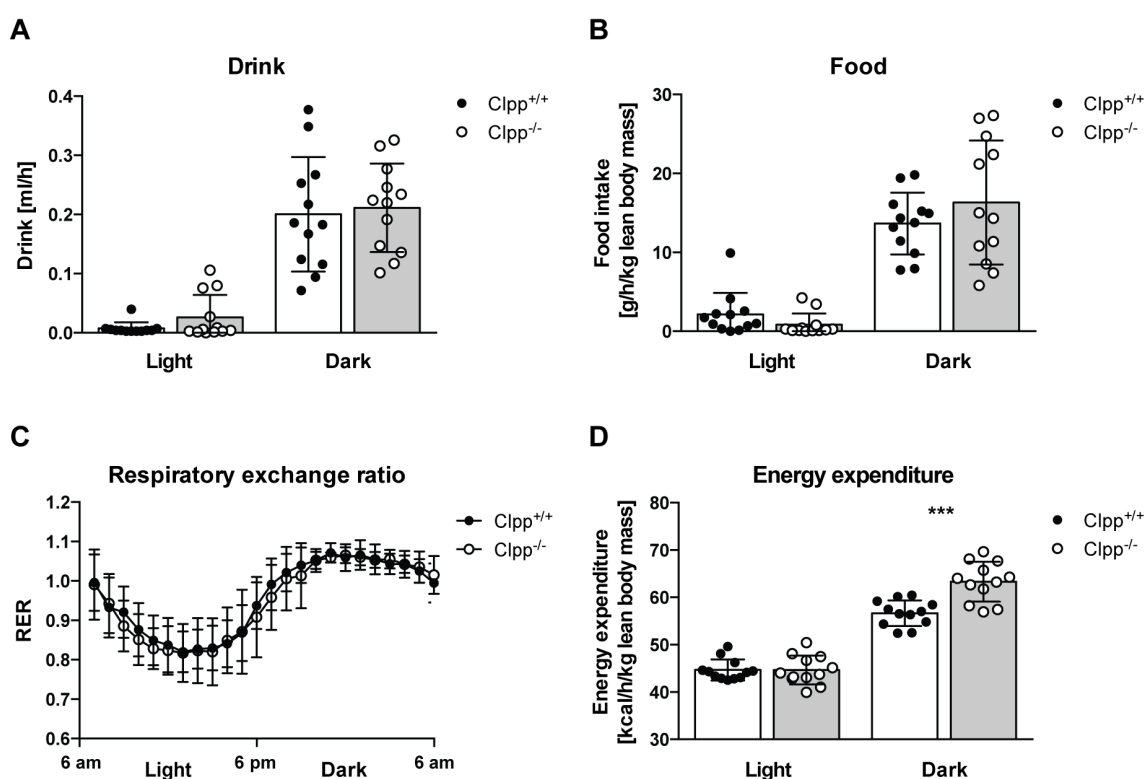


Figure 3.4 Loss of CLPP increases energy expenditure.

(A) Water intake of male $Clpp^{-/-}$ mice and control mice during the light and dark phase (n=7). (B) Food intake normalized to lean body mass of control and $Clpp^{-/-}$ mice during the dark and light phase (n=7). (C) Respiratory exchange ratio over period of 24 h of control and $Clpp^{-/-}$ mice (n=7). (D) Energy expenditure corrected for lean body mass of control and $Clpp^{-/-}$ mice during the dark and light phase (n=7). Data are presented as mean \pm SD (* P <0.05, ** P <0.01, *** P <0.001; unpaired two-tailed t-test). Phenomaster experiments were performed by Steffen Hermans.

To investigate whether increased physical activity contributes to the increased energy expenditure in CLPP deficient mice, locomotor activity was monitored. Surprisingly, $Clpp^{-/-}$ mice displayed decreased locomotor and rearing activity as compared to controls primarily during the dark phase (Figure 3.5 A, B). Hence, physical activity is not enhanced and thus is not contributing to the increased energy expenditure in CLPP

deficient mice.

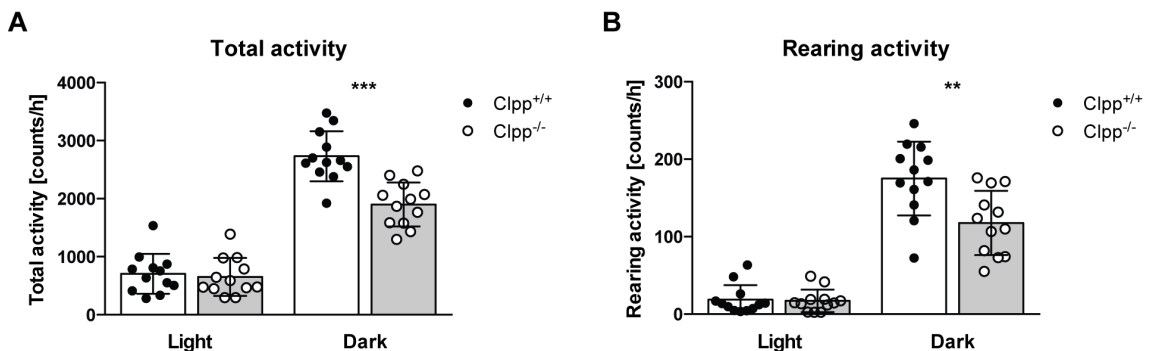


Figure 3.5 Reduced locomotor and rearing activities in Clpp^{-/-} mice.

(A) Average activity of Clpp^{-/-} and control mice per hour during light and dark phase (n=7). (B) Rearing activity of Clpp^{-/-} and control mice per hour during light and dark phase (n=7). Data are presented as mean ± SD (*P<0.05, **P<0.01, ***P<0.001; unpaired two-tailed t-test).

Since Clpp^{-/-} mice exhibit increased energy expenditure during the dark (active) phase, when mainly carbohydrates are metabolized, their glucose metabolism was further examined. When subjected to insulin tolerance tests, Clpp^{-/-} mice displayed an increased insulin sensitivity as compared to control mice (Figure 3.6 A). Notably, the insulin concentration had to be reduced to 0.6 U kg⁻¹ body weight (standard 0.75 U kg⁻¹ BW) due to the hyper responsiveness of CLPP deficient mice. Clpp^{-/-} mice further exhibited an improved glucose tolerance (Figure 3.6 B). Hence, both the ability of insulin to decrease blood glucose levels and the insulin mediated counter response to elevated glucose levels are enhanced in CLPP deficient mice. To further elucidate the reason for the enhanced glucose metabolism in Clpp^{-/-} mice, expression levels of the insulin dependent glucose transporter 4 (GLUT4) were determined in insulin target tissues. GLUT4 was strongly increased in SkM and EWAT of Clpp^{-/-} mice as compared to control mice, whereas no change in was observed in BAT (Figure 3.6 C, D). In contrast, the abundance of the insulin independent glucose transporter 1 (GLUT1) was not changed in liver and SkM tissue (Figure 3.6 E, F). Taken together, CLPP deficient mice display an enhanced glucose homeostasis facilitated by increased peripheral glucose uptake.

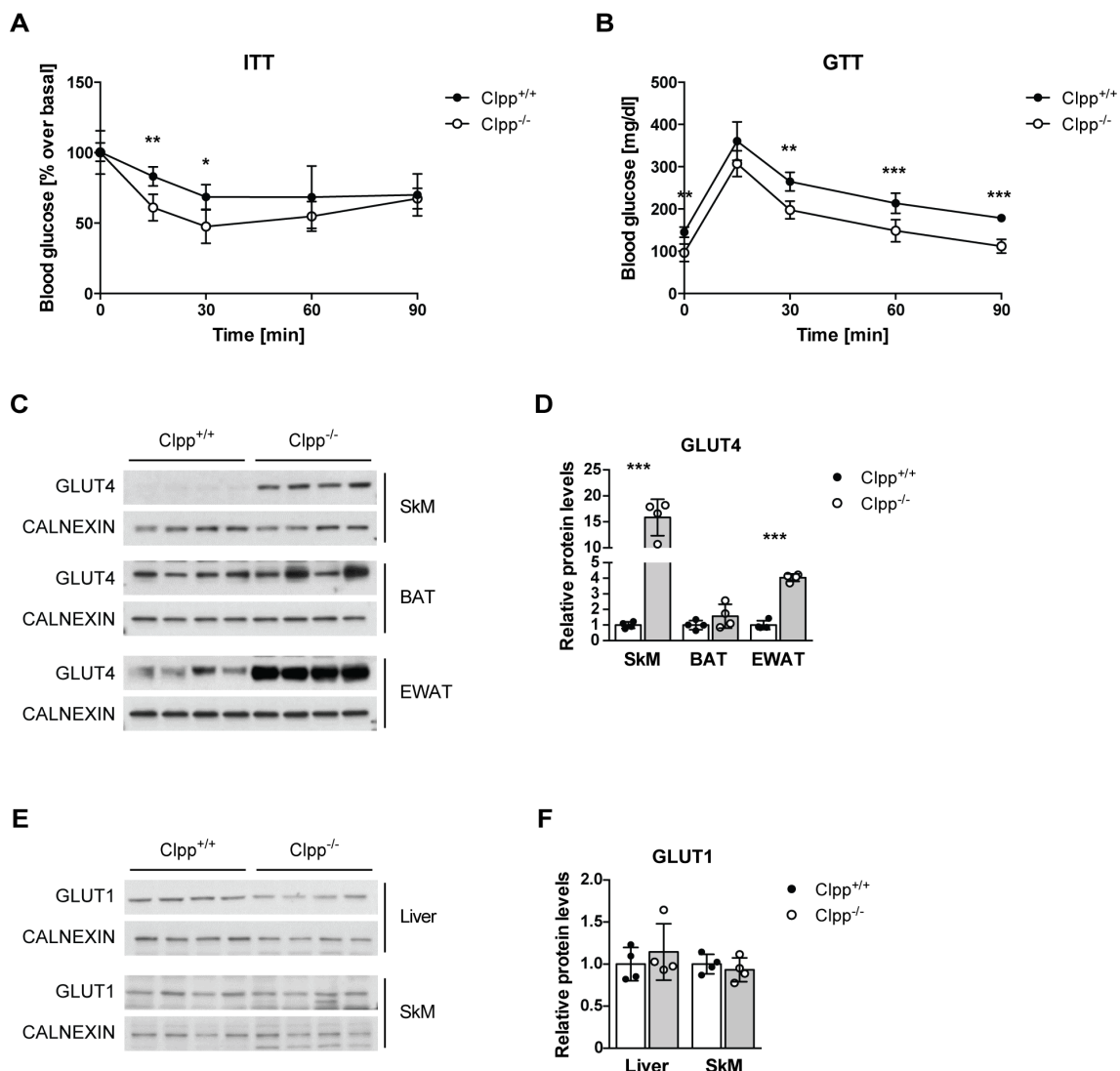


Figure 3.6 Improved glucose homeostasis in Clpp^{-/-} mice due to increased peripheral glucose uptake.

(A) Insulin tolerance test was performed on male control and Clpp^{-/-} mice fed NCD (n=10). (B) Glucose tolerance test was performed after 6 h fast on male control and Clpp^{-/-} mice fed NCD (n=10). (C) Western blot analyses for GLUT4 in CLPP deficient and control SkM, BAT and EWAT tissue lysates (n=4). CALNEXIN serves as loading control. (D) Quantification of GLUT4 Western blot analysis. (E) Western blot analysis for GLUT1 in CLPP deficient and control liver and SkM tissue lysates. CALNEXIN serves as loading control (n=4). (F) Quantification of GLUT1 Western blot analysis. Data are presented as mean \pm SD (*P<0.05, **P<0.01, ***P<0.001; unpaired two-tailed t-test). GTTs and ITTs were performed together with Katharina Senft.

3.1.3 CLPP deficiency causes a fasting-like phenotype

To further assess the basal metabolic state in CLPP deficient mice, blood and serum parameters were analyzed. Blood glucose levels were measured under fed and fasted conditions. In line with previous results, blood glucose levels were significantly reduced in Clpp^{-/-} mice as compared to controls in both conditions. Conversely, levels of free fatty acids, also called non-esterified fatty acids (NEFA) were not significantly changed in male Clpp^{-/-} mice and seem to be increased in female Clpp^{-/-} mice as compared to control mice (Figure 3.7 A, B), indicating an increased lipolysis in female Clpp^{-/-} mice.

Analysis of further metabolic markers revealed no changes in serum insulin, ghrelin, glucagon-like-peptide 1 (GLP-1), glucose-dependent insulinotropic polypeptide (GIP) and resistin levels in *Clpp*^{-/-} mice as compared to control mice in the fed state (Figure 3.7 C, E, G-I). GIP and GLP-1 are secreted from the intestine upon food ingestion to stimulate pancreatic insulin secretion (Baggio and Drucker, 2007). The absence of changes in GLP-1 and GIP levels is thus in line with comparable insulin levels in control and *Clpp*^{-/-} mice and further suggests a functional intestinal nutrient absorption. Moreover, a significant decrease in leptin levels was observed upon loss of CLPP corresponding to the decreased fat mass in *Clpp*^{-/-} mice (Figure 3.7 D). Leptin is a central hormone in the hypothalamic regulation of satiety. Glucagon instead is secreted upon fasting to increase blood glucose levels by decreasing glycogen synthesis and increasing gluconeogenesis. Accordingly, glucagon levels were increased in *Clpp*^{-/-} mice as compared to controls (Figure 3.7 F). Taken together, these data suggest that loss of CLPP leads to a fasting-like phenotype with lower blood glucose levels and altered hormone signature.

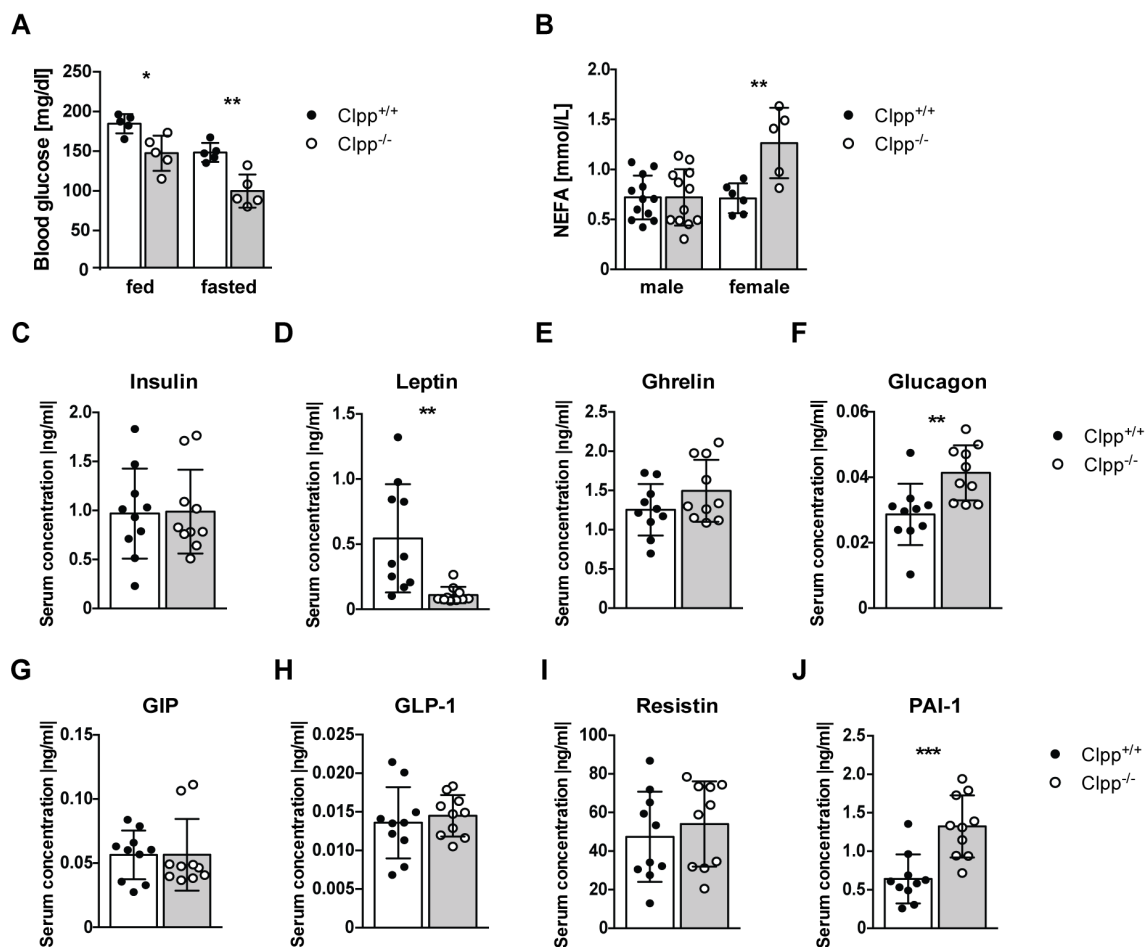


Figure 3.7 Serum parameters of control and CLPP deficient mice.

(A) Fed and fasted blood glucose levels of control and Clpp^{-/-} mice at 15 weeks of age. (B) Serum non-esterified fatty acid (NEFA) levels (male n=12, female n=5-6). (C-J) Analysis of serum metabolic markers in Clpp^{-/-} and control mice at 16 weeks of age (n=10) (C) Insulin (D) Leptin (E) Ghrelin (F) Glucagon (G) Glucose-dependent insulinotropic polypeptide (GIP) (H) Glucagon-like peptide 1 (GLP-1) (I) Resistin (J) Plasminogen activator inhibitor-1 (PAI-1). Data are presented as mean ± SD (*P<0.05, **P<0.01, ***P<0.001; unpaired two-tailed t-test).

At the tissue level, energy deficiency is sensed by the AMP-activated protein kinase (AMPK). AMPK plays a key role in the regulation of glucose and lipid metabolism in response to various stimuli as nutrient deprivation. To investigate the energy state at the tissue level of Clpp^{-/-} mice, phosphorylation of threonine-172 of AMPK α subunit in liver, SkM and EWAT was analyzed. The pAMPK/AMPK ratio was significantly increased in SkM of Clpp^{-/-} mice (Figure 3.8 A, B), indicating an energy deficient state with increased AMP/ATP ratio. In contrast, no difference was observed for liver and EWAT (Figure 3.8 A, B). Thus, the fasting-like phenotype of Clpp^{-/-} mice is also associated with AMPK activation in SkM.

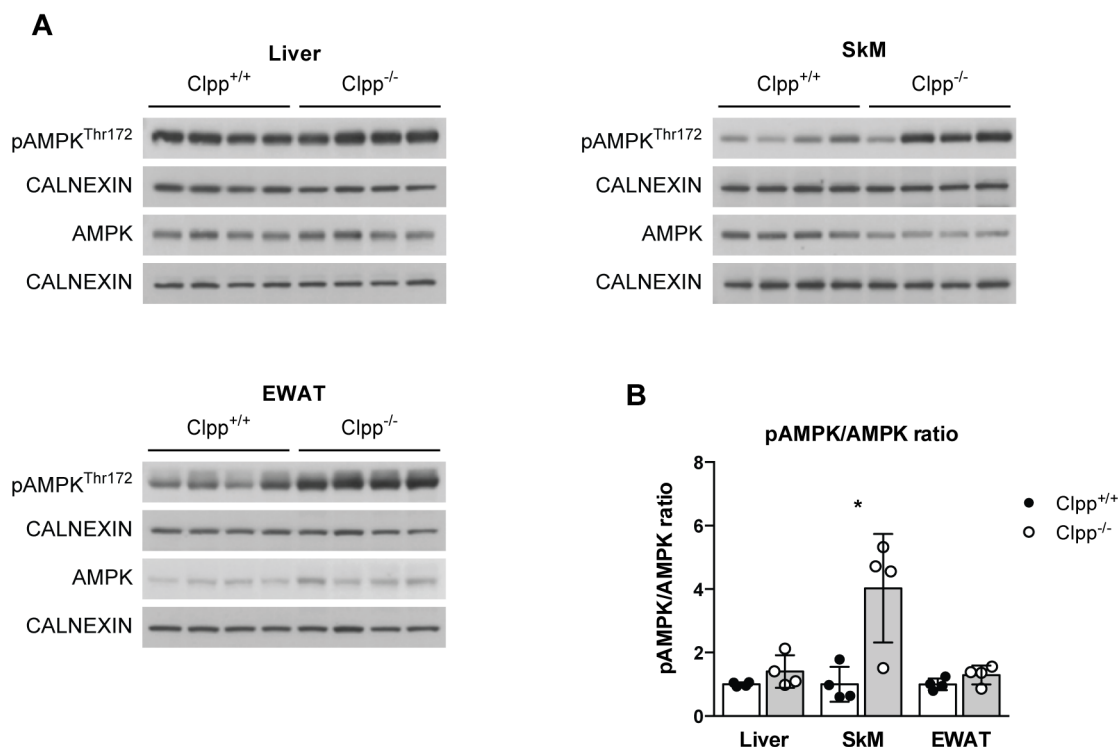


Figure 3.8 AMPK activation in SkM of CLPP deficient mice.

(A) Western blot analysis of phosphorylated Thr172 AMPK (pAMPK) and AMPK in liver, SkM and EWAT of Clpp^{-/-} mice. CALNEXIN serves as loading control (n=4). (B) Quantification of Western blots in (A) presented as ratio of pAMPK and AMPK. Data are presented as mean \pm SD (*P<0.05, **P<0.01, ***P<0.001; unpaired two-tailed t-test).

3.1.4 Lack of CLPP decreases glycogen content in liver and skeletal muscle

Hepatic and muscle glycogen metabolism are essential for glucose homeostasis and represent important energy sources during early starvation and physical exercise. Since CLPP deficient mice exhibit increased serum glucagon levels, which is known to decrease glycogen synthesis and enhance glucose metabolism, glycogen utilization/storage was investigated in CLPP deficient mice in liver and SkM. Notably, the glycogen content in liver and SkM was reduced in Clpp^{-/-} mice in comparison to control mice as shown by PAS reaction (Figure 3.9). No difference was observed for the general morphology of liver and SkM of Clpp^{-/-} mice as revealed by H&E staining of histological sections (Figure 3.9).

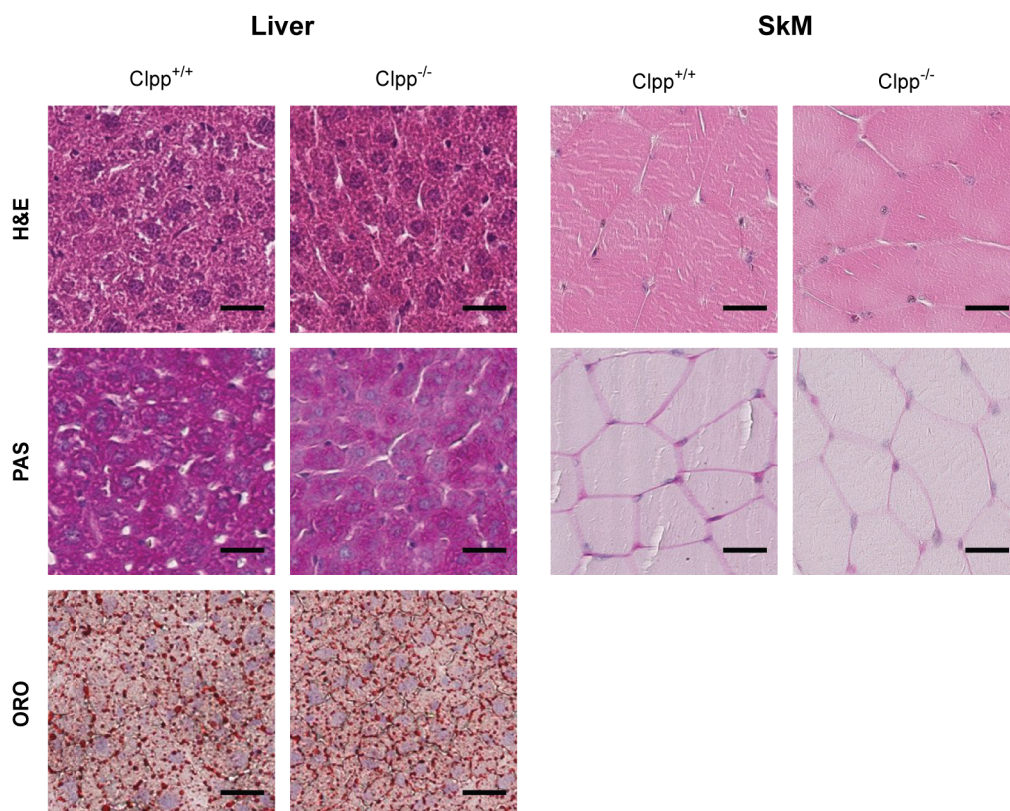


Figure 3.9 Loss of CLPP decreases glycogen content in liver and SkM.

Histological analysis of liver and SkM tissue sections. H&E - hematoxylin and eosin staining; PAS - periodic acid Schiff's reaction, assessment of glycogen content; ORO - oil red O staining, assessment of neutral lipids (n=4). Scale bar 50 μ m.

3.1.5 Effect of CLPP deficiency on fatty acid β -oxidation

Mitochondria are central to fatty acid β -oxidation (FAO). Since CLPP deficient mice display decreased fat mass, it was examined whether loss of CLPP affects fatty acid β -oxidation. First, β -oxidation was analyzed using [1- 14 C]-palmitate and measuring the incorporation into CO_2 and acid soluble metabolites (ASM) in liver, SkM and BAT mitochondria. Different than expected the β -oxidation rate was significantly reduced by about 25% in liver and SkM of CLPP deficient mice and no significant difference was observed for BAT (Figure 3.10 A).

Second, mitochondrial β -oxidation was analyzed exploiting high-resolution respirometry in isolated liver mitochondria in the presence of long chain palmitoylcarnitine (C16) and malate. The electrons from β -oxidation are supplied by the electron transferring flavoprotein (ETF) to Coenzyme Q. Malate is required to prevent the accumulation of acetyl-CoA and replenish CoA (Ojuka et al., 2016). In compliance with the previous result of the *ex vivo* FAO the ADP stimulated respiration on long chain palmitoylcarnitine (OXPHOS ETF + Col) was significantly reduced in CLPP deficient mice. However, mitochondria from control and Clpp $^{-/-}$ mice were equally coupled (LEAK) and also the maximal capacity of the electron transfer system (ETS) was not

changed (Figure 3.10 B). Remarkably, when substrates feeding electrons to complex I and complex II were applied, all respiratory states were unchanged in mitochondria from control and *Clpp*^{-/-} mice, (Figure 3.10 C). Thus, CLPP deficiency leads to decreased β -oxidation in liver and SkM, however, mitochondrial respiration is not affected in liver mitochondria.

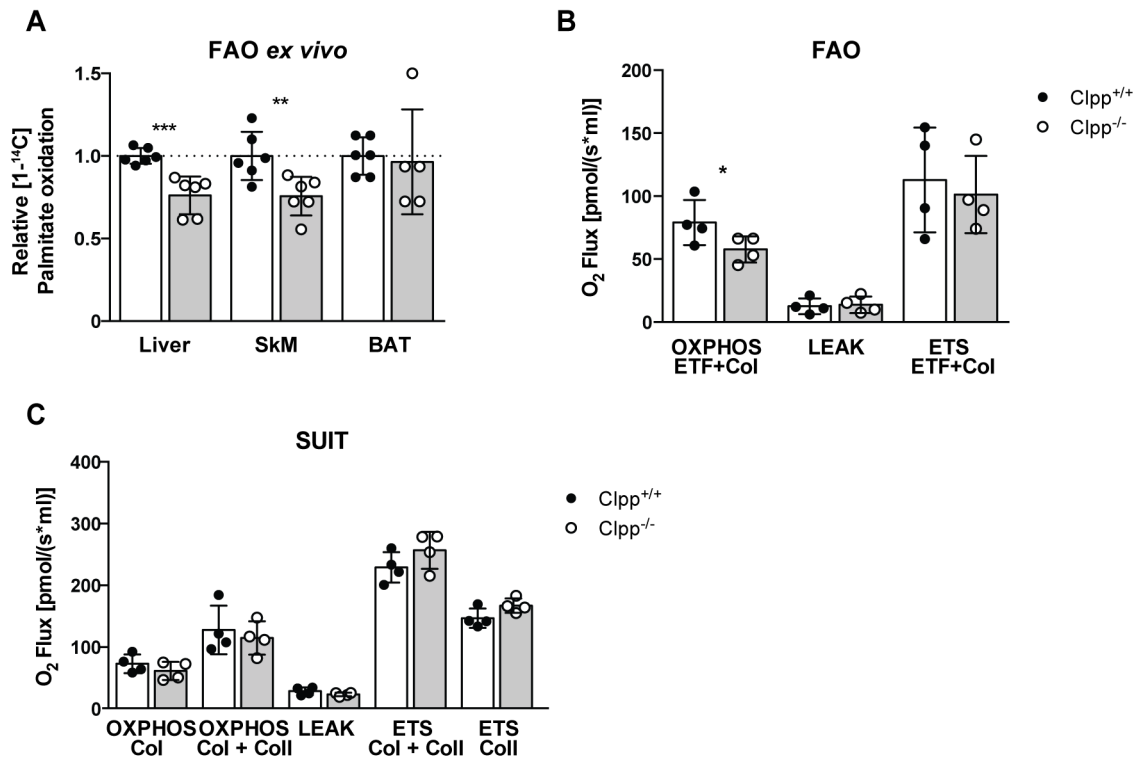


Figure 3.10 CLPP deficient mice exhibit decreased FAO in liver and SkM.

(A) *Ex vivo* fatty acid oxidation of long chain [¹⁴C]-palmitate in liver (n=6), SkM (n=6) and BAT (n=5) of control and *Clpp*^{-/-} mice. Data are presented as mean \pm SD (*P<0.05; unpaired two-tailed t-test). (B-C) Respiratory flux of isolated liver mitochondria in the presence of (B) fatty acid oxidation substrates (palmitoylcarnitine and malate) or (C) Col and Coll substrates (pyruvate, malate, glutamate and succinate) OXPHOS - ADP stimulated respiration, LEAK - upon addition of oligomycin and ETS - maximal respiration after FCCP titration (n=4). Data are presented as mean \pm SD (*P<0.05; paired two-tailed t-test). *Ex vivo* FAO experiments were performed together with Dr. Alexandra Kukat.

To gain further insights into the deregulated fatty acid β -oxidation in *Clpp*^{-/-} mice, expression of major enzymes involved in the catabolism of fatty acids were analyzed in various metabolic tissues. Mitochondrial fatty acid β -oxidation comprises different steps and requires uptake of long chain acyl-CoAs via the carnitine palmitoyltransferase system (CPT1, CACT and CPT2) before the β -oxidation involving four major enzymes acyl-CoA dehydrogenase, enoyl-CoA hydratase, hydroxyacyl-CoA dehydrogenase and ketoacyl-CoA thiolase can take place. The acyl-CoA dehydrogenases differ in their specificity for very long-, long-, medium- and short-chain acyl-CoAs.

Comparing the expression profiles of liver, SkM and BAT, the specific downregulation

of the carnitine palmitoyltransferase 2 (CPT2) and striking upregulation of the very long chain acyl CoA dehydrogenase (VLCAD) was observed in CLPP deficient mice (Figure 3.11 A-F), whereas no difference was detected for CPT1A (liver isoform), CPT1M (muscle and adipose tissue isoform), MCAD, SCAD and HADHA. In BAT, next to CPT2 also MCAD was downregulated. Since the liver, SkM and BAT are tissues highly dependent on fatty acid oxidation, also WAT depots were examined. WAT contains far less mitochondria and the role of fatty acid β -oxidation in this tissue is not very well understood, yet it was shown that fasting increases fatty acid oxidation in WAT of broiler chicken (Torchon et al., 2017). In both EWAT and IWAT strong upregulation of VLCAD was observed, consistent with the data from liver, SkM and BAT, while CPT2 levels were not altered (Figure 3.12 A-D). Taken together, the changes in proteins involved in FAO manifest in decreased rates of fatty acid oxidation in liver and SkM of CLPP deficient mice. Furthermore, there are tissue-specific differences in the adaptations to the CLPP dependent increase in VLCAD.

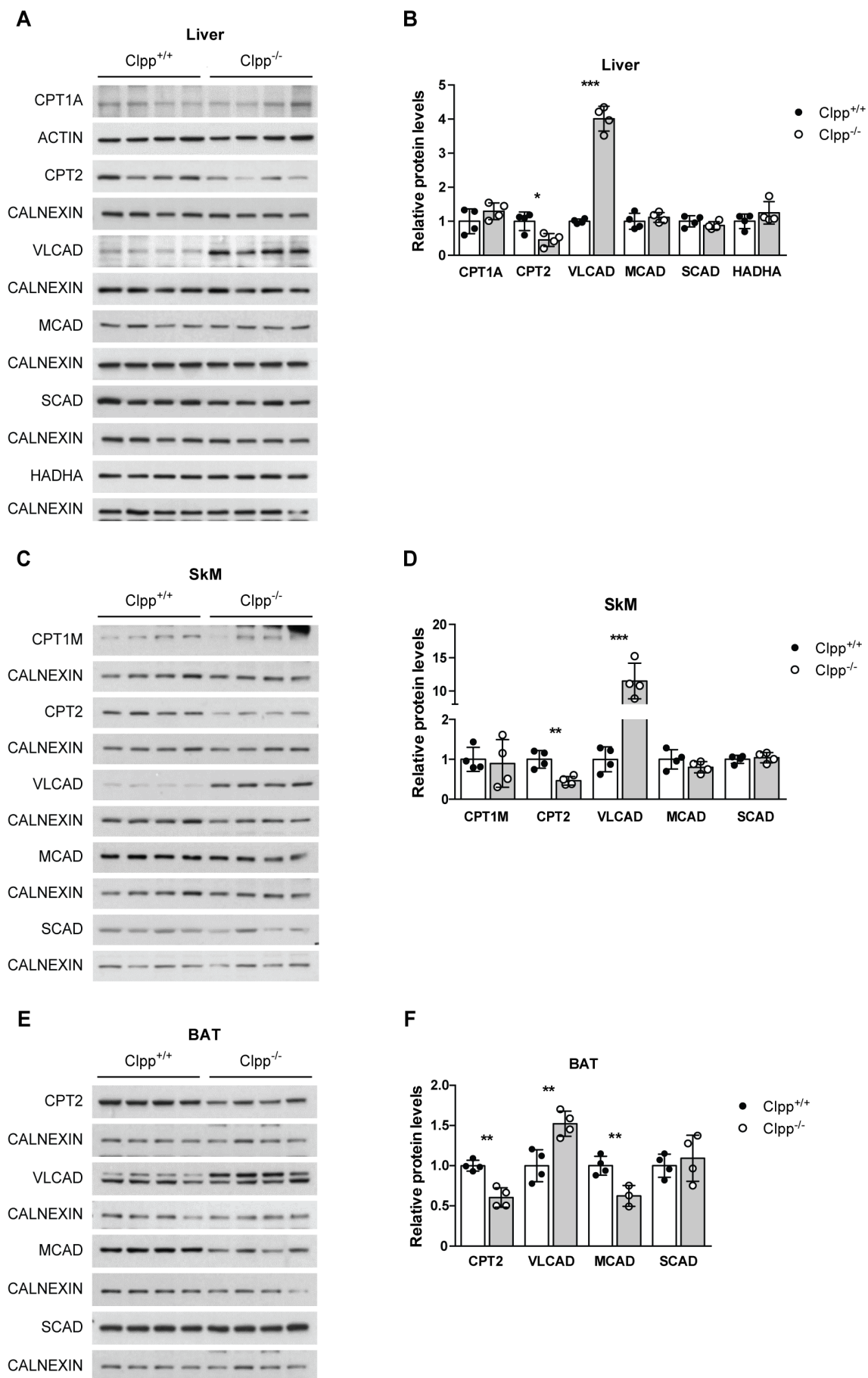
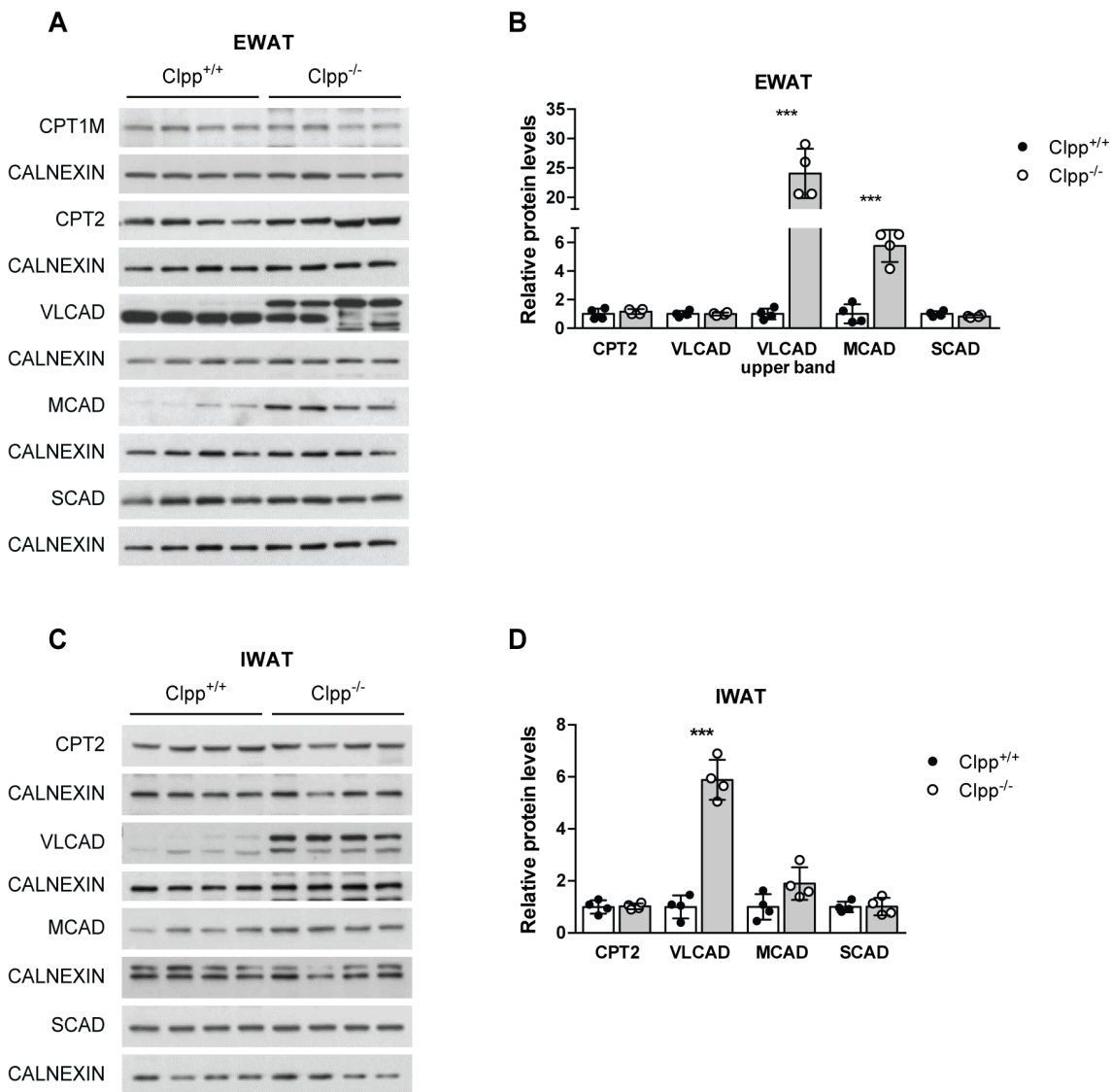


Figure 3.11 Profile of FAO enzymes in Clpp^{-/-} mice (1).

Figure 3.11 Profile of FAO enzymes in *Clpp*^{-/-} mice (1).

Loss of CLPP increases VLCAD steady state levels and decreases CPT2. (A, C, E) Western blot analysis of enzymes involved in FAO in (A) liver (C) SkM and (E) BAT lysates. CALNEXIN and ACTIN serve as loading controls. (B, D, F) Quantification of Western blots shown in (A, C, E). Data are presented as mean \pm SD (* P <0.05; paired two-tailed t-test). Western Blots were performed together with Katharina Senft.

**Figure 3.12 Profile of FAO enzymes in *Clpp*^{-/-} mice (2).**

In adipose tissue loss of CLPP increases VLCAD steady state levels (A, C) Western blot analysis of enzymes involved in FAO in (A) EWAT and (C) IWAT lysates. CALNEXIN serves as loading control. (B, D) Quantification of Western blots shown in (A, C). Data are presented as mean \pm SD (* P <0.05; paired two-tailed t-test).

Since CLPP is a mitochondrial matrix protease, upregulation of a matrix protein in a CLPP deficient background is an indication for possible substrate.

The universal upregulation of VLCAD proposes it as a novel CLPP substrate. To test this hypothesis, mRNA levels of *Acadvl* (gene encoding VLCAD) were analyzed. No significant difference at the transcript level, further supports VLCAD as a possible

CLPP substrate, indicating that increased VLCAD levels are not due increased gene expression, but rather due to increased stability of the protein (Figure 3.13 A). Moreover, transcript level analysis of *Cpt2* also revealed no significant difference (Figure 3.13 A), suggesting that the decreased abundance of CPT2 is not mediated by transcriptional repression, rather due to post-transcriptional modification or increased protein turnover.

To further assess whether VLCAD is a putative CLPP substrate, its expression was analyzed in immortalized *Clpp* knockout mouse embryonic fibroblasts (MEFs). CLPP dependent upregulation of VLCAD was detected, whereas the counter regulatory response of CPT2 downregulation was absent (Figure 3.13 B).

Clpp knockout MEFs were further used to assess the stability of VLCAD during a cycloheximide chase (CHX) experiment. While blocking the cytoplasmic translation with cycloheximide and following the turnover, no difference was observed regarding the steady state levels of VLCAD in the wildtype or CLPP deficient cells, due to long half-life (>12 h) of VLCAD (Figure 3.13 C). Therefore, this method is not sufficient to confirm the increased stability of VLCAD in *Clpp* knockout MEFs. A different approach could be the ³⁵S-methionine labeling of proteins and to follow the protein stability after immunoprecipitation of VLCAD. These results identify VLCAD as putative CLPP substrate and thus propose a role for CLPP in the regulation of fatty acid β -oxidation.

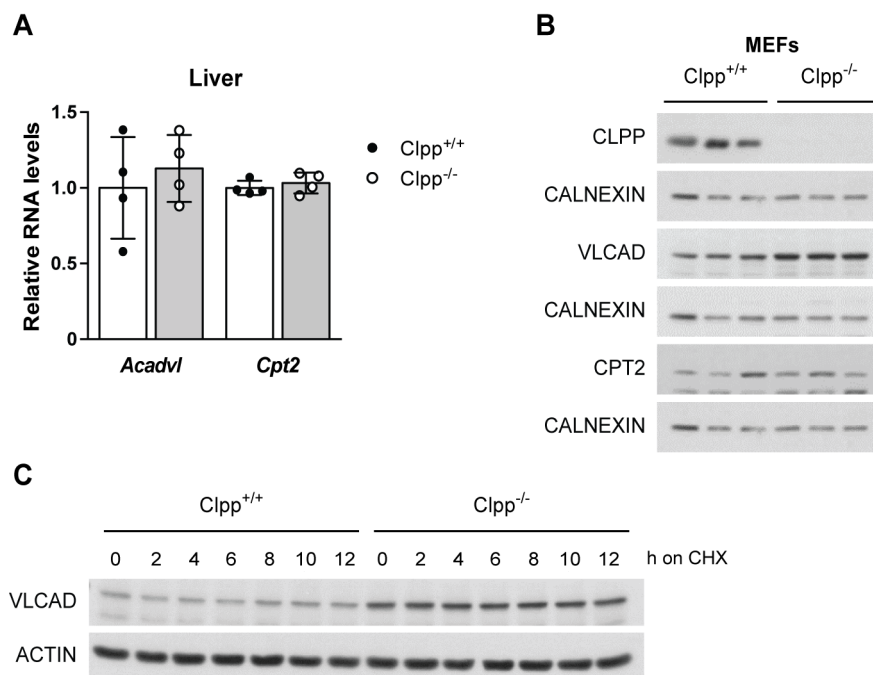


Figure 3.13 VLCAD is a putative substrate of CLPP.

(A) Relative expression levels of *Acadvl* and *Cpt2* in liver of control and $Clpp^{-/-}$ mice (n=4). (B) CLPP deficient MEFs were cultured and cell lysates were analyzed by Western blot for VLCAD and CPT2 expression (n=3). CALNEXIN serves as loading control. (C) Cycloheximide (CHX) chase experiment for the determination of the stability of VLCAD in the absence of CLPP. Cells were harvested 0, 2, 4, 6, 8, 10 and 12 h after starting the treatment with CHX and lysed for subsequent Western blot analysis (n=3). ACTIN serves as loading control. Data are presented as mean \pm SD. Cycloheximide chase assay was performed by Dr. Karolina Szczepanowska.

3.1.6 Loss of CLPP severely impairs cold tolerance

Brown adipose tissue is an organ actively contributing to whole body energy expenditure. Increased energy expenditure, as observed for $Clpp^{-/-}$ mice, can be caused by increased mitochondrial uncoupling due to enhanced adaptive thermogenesis. To examine the significance of CLPP deficiency for BAT function, first BAT morphology was analyzed. Upon dissection, CLPP deficient interscapular BAT was more lipid laden, having a much lighter appearance in contrast to the brown color of control BAT (Figure 3.14 A). Histological analysis of H&E stained BAT tissue slides confirmed the alterations by the presence of large unilocular lipid droplets in the BAT of $Clpp^{-/-}$ mice instead of the classic multilocular lipid droplets as seen in control mice. In accordance with these findings ORO staining of neutral lipids showed a slight increase and more dense appearance of lipid droplets in BAT of CLPP deficient mice in comparison to control mice (Figure 3.14 B). Finally, COX-SDH staining of BAT revealed no difference in mitochondrial function of control and $Clpp^{-/-}$ mice.

Next, thermogenic protein abundance was analyzed in BAT whole tissue lysates. Interestingly, gender specific differences could be observed for $Clpp^{-/-}$ mice. While UCP1 and TOMM20 levels were not changed in male $Clpp^{-/-}$ mice and only PGC1 α

levels were increased, an increase in TOMM20, a consistent increase in PGC1 α and decreased levels of UCP1 were detected in female Clpp^{-/-} mice (Figure 3.14 C, D). TOMM20 is an outer mitochondrial membrane protein and can thus not be directly linked to mitochondrial mass, since an increase in mitochondrial mass is often associated with an increase in mitochondrial size not in number. Whether the reduction in UCP1 protein in BAT of female Clpp^{-/-} mice results from a decrease in mitochondrial mass in a CLPP dependent manner or from the influence of sex hormones needs to be further investigated. It was previously reported about gender related differences in BAT thermogenesis in rats in response to cold or diet induced obesity (Rodríguez-Cuenca et al., 2002; Rodríguez et al., 2001).

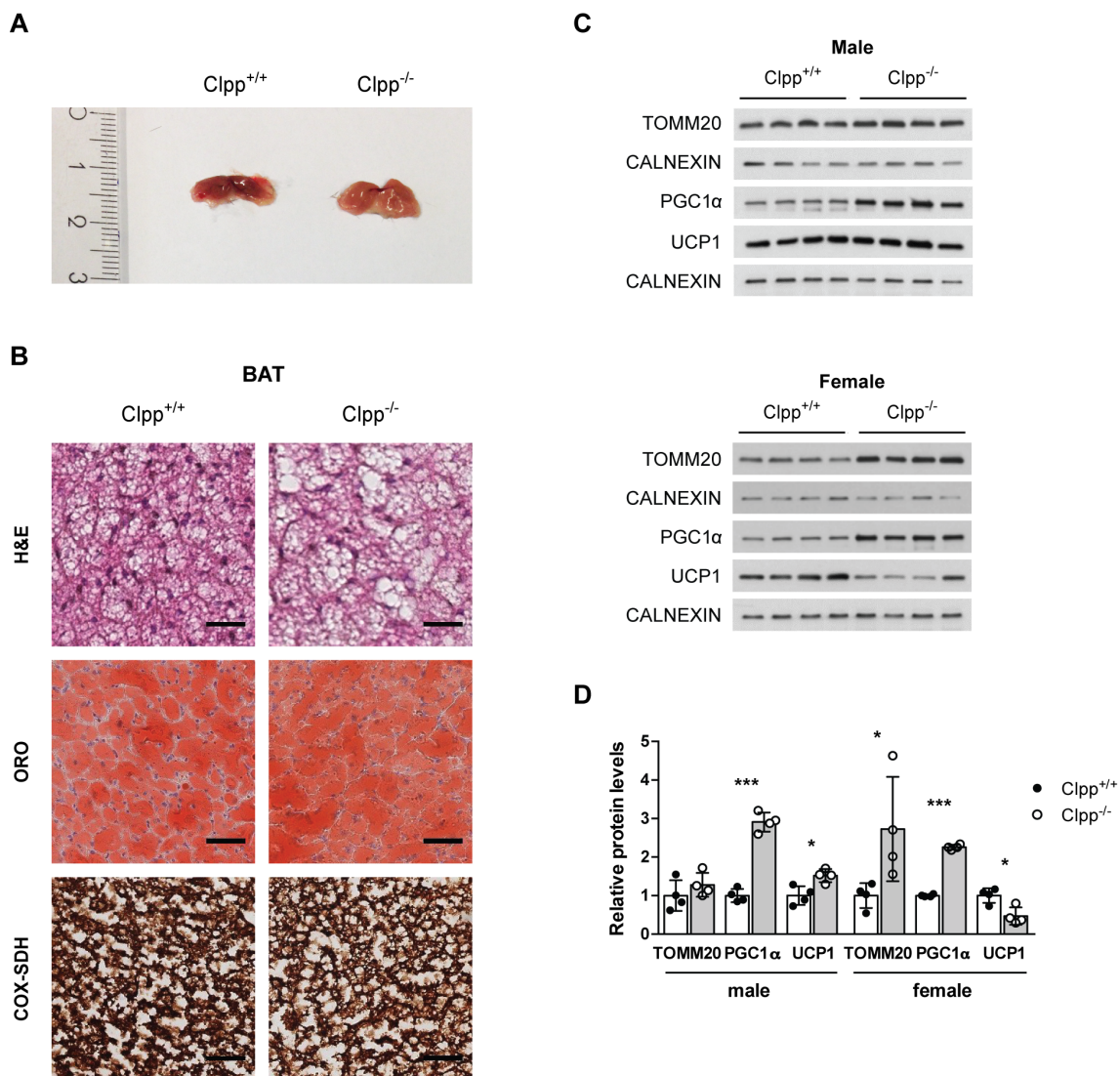


Figure 3.14 Lipid accumulation in BAT of Clpp^{-/-} mice.

(A) Gross morphology of BAT of control and Clpp^{-/-} mice. (B) Histological analysis of BAT, H&E - hematoxylin and eosin staining; ORO - oil red O staining, assessment of neutral lipids; COX-SDH - enzyme histochemical double staining for COX and SDH activities (n=4). Scale bar 50 μ m. (C) Western blot analysis of thermogenic proteins and mitochondrial mass (TOMM20) in BAT lysates of male and female control and Clpp^{-/-} mice. CALNEXIN serves as loading control. (D) Quantification of blots shown in (C). Data are presented as mean \pm SD (*P<0.05, **P<0.01, ***P<0.001; unpaired two-tailed t-test). Cryosections were done by Steffen Hermans.

To analyze whether the lipid accumulation in combination without altered UCP1 abundance in BAT of male Clpp^{-/-} mice has an impact on adaptive thermogenesis, control and Clpp^{-/-} mice were exposed to 5°C. Basal body temperature at room temperature (22°C) was not different between control and CLPP deficient mice (Figure 3.15 A), indicating functional maintenance of body temperature in Clpp^{-/-} mice. Intriguingly, cold exposure induced severe hypothermia in Clpp^{-/-} mice with a body temperature drop from 36°C to 27°C within 2 h, whereas the body temperature of control mice was only lowered by 2°C to 34°C (Figure 3.15 A). Based on the observation that UCP1 levels are not changed in male Clpp^{-/-} mice, yet these mice are

severely impaired in maintaining body temperature upon cold exposure, it was investigated whether UCP1 induction or mitochondrial function is impaired upon cold exposure. UCP1 levels examined in isolated BAT mitochondria showed a significant reduction in *Clpp*^{-/-} mice upon cold exposure (Figure 3.15 B). Next, mitochondrial complex and supercomplex levels were assessed in cold exposed *Clpp*^{-/-} mice by BN-PAGE and subsequent Western blot analysis. At complex level, *Clpp*^{-/-} mice exhibited a severe reduction for CoI, while CoIII and CoIV were less affected. No difference was observed for the entirely nuclear-encoded CoII and the levels of CoV were even increased in cold exposed *Clpp*^{-/-} mice as compared to control mice (Figure 3.15 C). Similar changes were observed for assembled mitochondrial supercomplexes (Figure 3.15 D).

Taken together, loss of CLPP leads to an aberrant BAT morphology due to lipid accumulation and leads to an impaired thermogenesis due to decreased UCP1 induction and severe mitochondrial dysfunction upon cold exposure. The severe decrease in mitochondrial complexes especially CoI in BAT of CLPP deficient mice does most likely not exclusively result from the short cold exposure (2 h), but rather from a further stress induced deterioration of a previous defect. However, whether a general reduction of mitochondrial complexes in BAT of *Clpp*^{-/-} mice is present needs to be further investigated.

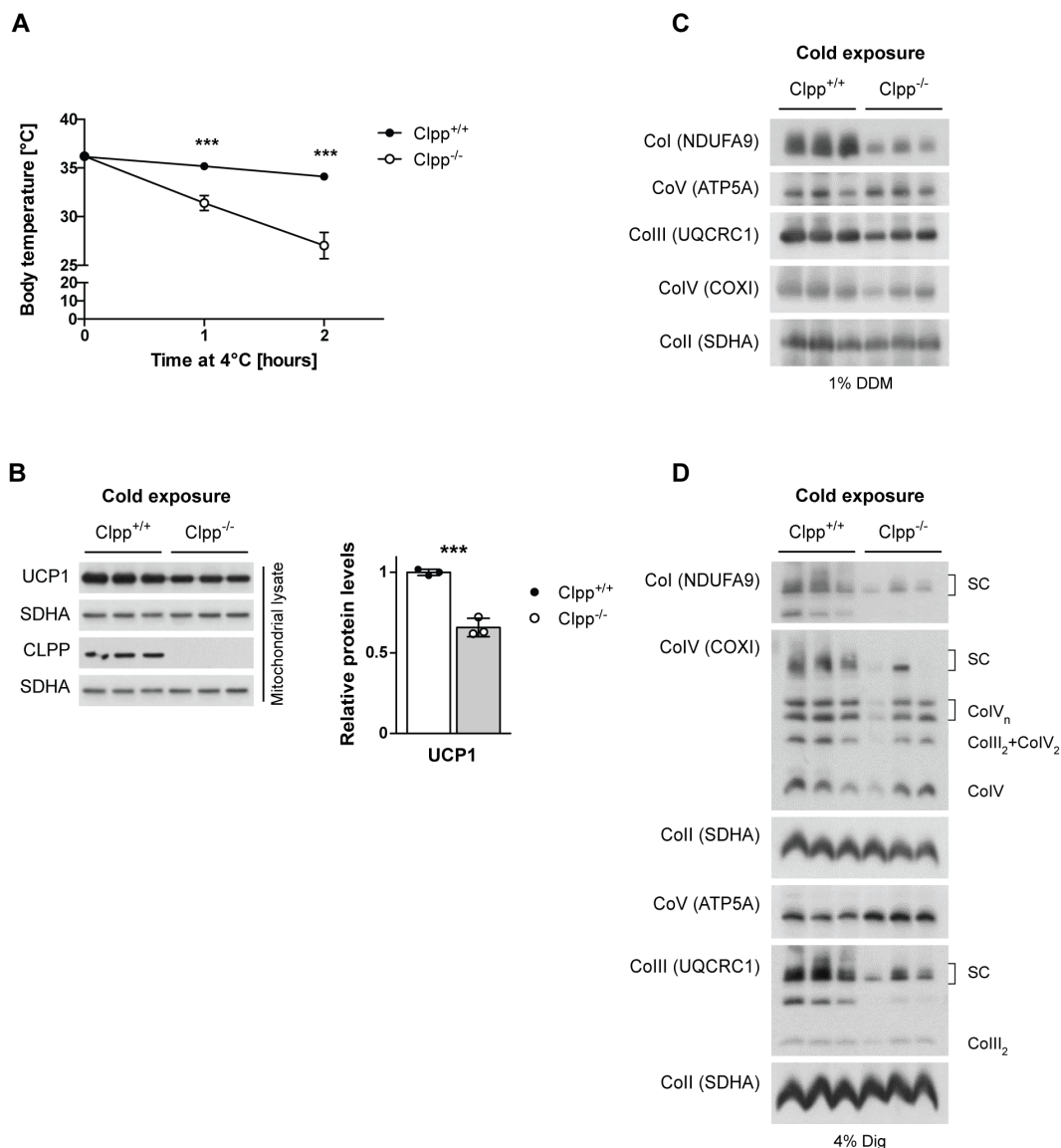


Figure 3.15 CLPP is essential for cold induced thermogenesis.

(A) Body temperature of control and Clpp^{-/-} mice exposed to 4°C for 2 h (n=3-4). (B) Western blot analysis of thermogenic proteins in mitochondrial lysates from BAT of Clpp^{-/-} and control mice exposed to 4°C for 2 h. (C-D) BN-PAGE and subsequent Western blot analysis of mitochondrial respiratory chain complexes (n=3) (C) and supercomplexes (D) of BAT mitochondria from control and Clpp^{-/-} mice exposed to 4°C for 2 h. Antibodies against individual complex subunits (indicated in parenthesis) were used for the detection of assembled complexes. Data are presented as mean ± SD (*P<0.05, **P<0.01, ***P<0.001; unpaired two-tailed t-test).

3.1.7 Loss of CLPP leads to enhanced browning of WAT

Another often-disregarded tissue related to energy expenditure is the WAT, since it usually exhibits energy storage function. Particularly in mouse models of mitochondrial dysfunction it was shown that “browning” of white adipose tissue increases energy expenditure (Vernochet et al., 2012). Browning is the emergence of adipocytes with brown properties, referred to as beige or brite adipocytes within classical WAT depots (Kishida et al., 2015). Therefore, different WAT depots were analyzed from Clpp^{-/-} mice. Consistent with the decreased body fat mass, EWAT (visceral) and IWAT

(subcutaneous) depots were smaller in *Clpp*^{-/-} mice as compared to control (Figure 3.16 A) and especially the EWAT displayed more brown-like appearance. This was further confirmed upon histological analysis of the fat depots. Adipocyte size of EWAT and IWAT was not different between control and *Clpp*^{-/-} mice, however, in EWAT of *Clpp*^{-/-} mice occasionally regions with brown like morphology were detected (Figure 3.16 B). A hallmark of white adipose tissue browning is the increase in transcript levels of thermogenic genes, which was also present in EWAT of *Clpp*^{-/-} mice, as shown by increased *Ucp1*, *Dio2* and *Cidea* mRNA levels (Figure 3.16 C). In IWAT of *Clpp*^{-/-} mice only the increase in *Cidea* mRNA levels was significantly different from control mice. In contrast, corresponding transcript levels in BAT of *Clpp*^{-/-} mice were decreased or not changed (Figure 3.16 C right panel), indicating a whitening of the BAT in the absence of CLPP (Shimizu and Walsh, 2015). Thus, it can be concluded that *Clpp*^{-/-} EWAT acquired thermogenic capacity, which might contribute to increased energy expenditure of *Clpp*^{-/-} mice. This effect is not as strong in IWAT of *Clpp*^{-/-} mice and almost reversed for BAT, again indicating tissue-specific differences in the consequences of CLPP deficiency.

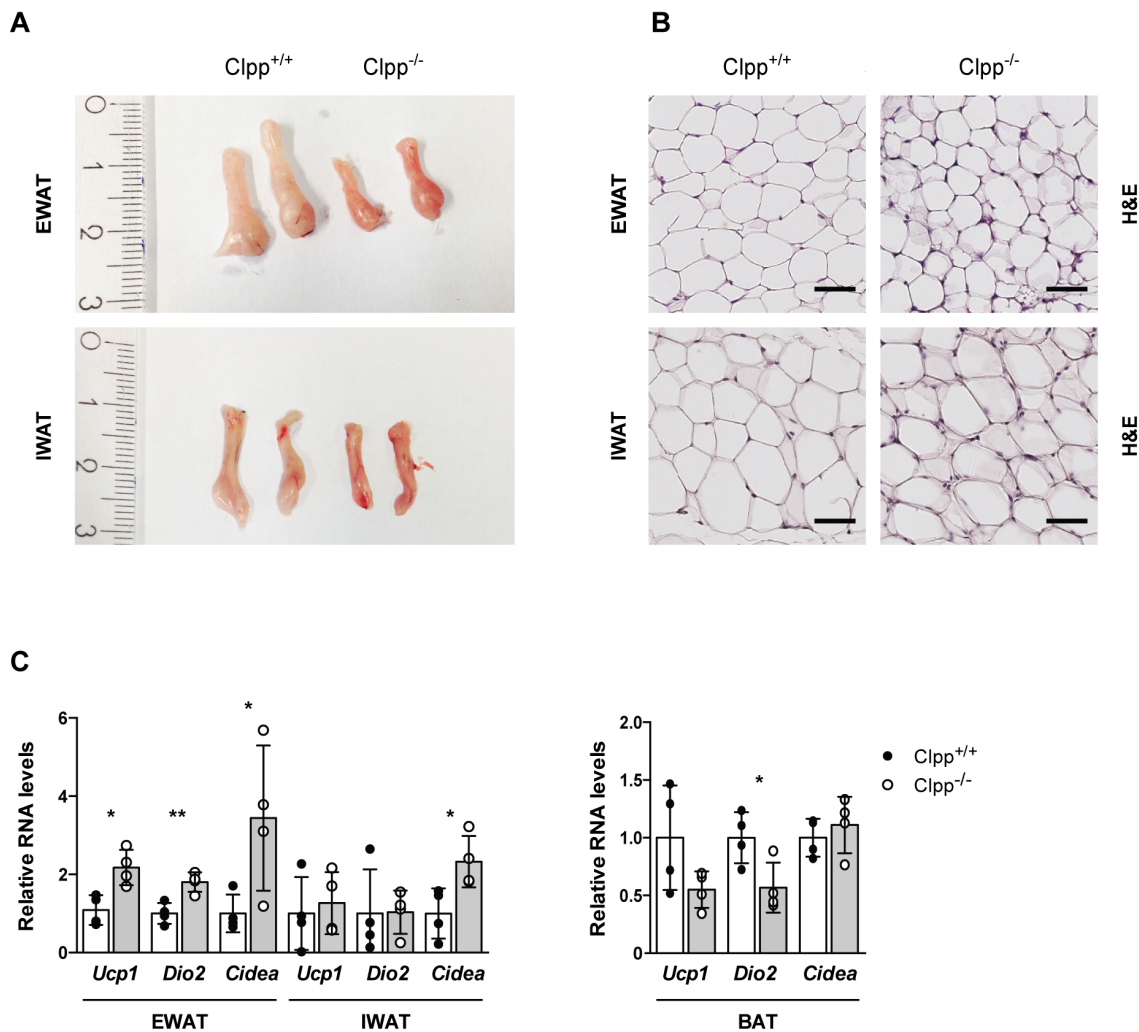


Figure 3.16 Browning of WAT in *Clpp*^{-/-} mice.

(A) Gross morphology of EWAT and IWAT of control and *Clpp*^{-/-} mice. (B) Hematoxylin and eosin staining of EWAT and IWAT tissue sections (n=7). Scale bar 50 μ m. (C) Relative expression of thermogenic genes (*Ucp1*, *Cidea*, *Dio2*) in EWAT, IWAT and BAT of control and *Clpp*^{-/-} mice (n=3). Data are presented as mean \pm SD (*P<0.05, **P<0.01, ***P<0.001; unpaired two-tailed t-test).

Fibroblast growth factor 21 (FGF21) is an important metabolic hormone secreted upon fasting from the liver (Badman et al., 2007; Inagaki et al., 2007). Moreover, FGF21 was suggested as a marker for mitochondrial dysfunction that functions as mitokine and elicits a global response (Tynismaa et al., 2010). Given that many of the observed phenotypes in *Clpp*^{-/-} mice resemble those reported for FGF21 transgenic mice with hepatic overexpression of FGF21 like reduced body weight, reduced body size, enhanced insulin sensitivity, it was investigated whether FGF21 could be mediating the phenotype of CLPP deficient mice (Zhang et al., 2012b). Therefore, *Fgf21* induction was explored at the transcript level in metabolically important tissues. Remarkably, in all observed tissues *Fgf21* levels were increased at least 3-fold (Figure 3.17 A), whereas the strongest increase was found in the heart of *Clpp*^{-/-} mice. This is in line with the highest degree of mitochondrial dysfunction observed in heart of *Clpp*^{-/-} mice

(Szczepanowska et al., 2016). The transcriptional increase in *Fgf21* was associated with 2-fold increase in circulating serum FGF21 (Figure 3.17 B). Hence, increased serum FGF21 could facilitate some of the phenotypes observed for CLPP deficient mice.

Transcriptional activation of *Fgf21* expression is regulated by ATF4 and PPAR α . The *Fgf21* promoter harbors two PPAR α response elements (PPRE) as well as three amino acid response elements (AARE) and is directly bound by PPAR α and ATF4 (Inagaki et al., 2008; Maruyama et al., 2016). Besides an increased *Atf4* expression in heart no difference in *Atf4* and *Ppara* expression was observed in the other analyzed tissues of *Clpp*^{-/-} mice. In addition, transcript levels of the bZIP transcription factors CHOP and ATF5 were assessed. *Chop* was again only elevated in heart, whereas in all analyzed tissues *Atf5* was upregulated. Although ATF5 was not reported to induce *Fgf21* expression so far, a recent study analyzing *Fgf21* induction in liver in response to different diet combinations using microarray data, found the closest correlation of *Atf5* and *Fgf21* expression (Solon-Biet et al., 2016).

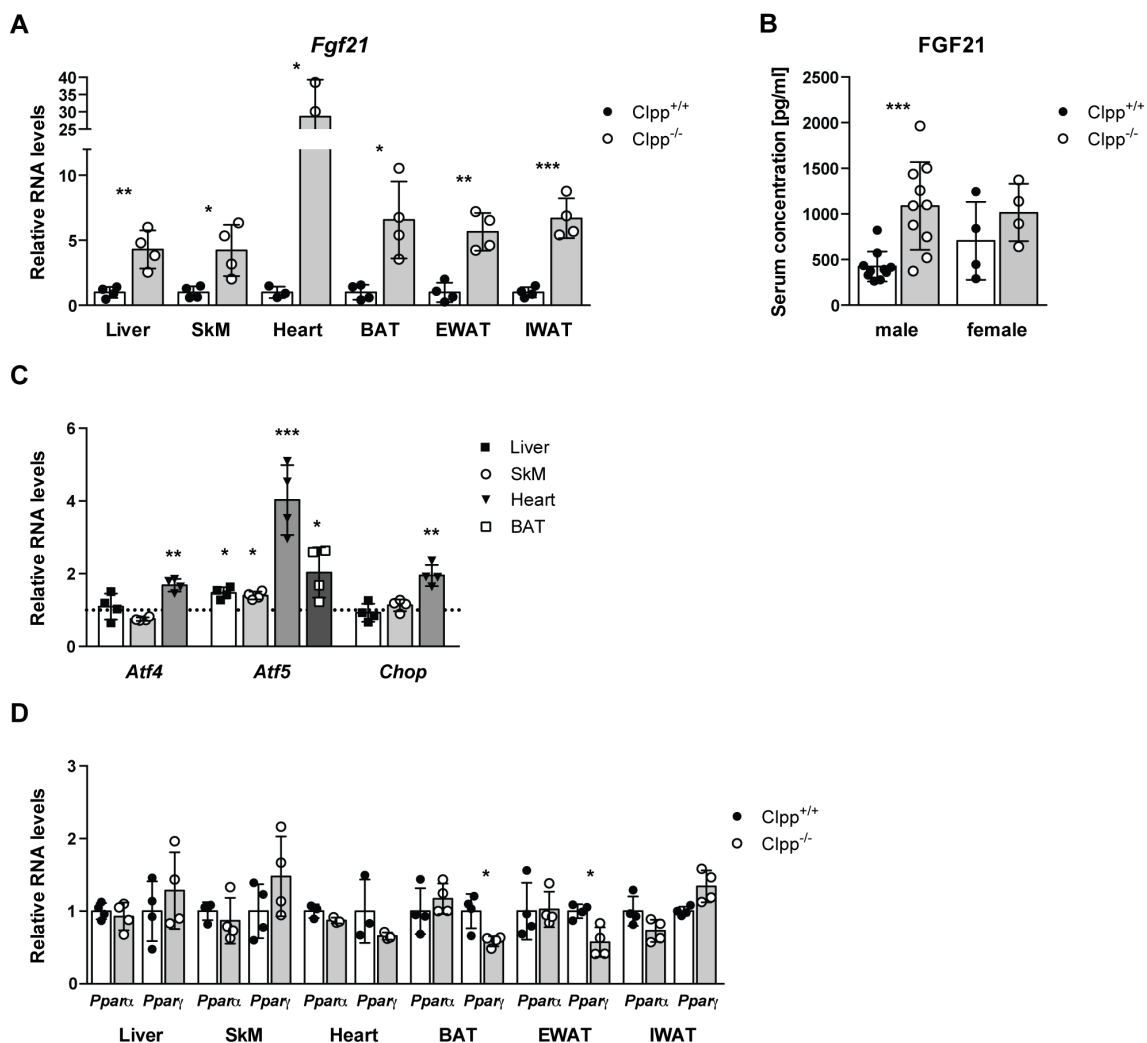


Figure 3.17 Systemic induction of *Fgf21* and increased circulating levels in *Clpp*^{-/-} mice.

(A) Relative expression of *Fgf21* in liver, SkM, heart, BAT, EWAT and IWAT (n=4). (B) Circulating serum levels of FGF21 in control and CLPP deficient mice (male n=10, female n=4). (C) *Atf4*, *Atf5* and *Chop* expression levels in liver, SkM, Heart and for BAT only *Atf5* (n=4). (D) Relative expression of *Ppara* and *Ppar*_γ in all metabolically relevant tissues (n=4). Data are presented as mean ± SD (*P<0.05, **P<0.01, ***P<0.001; unpaired two-tailed t-test).

3.2 Phenotype of *Clpp*^{-/-} mice is independent of FGF21

To analyze the functional relevance of FGF21 in mediating the phenotype of *Clpp*^{-/-} mice, double deficient mice lacking CLPP and FGF21 (DKO) were generated and as control homozygous *Clpp* (*Clpp*^{-/-}) and *Fgf21* (*Fgf21*^{-/-}) knockout mice. Many of the observed phenotypes for *Clpp*^{-/-} mice are in accordance with *Fgf21* overexpression or pharmacological effects of FGF21 treatment. Unexpectedly, despite the loss of *Fgf21* (Figure 3.18 B) the phenotype of DKO mice was almost identical to *Clpp*^{-/-} mice. The body weight gain of DKO mice was similar to *Clpp*^{-/-} mice till 15 weeks of age (Figure 3.18 A) and *Fgf21*^{-/-} mice only slightly deviate from the weight curve of the wildtype control animals. Furthermore, FGF21 is not involved in the regulation of the fat metabolism in *Clpp*^{-/-} mice. Both genotypes, *Clpp*^{-/-} and DKO mice had a similar body

fat mass, although fat mass of FGF21 deficient mice was significantly increased as compared to control mice (Figure 3.18 C). Thus, endogenous FGF21 only has a negligible role in regulating body weight and fat mass in $Clpp^{-/-}$ mice.

Since FGF21 was further shown to blunt growth hormone action and thereby reduce longitudinal growth (Inagaki et al., 2008; Wu et al., 2013), femur lengths were measured to determine whether endogenous FGF21 in $Clpp^{-/-}$ mice is responsible for the growth retardation. From visible inspection of the DKO mice it was already apparent that despite loss of FGF21 action, these mice are indistinguishable from $Clpp^{-/-}$ mice. This relates well with equivalent femur lengths of $Clpp^{-/-}$ and DKO mice (Figure 3.18 D). Hence, the growth defect in $Clpp^{-/-}$ mice is independent of FGF21. To decipher whether FGF21 serves as a cell autonomous stress response to enhance mitochondrial function (Ji et al., 2015), mitochondrial complex levels were examined in liver tissue. However, mitochondrial complex as well as supercomplex levels did not differ between all four groups (Figure 3.18 E, F). Albeit of similar mitochondrial complex levels, increased levels of LONP1 and TFAM were observed in DKO mice, indicating a possible induction of UPR^{mt} and increased mitochondrial mass (Figure 3.19). To conclude, FGF21 has a dispensable function for the systemic metabolic adaptations of $Clpp^{-/-}$ mice.

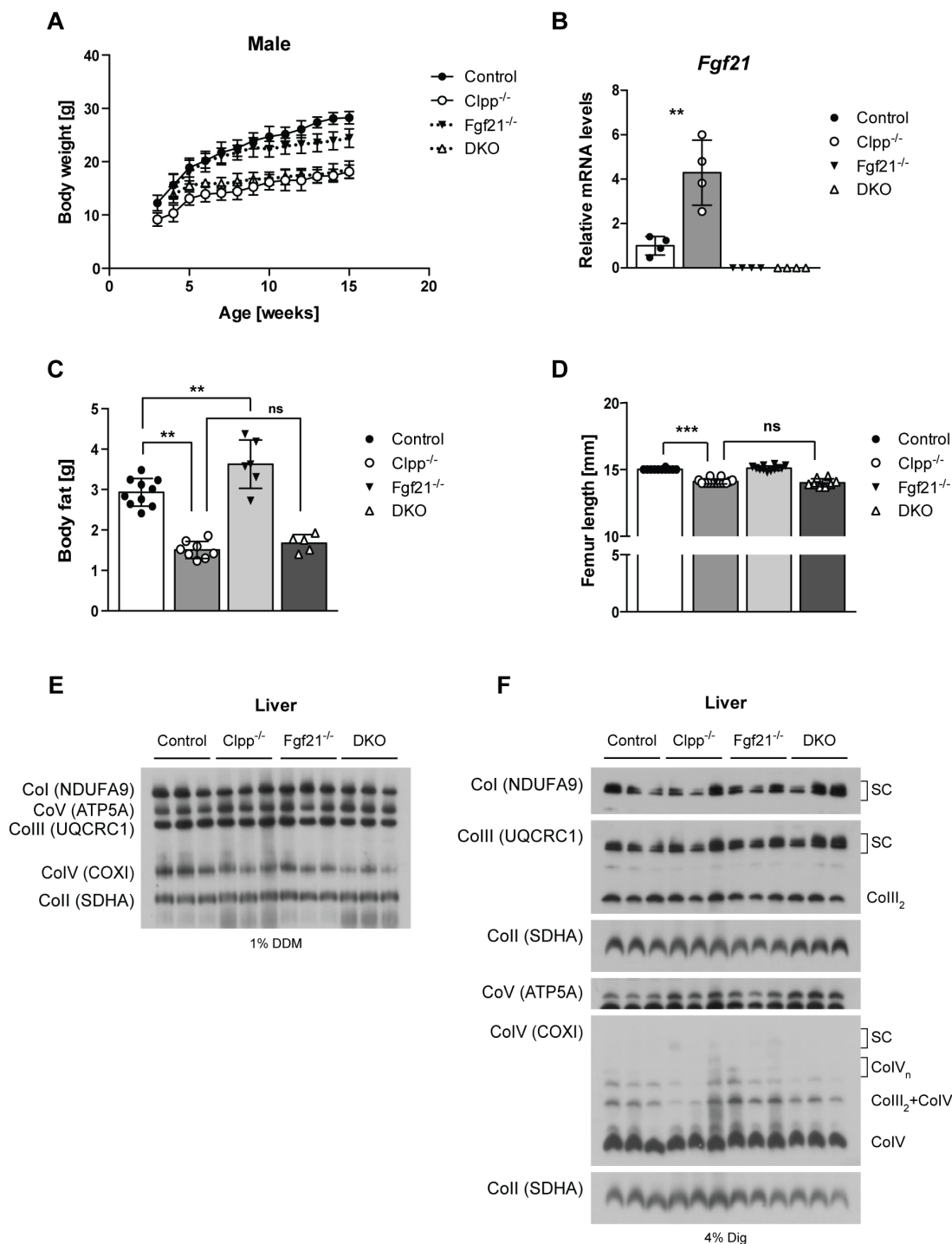


Figure 3.18 Loss of FGF21 in CLPP deficient mice does not normalize whole body physiology.

(A) Body weight of male control mice, *Clpp*^{-/-}, *Fgf21*^{-/-}, and DKO mice (n=6-10) was monitored till 15 weeks of age on normal chow diet (NCD). (B) Relative *Fgf21* transcript levels in liver of control, *Clpp*^{-/-}, *Fgf21*^{-/-} and DKO mice (n=4). (C) Body fat mass of control, *Clpp*^{-/-}, *Fgf21*^{-/-} and DKO mice fed NCD determined by NMR (n=8). (D) Femur length of control, *Clpp*^{-/-}, *Fgf21*^{-/-} and DKO mice (n=5-7). (E, F) BN-PAGE and subsequent Western blot analysis of mitochondrial complexes (E) and mitochondrial respiratory supercomplexes (F) of liver mitochondria from control, *Clpp*^{-/-}, *Fgf21*^{-/-} and DKO mice (n=3). Antibodies against individual complex subunits (indicated in parenthesis) were used for the detection of assembled complexes. Data are presented as mean ± SD (*P<0.05, **P<0.01, ***P<0.001; unpaired two-tailed t-test).

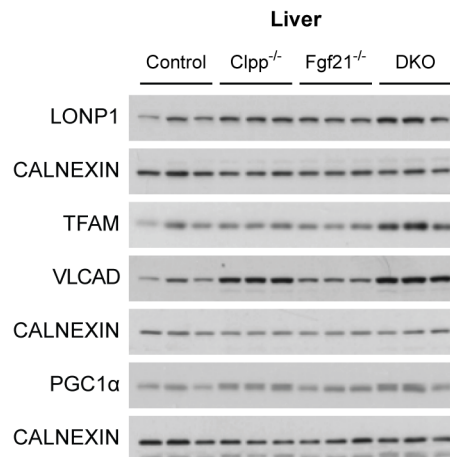


Figure 3.19 FGF21 deletion in CLPP deficient liver alters LONP1 and TFAM abundance. Western blot analysis of various proteins in liver tissue. CALNEXIN is used as loading control (n=3).

3.3 Tissue-specific disruption of *Clpp*

In order to dissect the role of CLPP in different tissues and to elucidate the contribution of CLPP deficiency in individual organs to the whole body metabolism, two tissue-specific mouse models were generated:

- (I) by ablating *Clpp* expression in liver using transgenic mice expressing Cre recombinase under control of the albumin enhancer and promoter and the α -fetoprotein enhancer (Afp-Cre) and
- (II) by disrupting the *Clpp* gene in heart and skeletal muscle by mating Clpp^{fl/fl} mice with mice expressing Cre from the muscle creatine kinase promoter (Ckmm-Cre).

3.3.1 Liver restricted loss of CLPP does not affect body weight and glucose homeostasis

CLPP ablation in liver was mediated by Cre recombinase under control of the albumin promoter and enhancer and the α -fetoprotein enhancer to produce Clpp^{fl/fl, +/Afp-Cre} mice, denoted as Clpp^{LKO}. The liver is composed of different cell types; hepatocytes are the most abundant cells with about 80%, Kupffer cells, Ito cells, endothelial cells and biliary duct cells. The albumin promoter is fully active before embryonic day 10.5 (E10.5) in hepatocytes and biliary duct cells (Kellendonk et al., 2000). First, the complete loss of CLPP in the target tissue was confirmed at 15 weeks of age. Although not all liver cell types were targeted, no residual CLPP was observed (Figure 3.20 A). CLPP abundance in peripheral tissue (SkM) was not affected (Figure 3.20 A). In contrast to full body Clpp^{-/-} mice, Clpp^{LKO} and respective control mice were born at the expected Mendelian ratio, were fertile and did not display any signs of growth retardation (data not shown).

To investigate whether mitochondrial dysfunction due to CLPP deletion in liver is sufficient to alter whole body metabolism, body weight of $Clpp^{LKO}$ and $Clpp^{fl/fl}$ control mice was monitored. No significant difference in body weight was detected for males fed NCD until 15 weeks of age (Figure 3.20 B). Furthermore, glucose homeostasis of liver-specific $Clpp$ mice was analyzed by glucose and insulin tolerance tests at 15 and 16 weeks of age, respectively. Consistent with the unaltered body weight, the insulin sensitivity and glucose tolerance was not altered in $Clpp^{LKO}$ mice as compared to control mice (Figure 3.20 C, D).

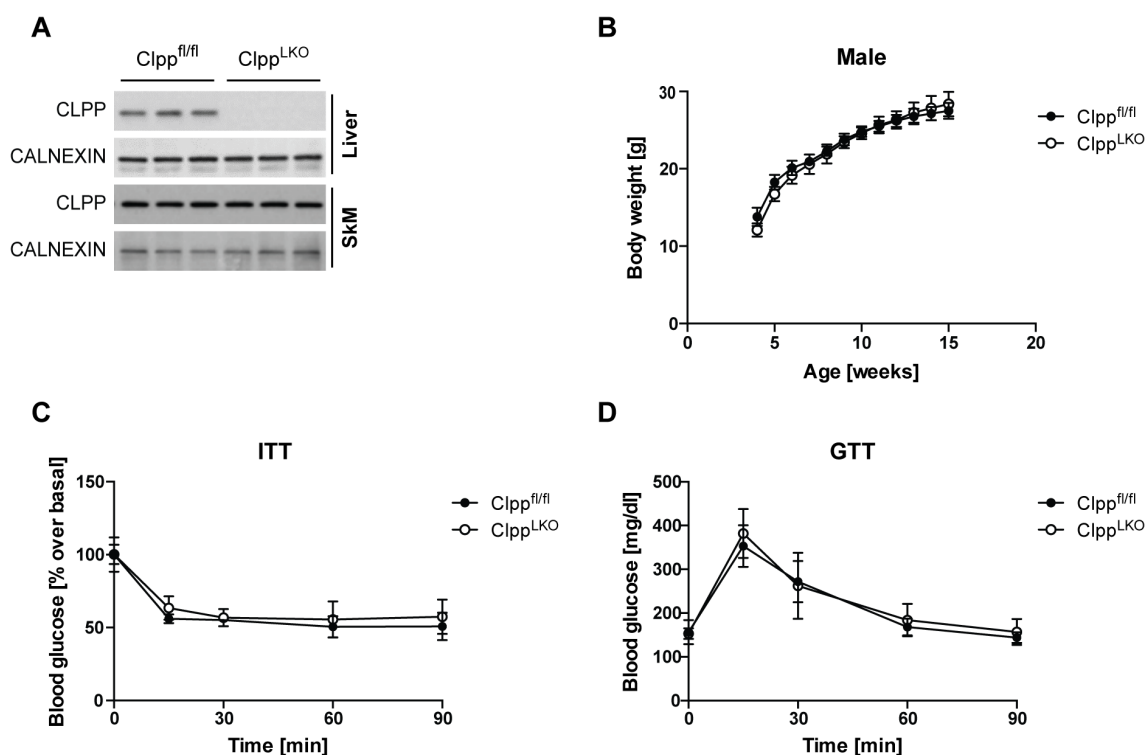


Figure 3.20 Liver restricted loss of CLPP does not alter body weight and glucose homeostasis. (A) Western Blot analysis of CLPP levels in liver and SkM of control ($Clpp^{fl/fl}$) and $Clpp^{LKO}$ mice. CALNEXIN serves as loading control (n=3). (B) Body weight of male control mice and $Clpp^{LKO}$ mice (n=7) was monitored till 15 weeks of age on normal chow diet (NCD). (C) Insulin tolerance test was performed on male control and $Clpp^{LKO}$ mice fed NCD (n=6). (D) Glucose tolerance test was performed after 6 h fast on male control and $Clpp^{LKO}$ mice fed NCD (n=6). Data are presented as mean \pm SD. GTT and ITT were performed together with Katharina Senft.

3.3.2 Liver restricted loss of CLPP alters FAO enzyme levels and leads to moderate mitochondrial dysfunction

Given the absence of a whole body phenotype of $Clpp^{LKO}$ mice, it was investigated whether liver-specific loss of CLPP causes tissue-specific alterations at the molecular level. First, the expression profile of FAO enzymes was examined in liver and SkM tissue lysates, SkM serving as negative control. Identical to full body $Clpp$ knockout

mice, the $Clpp^{LKO}$ mice present decreased CPT2 and increased VLCAD levels in liver, while the levels in SkM were not changed for CPT2 and downregulated for VLCAD in the presence of CLPP (Figure 3.21 A), thus further supporting VLCAD as possible CLPP substrate.

Next, mitochondrial complex levels were evaluated in liver of $Clpp^{LKO}$ and control mice. Deletion of hepatic CLPP results in decreased levels of assembled respiratory supercomplexes, while monomers or dimers of CoIII and CoIV, CoII and CoV were not altered (Figure 3.21 B). Thus, it can be suggested that mostly CoI and CoI-enclosing supercomplexes are affected by the absence of CLPP. Although the liver is an important organ contributing to whole body energy expenditure and glucose homeostasis, ablation of CLPP in liver does not alter body weight and glucose homeostasis, despite moderate hepatic mitochondrial dysfunction.

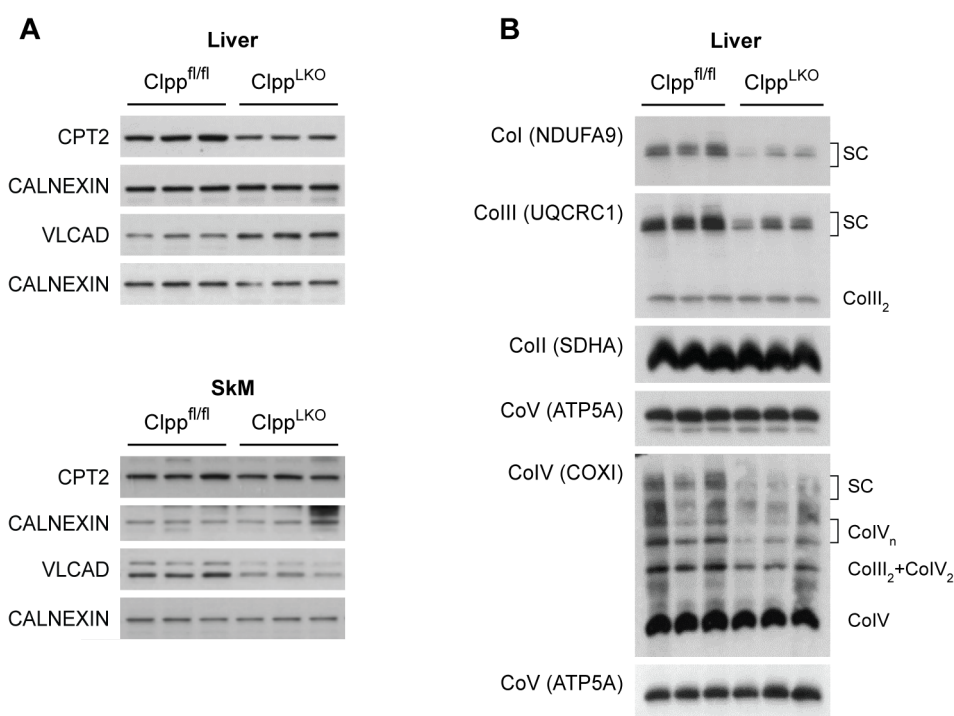


Figure 3.21 Hepatic deficiency of CLPP causes mitochondrial dysfunction and similar FAO profile as observed for $Clpp^{-/-}$ mice.

(A) Western blot analysis of CPT2 and VLCAD in liver tissue lysates of control and $Clpp^{LKO}$ mice ($n=3$). (B) BN-PAGE and subsequent Western blot analysis of mitochondrial respiratory chain supercomplexes of liver mitochondria from $Clpp^{fl/fl}$ and $Clpp^{LKO}$ mice ($n=6$). Antibodies against individual complex subunits (indicated in parenthesis) were used for the detection of assembled supercomplexes.

3.3.3 CLPP ablation in skeletal muscle and heart does not alter body weight and glucose homeostasis

Whole body loss of CLPP causes a substantial alteration of whole body energy metabolism. To elucidate the contribution of muscle tissue to this phenotype, CLPP was selectively ablated in heart and SkM. Therefore, $Clpp^{fl/fl}$ mice were mated with

mice expressing Cre recombinase under control of the creatine kinase promoter (Ckmm-Cre). The promoter is fully active in skeletal muscle and heart after embryonic day 15.5 (E15.5) (Lyons et al., 1991). Cre expression induced a selective disruption of the *Clpp* gene in SkM and heart of $Clpp^{MKO}$ mice as evidenced by Western blot analysis at 15 weeks of age (Figure 3.22 A). Liver extracts were used as negative control. In line with the liver-specific *Clpp* knockout mice, $Clpp^{MKO}$ were also born in the expected Mendelian proportions without any visible defects and further $Clpp^{MKO}$ were fertile. Again the body weight was followed for $Clpp^{MKO}$ and control mice ($Clpp^{fl/fl}$) fed NCD, to investigate the impact of muscle-specific CLPP deficiency on whole body metabolism. Both genotypes exhibited a similar weight gain reaching approximately 27 g body weight at the age of 15 weeks (Figure 3.22 B). To examine if the glucose homeostasis is still enhanced, while CLPP is merely ablated in muscle tissue, glucose and insulin tolerance tests were conducted. However, insulin sensitivity and glucose tolerance in $Clpp^{MKO}$ mice was indistinguishable from control animals (Figure 3.22 C, D).

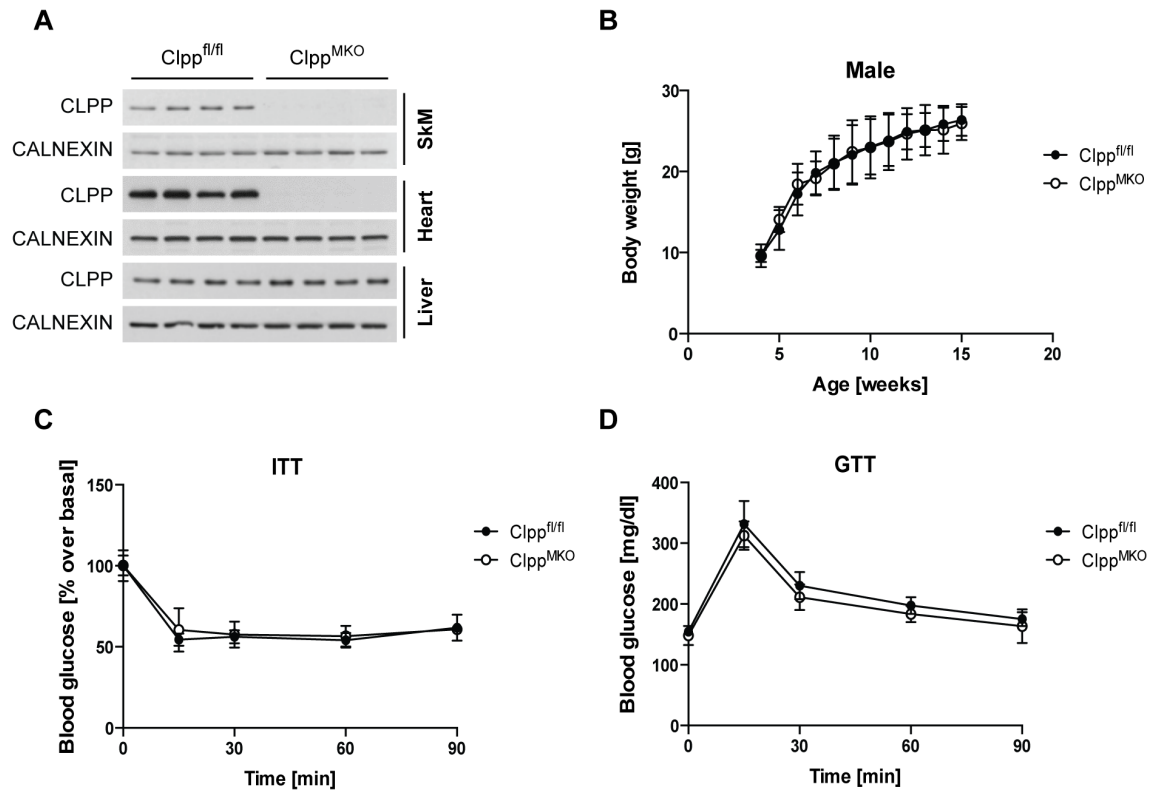


Figure 3.22 Skeletal muscle and heart restricted loss of CLPP does not alter body weight and glucose homeostasis.

(A) Western Blot analysis of CLPP levels in SkM, heart and liver of control mice (Clpp^{fl/fl}) and Clpp^{MKO} mice. CALNEXIN serves as loading control (n=4). (B) Body weight of male control mice and Clpp^{MKO} mice (n=6-7) was monitored till 15 weeks of age on normal chow diet (NCD). (C) Insulin tolerance test was performed on male control and Clpp^{MKO} mice fed NCD (n=6). (D) Glucose tolerance test was performed after 6 h fast on male control and Clpp^{MKO} mice fed NCD (n=6). GTT and ITT were conducted together with Katharina Senft.

3.3.4 Muscle restricted loss of CLPP induces FAO oxidation profile and causes mitochondrial dysfunction

To complement the analysis of VLCAD and CPT2 protein abundance, SkM, heart and liver were analyzed in Clpp^{MKO} and control mice. Consistently, VLCAD levels were increased in the absence of CLPP in SkM and heart of Clpp^{MKO} mice and CPT2 was downregulated, while the abundance of both proteins was similar in liver (Figure 3.23 A). If this finding has functional implications and leads to reduced fatty acid β -oxidation needs to be further addressed.

CLPP ablation in liver resulted in specific decrease of mitochondrial supercomplexes, most likely due to decreased levels of CoI. Thus, it was analyzed whether muscle mitochondrial complexes are affected in a similar manner by loss of CLPP. Interestingly, in SkM of Clpp^{MKO} a decrease in supercomplex levels was only apparent when probing with a CoI specific antibody (NDUFA9) (Figure 3.23 B, left panel). Supercomplex levels were not changed when antibodies against CoIII (UQCRC1) or CoIV (COXI) were used for immunodetection (Figure 3.23 B, left panel). Instead, liver

mitochondrial complex assembly and steady state levels were comparable between $Clpp^{MKO}$ and control mice. These results favor the assumption that there are no cell autonomous effects, nonetheless, relative *Fgf21* expression was determined in SkM and liver tissue. In line with the mitochondrial dysfunction, SkM of $Clpp^{MKO}$ exhibit increased *Fgf21* transcript levels as compared to $Clpp^{fl/fl}$ mice (Figure 3.23 C).

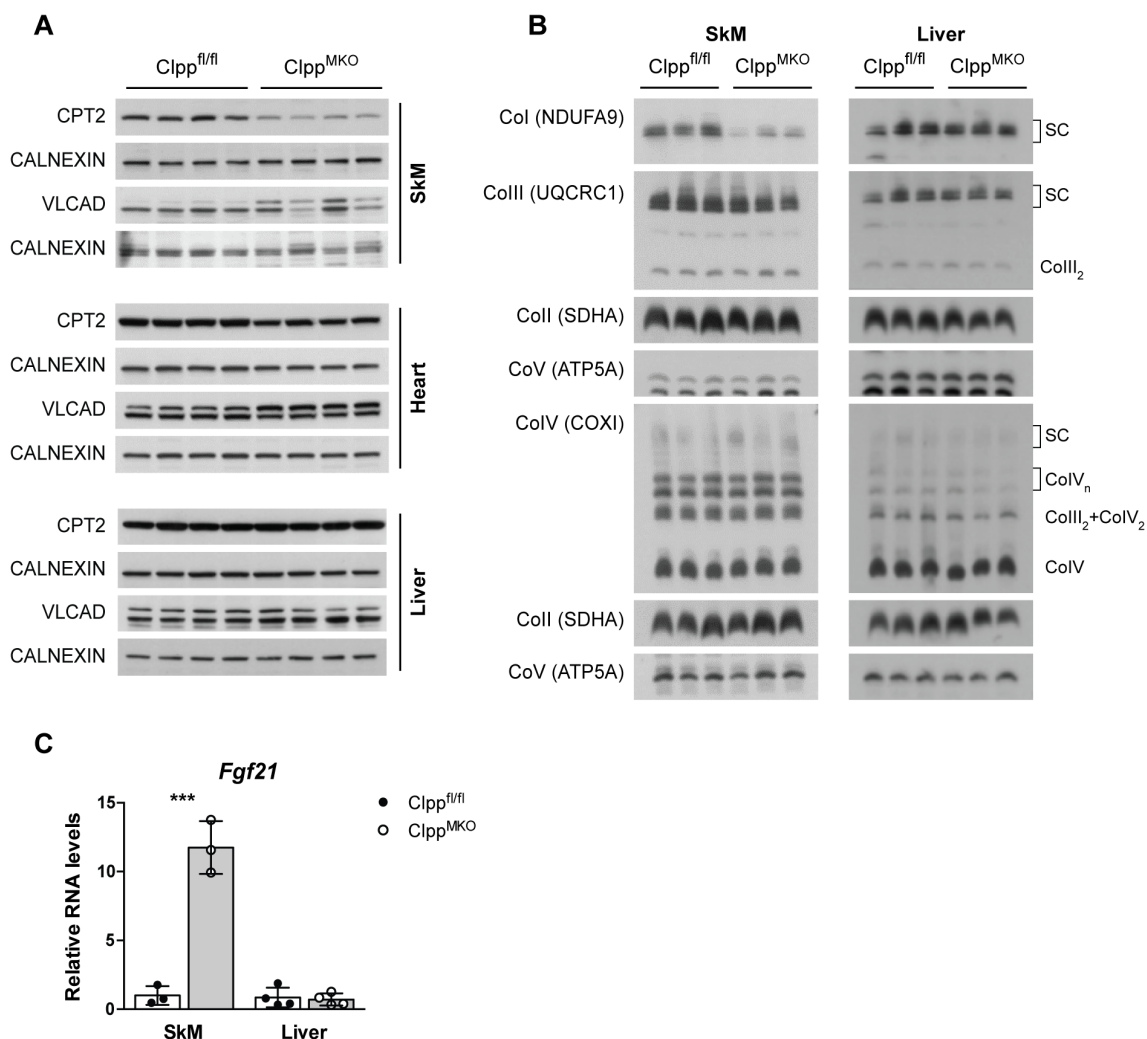


Figure 3.23 Muscle deficiency of CLPP causes mitochondrial dysfunction and similar FAO profile as observed for $Clpp^{-/-}$ mice.

(A) Western blot analysis of CPT2 and VLCAD in SkM, heart and liver tissue lysates of control and $Clpp^{MKO}$ mice (n=3). (B) BN-PAGE and subsequent Western blot analysis of mitochondrial respiratory chain supercomplexes of SkM mitochondria from $Clpp^{fl/fl}$ and $Clpp^{MKO}$ mice (n=6). Antibodies against individual complex subunits (indicated in parenthesis) were used for the detection of assembled supercomplexes. (C) *Fgf21* expression levels in SkM and liver of $Clpp^{fl/fl}$ and $Clpp^{MKO}$ mice (n=3-4). Data are presented as mean \pm SD (*P<0.05, **P<0.01, ***P<0.001; unpaired two-tailed t-test).

3.3.5 $Clpp^{MKO}$ mice exhibit functional shivering activity

Heat production is acquired by either shivering thermogenesis mediated by the SkM or non-shivering thermogenesis facilitated by BAT (Cannon and Nedergaard, 2010). Conventional whole body deletion of CLPP strongly impairs thermogenesis. Impaired

BAT function has been shown for $Clpp^{-/-}$ mice, however, it is not known to which extent shivering thermogenesis is affected. Thus, $Clpp^{MKO}$ mice were cold exposed to test whether loss of CLPP in muscle impairs shivering thermogenesis. The resting body temperature of control and $Clpp^{MKO}$ mice was not different ($t=0$) and also upon cold exposure both genotypes were equally capable in maintaining body temperature during the 7 h cold exposure (Figure 3.24 A). Hence, $Clpp^{MKO}$ mice display comparable shivering capacity and endurance than control mice. To exclude a compensatory increase of non-shivering thermogenesis in BAT of $Clpp^{MKO}$ mice, UCP1 was analyzed in BAT tissue lysates. UCP1 levels were decreased in BAT lysates of $Clpp^{MKO}$ mice, thus omitting increased non-shivering thermogenesis as a compensatory mechanism (Figure 3.24 B). The nature of decreased UCP1 expression needs to be further investigated, since PGC1 α levels were not changed, indicating no increase or decrease in mitochondrial biogenesis and therefore most likely also no change in mitochondrial mass.

Taken together, these data demonstrate, that tissue-specific loss of CLPP despite causing a tissue-restricted mild to moderate mitochondrial dysfunction, does not affect whole body metabolism.

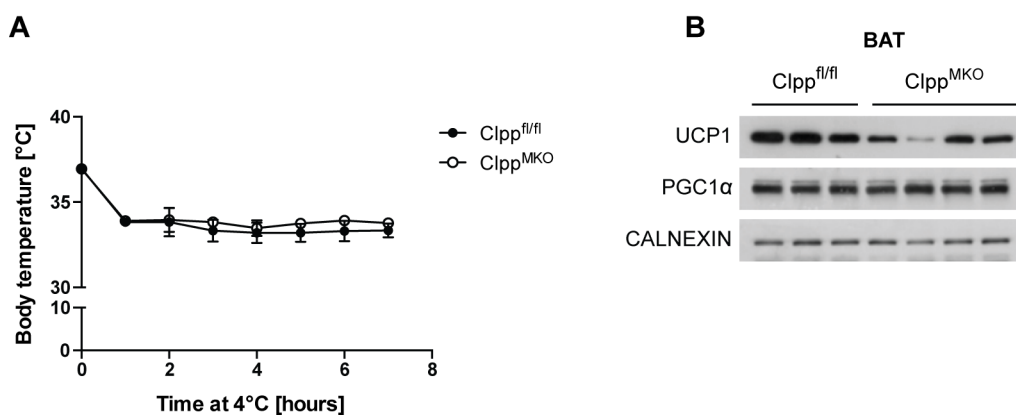


Figure 3.24 Cold induced adaptive thermogenesis is not impaired in $Clpp^{MKO}$ mice.

(A) Body temperature of $Clpp^{fl/fl}$ and $Clpp^{MKO}$ exposed to 4°C for 7 h ($n=3-4$). (B) Western blot analysis of thermogenic proteins in BAT lysates of $Clpp^{MKO}$ and control mice exposed to 4°C for 7 h ($n=3$).

3.4 High fat feeding impairs hepatic mitochondrial translation in the absence of CLPP

3.4.1 $Clpp^{-/-}$ mice maintain lean phenotype and enhanced glucose metabolism during HFD-feeding

To examine how CLPP deficient mice are able to cope with metabolic stress, $Clpp^{-/-}$ mice and control mice were fed high fat diet (HFD) providing 60% calories from fat (lard) from 8 weeks of age for a period of 8 weeks. CLPP ablated mice gained

significantly less weight in comparison to control mice irrespective of the gender (Figure 3.25 A, B). After 3 weeks on HFD the difference in body weight accounted for 35% and increased to 45%-50% after 7 weeks on HFD. Therefore, all subsequent experiments were performed at the age of 15-16 weeks after 8 weeks on HFD. First, the effect of HFD-feeding on the enhanced glucose homeostasis of $Clpp^{-/-}$ was investigated. In accordance with the preserved lean phenotype, the enhanced insulin sensitivity and glucose tolerance was retained in CLPP deficient mice as compared to control. Blood glucose levels of control mice were only marginally reduced by insulin (Figure 2.25 C), pointing out an insulin resistant state. To link the enhanced glucose metabolism with insulin signaling, the levels of insulin-stimulated phosphorylation of AKT and GLUT1 was analyzed in liver tissue. No difference was observed in the insulin-stimulated AKT phosphorylation and GLUT1 levels between $Clpp^{-/-}$ and control mice. However, a strong increase was observed for $Clpp^{-/-}$ mice when comparing basal (NaCl injected) and stimulated pAKT levels (insulin injected) (Figure 3.25 E, F), whereas there was no difference for control mice. This finding supports the result of the ITT, confirming the HFD induced insulin resistant state of control mice, while $Clpp^{-/-}$ mice remain insulin sensitive.

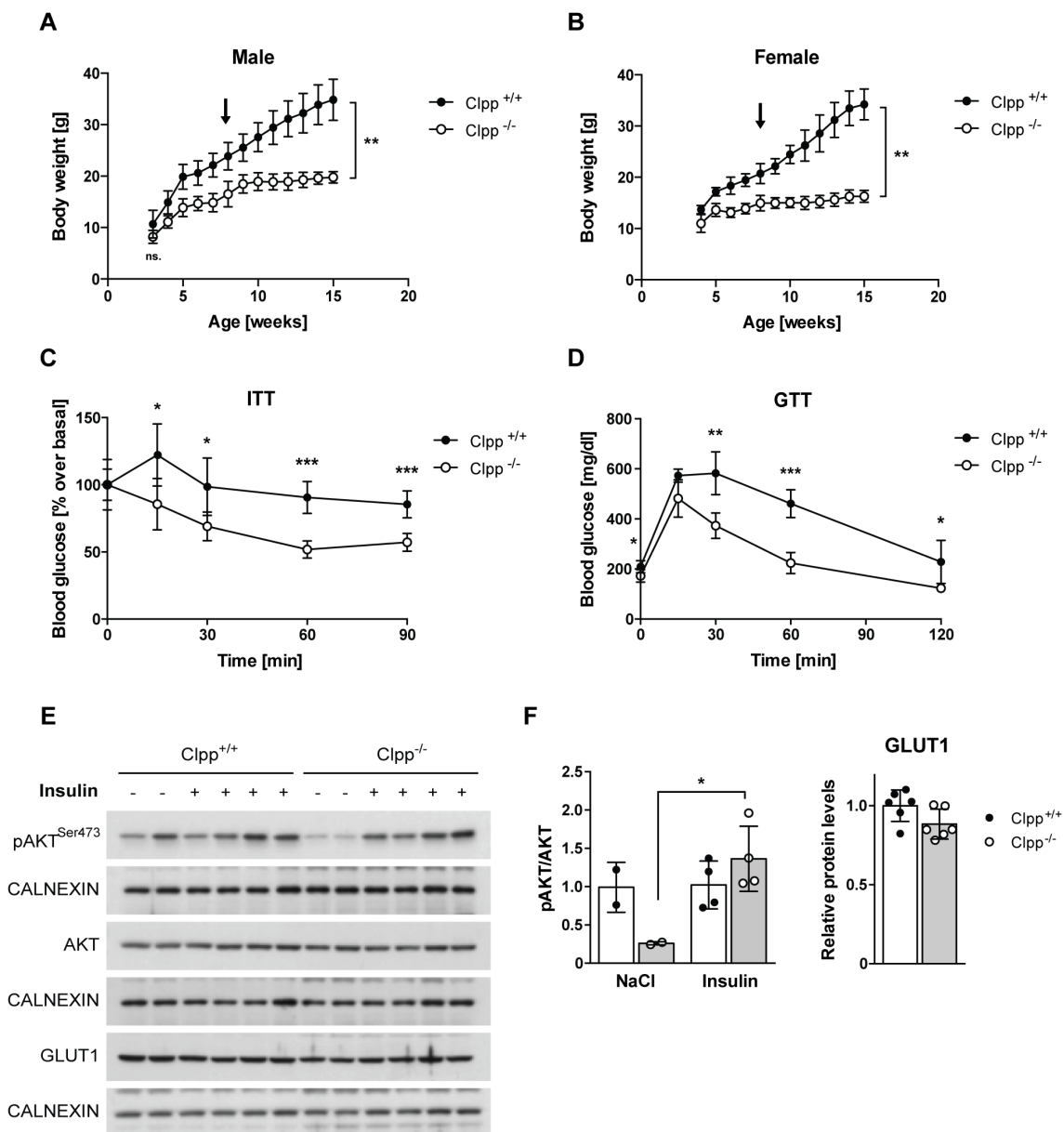


Figure 3.25 Loss of CLPP protects against HFD induced obesity.

(A) Body weight of male control and Clpp^{-/-} mice was monitored till 15 weeks of age fed HFD from 8 weeks of age. Arrow indicates start of HFD. (B) Body weight of female control and Clpp^{-/-} mice was monitored till 15 weeks of age fed high fat diet. (C) Insulin tolerance test was performed with 15-week-old control mice and Clpp^{-/-} mice after 7 weeks on HFD. (D) Glucose tolerance test was performed after 6 h fast with 16-week-old control mice and Clpp^{-/-} mice after 8 weeks on HFD. (E) Western blot analysis of phosphorylated and total AKT in liver tissue lysates of control and Clpp^{-/-} mice, which were fasted for 2 h and then insulin-stimulated for 30 min (-/+). CALNEXIN serves as loading control. (F) Quantification of Western blots shown in (E). Data are presented as mean \pm SD (*P<0.05, **P<0.01, ***P<0.001; unpaired two-tailed t-test). GTT, ITT and Insulin signaling experiment were performed together with Dr. Alexandra Kukat.

To further corroborate the resistance to diet induced obesity of Clpp^{-/-} mice serum parameters were analyzed. As it was revealed for the NCD, non-fasting and fasting blood glucose levels of Clpp^{-/-} mice were also significantly lower during HFD-feeding. In addition, HFD exposure induced a strong increase in insulin and leptin in control mice,

whereas $Clpp^{-/-}$ mice displayed levels comparable to NCD conditions (Figure 3.26 B, C). Further, increased levels of ghrelin and glucagon were obtained for $Clpp^{-/-}$ mice, thus demonstrating an augmentation of the fasting-like phenotype previously observed during NCD feeding (Figure 3.26 D, E). In line with reduced insulin levels, GIP serum levels were also decreased in $Clpp^{-/-}$ mice although GLP-1 was not distinctive between control and CLPP deficient mice (Figure 3.26 F, G). Resistin is secreted from adipocytes and links obesity and insulin resistance (Steppan et al., 2001). In agreement with this, $Clpp^{-/-}$ mice exhibit lower levels of resistin compared to control mice fed HFD (Figure 3.26 H). Taken together, HFD-feeding affirms the fasting-like phenotype of $Clpp^{-/-}$ mice.

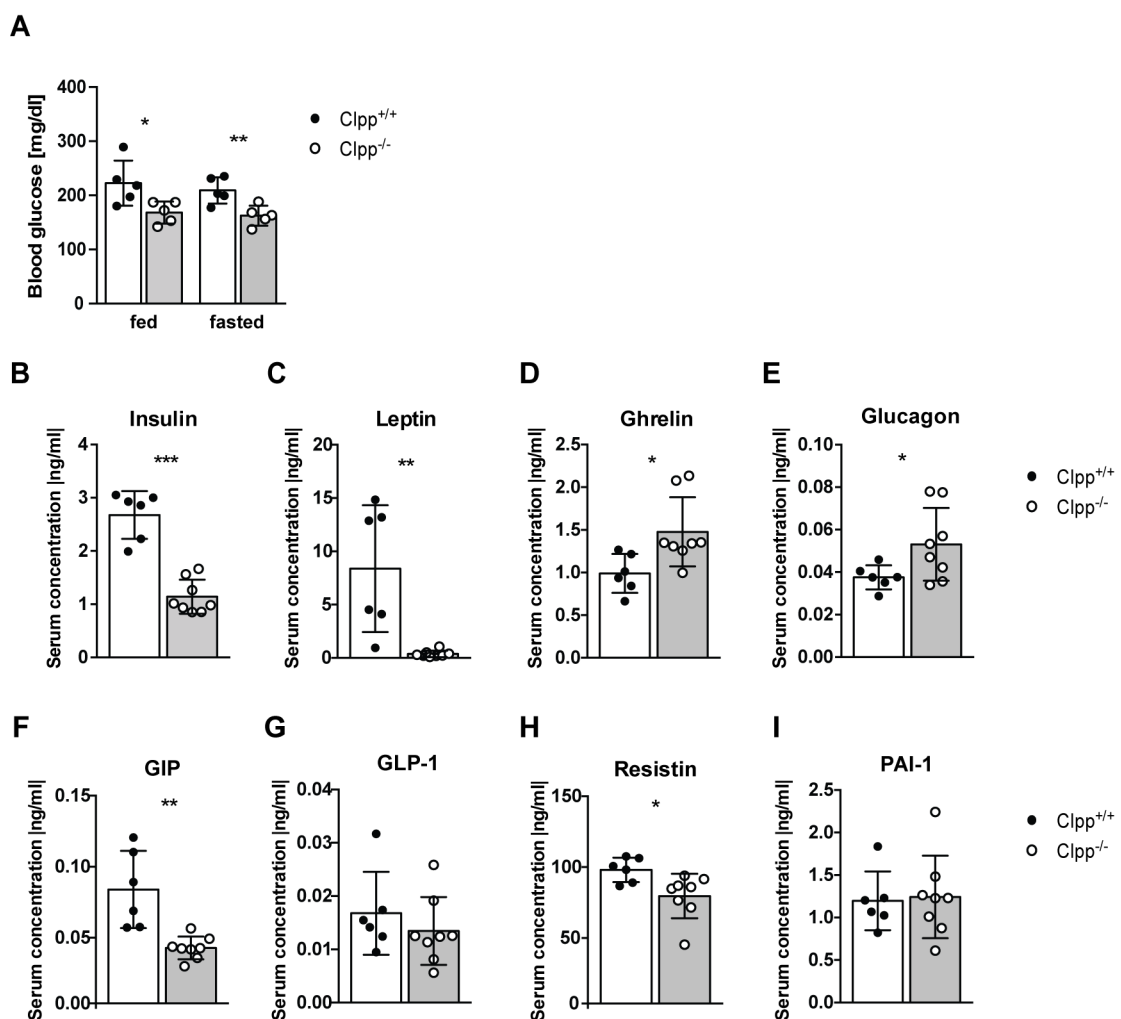


Figure 3.26 Serum parameters of control and CLPP deficient mice fed HFD.

(A) Fed and fasted blood glucose levels of control and $Clpp^{-/-}$ mice at 15 weeks of age after 7 weeks on HFD. (B-I) Analysis of serum metabolic markers in $Clpp^{-/-}$ and control at 16 weeks of age (B) Insulin (C) Leptin (D) Ghrelin (E) Glucagon (F) Glucose-dependent insulinotropic polypeptide (GIP) (G) Glucagon-like peptide 1 (GLP-1) (H) Resistin (I) Plasminogen activator inhibitor-1 (PAI-1). Data are presented as mean \pm SD (* P <0.05, ** P <0.01, *** P <0.001; unpaired two-tailed t-test).

Since the uptake of excess nutrients leads to lipid accumulation not only in adipose tissue but also in liver, it was investigated whether loss of CLPP protects against HFD induced lipid accumulation. Whereas control mice fed HFD exhibit a clear hypertrophy of adipocytes of the EWAT, $Clpp^{-/-}$ mice failed to accumulate lipids relative to NCD fed $Clpp^{-/-}$ mice (Figure 3.27). In contrast, for the subcutaneous adipose depot no difference was observed and the lipid accumulation in BAT of $Clpp^{-/-}$ mice was deteriorated by HFD-feeding. For liver no significant difference was observed for the lipid accumulation based on the histological analysis (Figure 2.27).

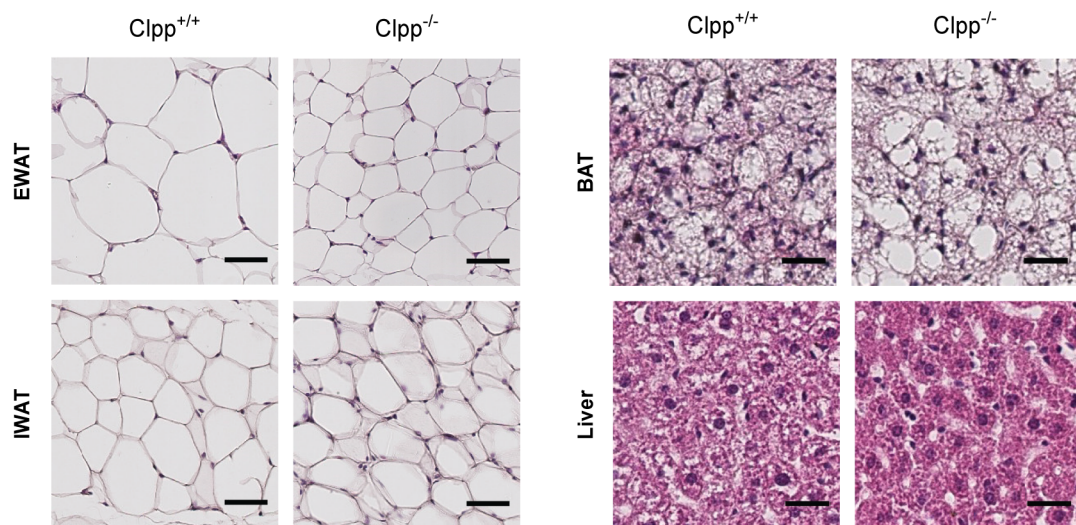


Figure 3.27 $Clpp^{-/-}$ mice are protected against HFD induced hypertrophy of EWAT.

Histological analysis of EWAT, IWAT, BAT and liver tissue of control and $Clpp^{-/-}$ mice on HFD-feeding (n=4). Scale bar 50 μ m.

Considering the decreased FAO rate in liver of $Clpp^{-/-}$ mice fed NCD and the similar liver morphologies of control and $Clpp^{-/-}$ mice fed HFD, the question arose whether the FAO gene expression profile would have changed due to the change in diet. Interestingly, HFD-feeding increased CPT2 abundance in CLPP deficient liver to a similar level of control mice (Figure 3.28 A, B). As expected for a putative CLPP substrate, VLCAD expression was not changed by the HFD treatment and was 3-fold increased in $Clpp^{-/-}$ mice as previously revealed for the NCD. Thus, it can be concluded that due to the increased VLCAD protein levels in $Clpp^{-/-}$ mice, CPT2 is regulated dependent on the metabolic requirements.

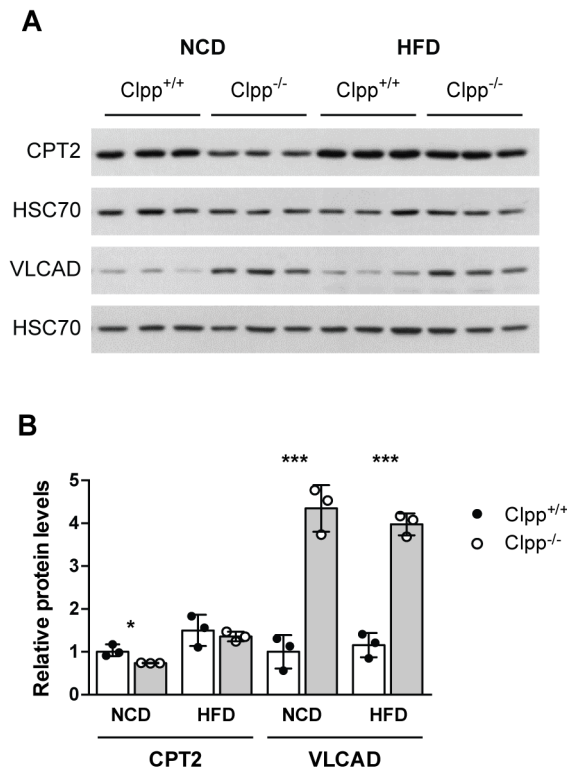


Figure 3.28 CPT2 is upregulated upon HFD-feeding in Clpp^{-/-} mice.

(A) Western blot analysis of CPT2 and VLCAD in liver of control and Clpp^{-/-} mice at 5 weeks of age, fed NCD or HFD (n=3). HSC70 serves as loading control. (B) Quantification of CPT2 and VLCAD Western blots shown in (A). Data are presented as mean \pm SD (*P<0.05, **P<0.01, ***P<0.001; unpaired two-tailed t-test).

3.4.2 Label-free quantitative proteomic profiling of liver reveals deregulated OXPHOS subunit levels due to HFD-feeding upon loss of CLPP

Mass spectrometric analysis of liver tissue was performed to establish a comprehensive map of protein abundance to understand the impact of loss of CLPP during NCD or HFD-feeding. Using label-free quantitative proteomics it was possible to quantify a total of 1050 proteins of which 278 were annotated mitochondrial proteins. The approach applied (4h gradient) generally recovers between 4000 and 5000 proteins. The low recovery observed here was due to low resolution of the mass spectrometric device and the requirement that peptides were quantified in at least three samples out of four (NCD) or five (HFD). Proteins were considered significantly deregulated for p-values <0.05 (-log p-value >1.3) and a false discovery rate (q-value) of 0.1. In liver of NCD fed Clpp^{-/-} mice only 17 proteins were found to be differently abundant as compared to NCD fed control mice (Figure 3.29 A), which is in line with previous experiments, which showed that the phenotype of liver tissue was not much changed by loss of CLPP. Proteins, which were significantly changed in abundance, are involved in the following processes; protein folding, mitochondrial transcription and translation and TCA cycle. An increase in the mitochondrial chaperones TRAP1,

mtHSP70 and GRPEL1 indicates a mildly disturbed mitochondrial proteome in liver of *Clpp*^{-/-} mice. LRPRRC, EFG1 and OGDH are putative CLPP substrates involved in mitochondrial transcription, translation and TCA cycle and were elevated in the absence of CLPP, as we previously published for heart mitochondria (Szczepanowska et al., 2016). Loss of CLPP during HFD-feeding leads to more pronounced proteomic changes in the liver with a total of 128 proteins changed in relative abundance (Figure 3.29 B). The most affected biological processes are identical to the NCD, however, in addition OXPHOS was strongly affected. Both nuclear- and mitochondrial-encoded respiratory chain subunits were upregulated or downregulated due to the loss of CLPP only during HFD-feeding with predominantly altered CoI subunits. Moreover, almost every enzyme of the TCA cycle was found to be increased or decreased in CLPP ablated liver confirming previous results (Fischer et al., 2015). Interestingly, 18 proteins of the large (60S) and small (40S) cytosolic ribosomal subunits were downregulated in liver of HFD fed *Clpp*^{-/-} mice, most likely due to a secondary effect. Taken together, liver proteomic analysis revealed only minor changes of the liver proteome due to loss of CLPP during NCD conditions, which correlates with previous results, whereas HFD-feeding in the absence of CLPP strongly affects OXPHOS subunits.

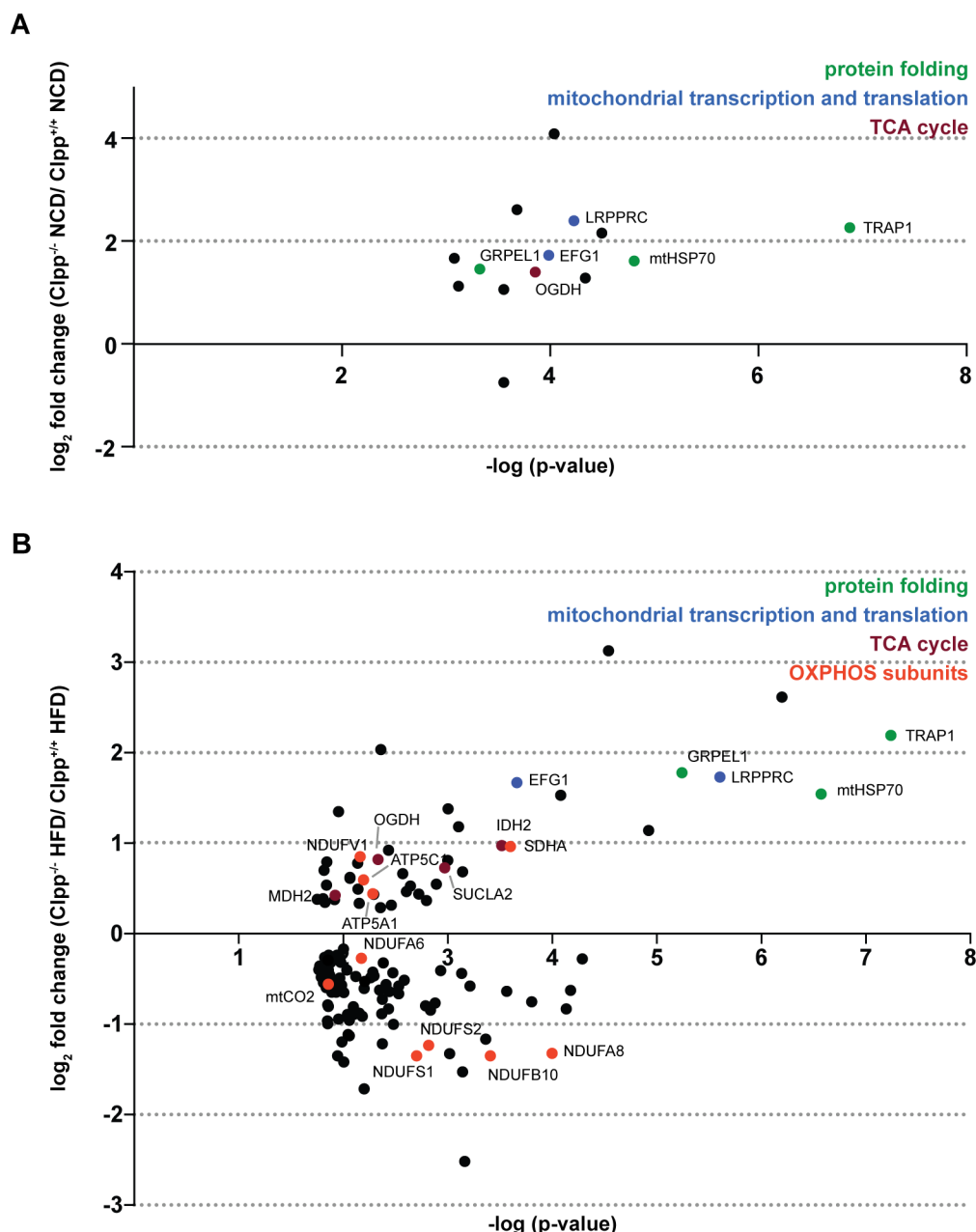


Figure 3.29 Quantitative assessment of liver proteomes of CLPP deficient mice fed NCD or HFD. Proteins were quantified by label-free proteomic analysis. (A-B) Volcano plots of differential abundance of liver proteins between *Clpp*^{-/-} and *Clpp*^{+/+} NCD (A) and *Clpp*^{-/-} and *Clpp*^{+/+} HFD (B) (n=4). Proteins are plotted according to statistical significance ($-\log_{10}$ p-value) and relative abundance (\log_2 fold change) (FDR<0.1).

3.4.3 Loss of CLPP during HFD-feeding leads to strong decrease only in hepatic mitochondrial respiratory chain complexes

Proteomic analysis disclosed changes in hepatic mitochondrial OXPHOS subunit levels in response to HFD-feeding in the absence of CLPP. To assess whether these changes impair mitochondrial function, assembly of mitochondrial complexes was investigated in liver mitochondria of NCD and HFD fed mice. BN-PAGE analysis demonstrates that lack of CLPP only had a minor effect on complex and supercomplex

levels under NCD, while having a profound effect on the levels of CoI, CoIII and CoIV comprising supercomplexes upon HFD (Figure 3.30 A). Notably, almost no difference was observed for CoIV monomers, CoIII and CoIV dimers, CoII and CoV complexes, suggesting CoI to be the primary cause for the decreased supercomplexes. Thus, loss of CLPP during HFD-feeding severely impairs OXPHOS integrity.

A similar dietary intervention to HFD-feeding with a large proportion of dietary fat is the maternal lactation period during the first weeks after birth. Maternal milk contains roughly 29.8% fat compared to 34% crude fat in the HFD, that corresponds to 53% and 60% calories provided from fat during lactation and HFD, respectively (Görs et al., 2009). Thus, it was analyzed if maternal lactation has the same effect as HFD-feeding upon loss of CLPP in liver. To do so, liver mitochondria of 5-week-old CLPP deficient and control mice were used for the examination of complex levels. Mitochondrial supercomplex levels were decreased to the same extent as shown for liver mitochondria of HFD fed *Clpp*^{-/-} mice (Figure 3.30 B). Thus, it can be concluded that loss of CLPP during metabolic challenging conditions like HFD-feeding or during lactation is detrimental for mitochondrial supercomplex abundance. Although, the levels of assembled complexes haven't been analyzed in the liver it can be assumed that they would also be reduced during HFD-feeding as it was observed for loss of CLPP in heart mitochondria under NCD conditions (Szczepanowska et al., 2016).

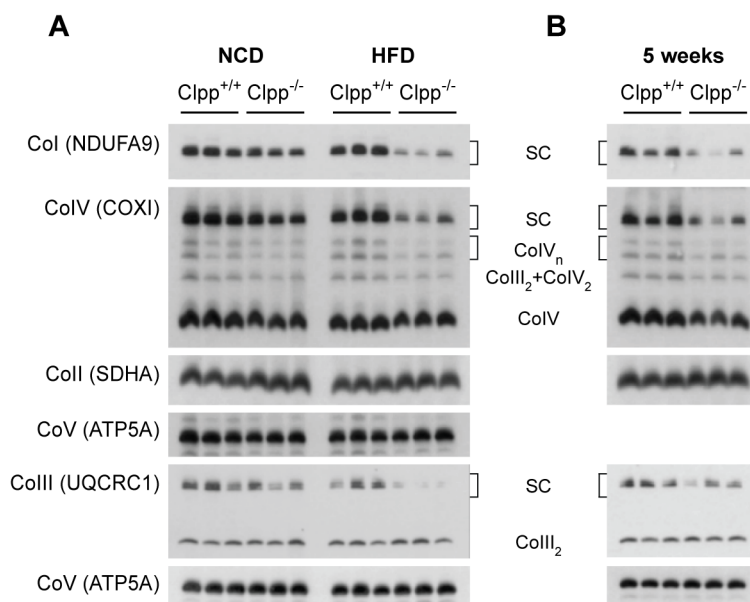


Figure 3.30 High dietary fat content causes mitochondrial dysfunction in liver.

(A-B) BN-PAGE and subsequent Western blot analysis of mitochondrial supercomplexes of liver mitochondria from control and *Clpp*^{-/-} mice fed either NCD or HFD (A) and 5-week-old *Clpp*^{-/-} mice and controls (B) (n=3). Antibodies against individual complex subunits (indicated in parenthesis) were used for the detection of assembled complexes.

To distinguish whether an assembly defect or decreased abundance of individual complex subunits during metabolic stress conditions could account for the observed phenotype, steady state levels of several mitochondrial complex subunits were assessed. On NCD, CLPP deficient liver displayed decreased levels of mitochondrial complex subunits for two out five analyzed CoI subunits, ND1 (mitochondrial-encoded) and NDUFS2 (nuclear-encoded)(Figure 3.31 A, C). In addition, CoIII subunits (UQCRC1 and UQCRFS1) and the mitochondrial-encoded CoIV subunit COXI were decreased. In contrast, steady state levels of SDHA and ATP5A were increased in *Clpp*^{-/-} liver mitochondria (Figure 3.31 A, C). Certainly, HFD-feeding had an even stronger influence on the level of complex subunits when CLPP was lost. The levels of ND1 and NDUFS2 were further reduced and in addition also the CoI subunits NDUFA9 and NDUFB6 were decreased in the absence of CLPP (Figure 3.31 A, D). Furthermore, steady state levels of two CoIV subunits, COXII (mitochondrial-encoded) and COXIV (nuclear-encoded) were reduced in CLPP deficient liver mitochondria of HFD fed mice. Unlike on NCD, CoIV subunit COXI was not decreased in HFD CLPP deficient liver mitochondria. Similar to the HFD data, CoI mitochondrial subunits were strongly decreased in liver mitochondria isolated from 5-week-old *Clpp*^{-/-} mice. Besides the CoI subunits, only the CoIII subunit UQCRFS1 was downregulated in CLPP deficient liver mitochondria at the age of 5 weeks (Figure 3.31 B, E). Hence, the decreased assembled supercomplexes during HFD-feeding and after lactation are resulting from diminished individual complex subunits, in particular of CoI.

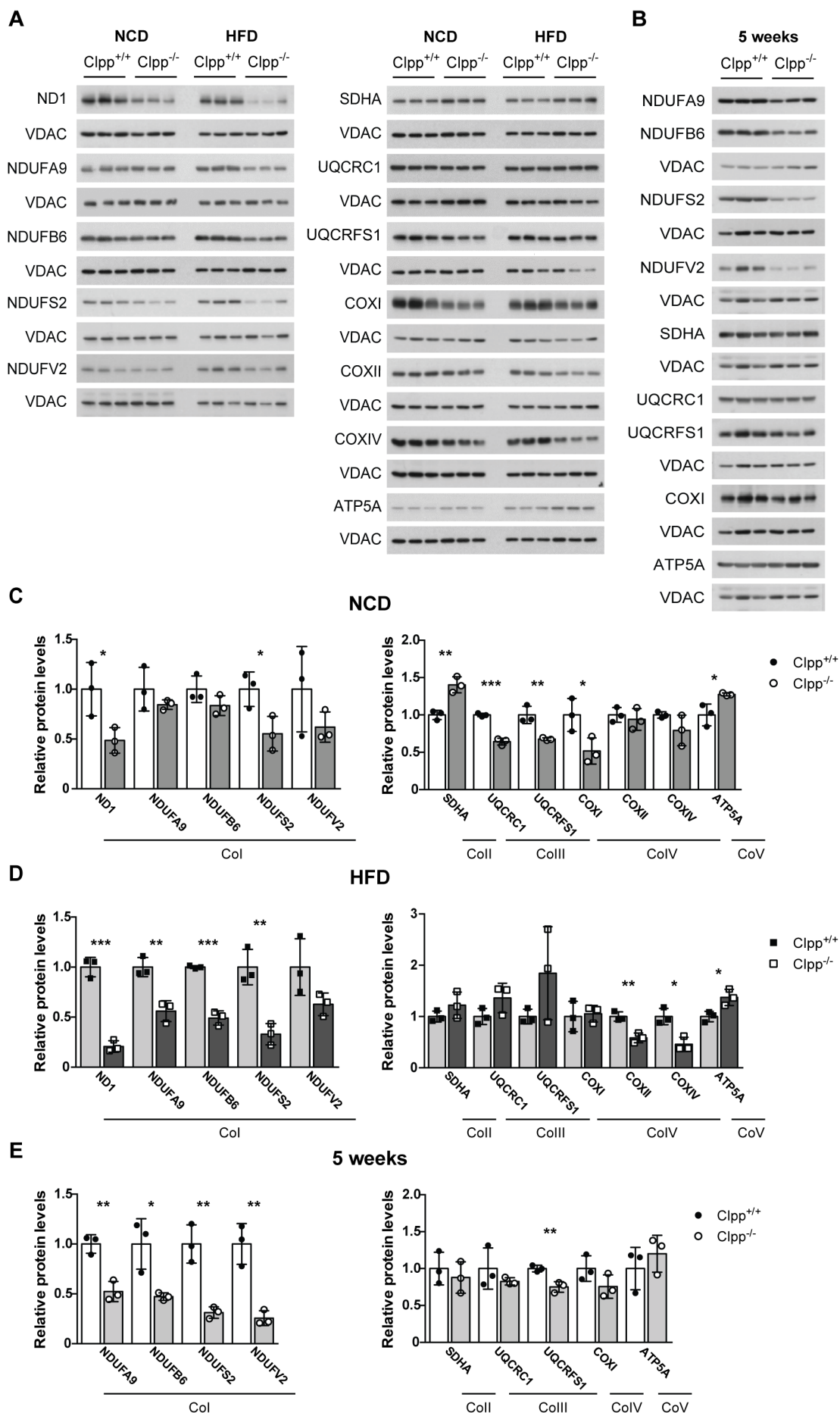


Figure 3.31 Decreased steady state levels of mitochondrial and nuclear-encoded complex I subunits in 5-week-old and HFD fed Clpp^{-/-} mice.

Figure 3.31 Decreased steady state levels of mitochondrial and nuclear-encoded complex I subunits in 5-week-old and HFD fed Clpp^{-/-} mice.

(A) Western blot analysis of individual complex subunits in liver mitochondria of 15-week-old NCD and HFD diet fed control and Clpp^{-/-} mice. Left panel - complex I subunits, right panel - other complex subunits (n=3-6). (B) Western blot analysis of individual complex subunits in liver mitochondria of 5-week-old control and Clpp^{-/-} mice (n=3). VDAC serves as loading control. (C) Quantification of relative mitochondrial complex subunit levels in liver of control and Clpp^{-/-} mice fed NCD. (D) Quantification of relative mitochondrial complex subunit levels in liver of control and Clpp^{-/-} mice fed HFD. (E) Quantification of relative mitochondrial complex subunit levels in liver of control and Clpp^{-/-} mice at 5 weeks of age. Data are presented as mean ± SD (*P<0.05, **P<0.01, ***P<0.001; unpaired two-tailed t-test).

Having found this effect in liver, it was examined whether this response to HFD is conserved and is likewise present in SkM. Therefore, SkM muscle mitochondria from NCD and HFD fed Clpp^{-/-} mice and control mice were analyzed for levels of respiratory supercomplexes and the levels of individual complex subunits. Strikingly, reduction of mitochondrial supercomplexes and complexes was not differently affected by either NCD or HFD-feeding upon loss of CLPP (Figure 3.32 A). The same could be observed for heart mitochondria (personal communication with Dr. Karolina Szczepanowska). To confirm this finding the levels of individual mitochondrial complex subunits were determined in SkM mitochondria. There was not a consistent tendency for the different complex subunits evident, since some subunits were decreased, whereas others were not changed (Figure 3.32 B, C). Hence, HFD-feeding does not affect SkM and heart mitochondrial complex levels upon loss of CLPP. Since SkM mitochondria do not display the differential response to HFD due to loss of CLPP, the further analysis focused on liver.

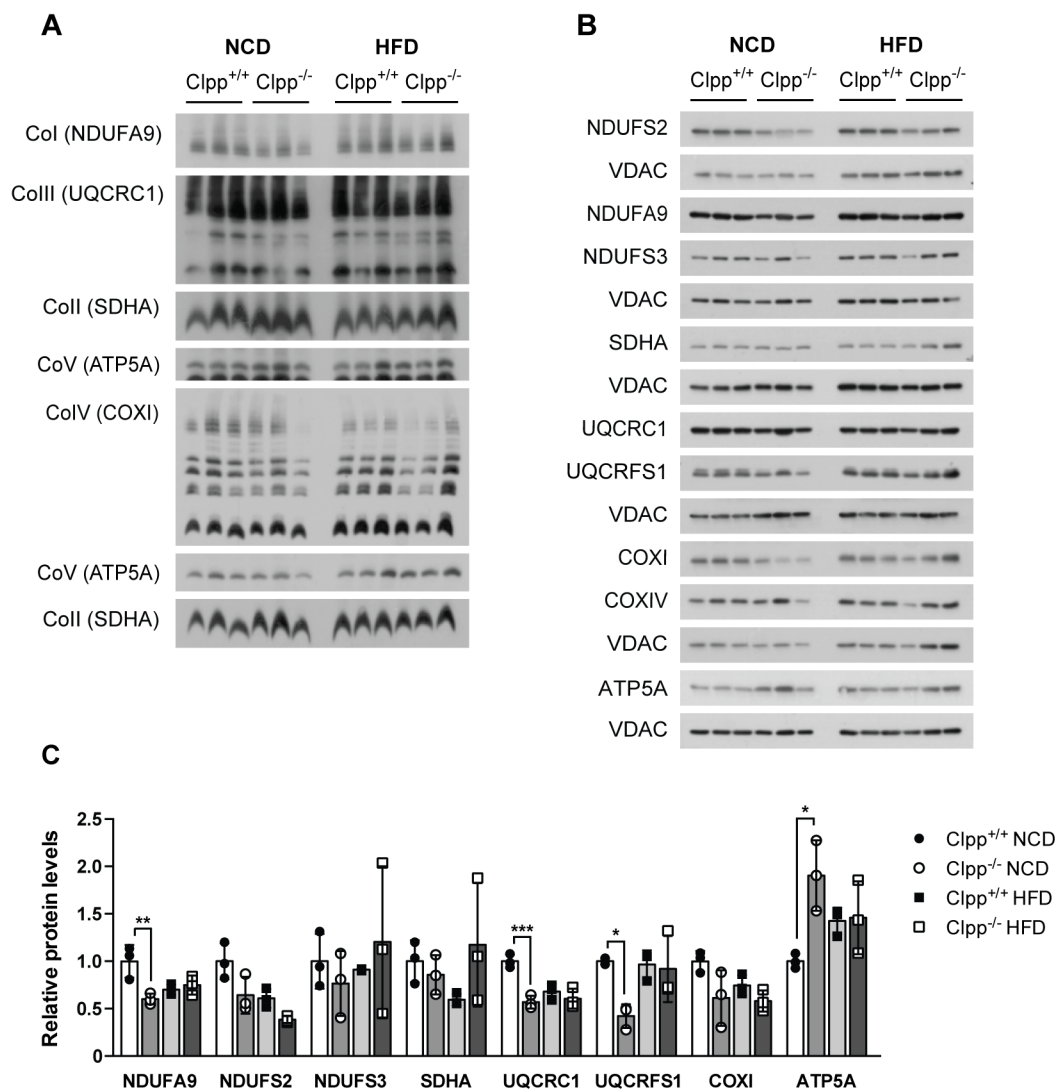


Figure 3.32 Complex composition is not affected by HFD-feeding in CLPP deficient SkM mitochondria.

(A) Mitochondrial supercomplex levels in SkM mitochondria of control and Clpp^{-/-} mice fed NCD or HFD assessed by BN-PAGE and subsequent Western blot analysis. Antibodies against individual complex subunits (indicated in parenthesis) were used for the detection of assembled complexes. (B) Western blot analysis and (C) relative quantification of individual mitochondrial respiratory complex subunits in SkM mitochondria (n=3). VDAC serves as loading control. Data are presented as mean \pm SD (*P<0.05, **P<0.01, ***P<0.001; one-way ANOVA, Tukey's post hoc test).

3.4.4 Decreased hepatic mitochondrial complex subunits in HFD fed Clpp^{-/-} mice are not caused by increased turnover

CLPP was previously shown to have a function in mitochondrial translation in heart (Szczepanowska et al., 2016). Therefore, the reduced levels of mitochondrial respiratory complex subunits in CLPP deficient liver could likewise result from impaired mitochondrial translation and a consequential imbalance of nuclear-encoded subunits. To exclude other mechanisms of being involved, it was first analyzed whether decreased complex subunits result from increased turnover by the protein quality control machinery. Since only few mitochondrial complex subunits are known targets of

the m-AAA protease (Edgar et al., 2009; Hornig-Do et al., 2012), AFG3L2 and also LONP1 and mtHSP70 levels were examined in liver mitochondrial lysates. However, AFG3L2 was decreased in liver of $Clpp^{-/-}$ mice fed NCD compared to control mice and the levels were further decreased in $Clpp^{-/-}$ mice when fed HFD, whereas AFG3L2 levels of control mice did not differ between NCD and HFD (Figure 3.33 A). No significant difference was observed for LONP1 between control and $Clpp^{-/-}$ mice fed either NCD or HFD, yet LONP1 levels increased for both genotypes on HFD as compared to NCD. For the mitochondrial chaperone mtHSP70 increased levels were observed in CLPP deficient liver mitochondria only on NCD, whereas no difference was observed for control and $Clpp^{-/-}$ mice on HFD (Figure 3.33 A). Since the proteomic analysis of liver tissue revealed an increase of mtHSP70 for $Clpp^{-/-}$ mice in both dietary conditions, there seems to be a biogenesis effect. Thus, the decreased levels of mitochondrial complex subunits are most likely not a result of increased turnover or impaired folding.

To explore whether increased mitochondrial biogenesis could contribute to the reduction of mitochondrial complex subunits, the steady state levels of biogenesis-related transcription factors and markers of mitochondrial mass were analyzed in liver tissue lysates. Both markers of mitochondrial content (VDAC and TOMM20) as well as transcription factors TFAM and PGC1 α were significantly increased upon loss of CLPP during HFD-feeding in liver tissue as compared to HFD fed control mice (Figure 3.33 C, D), indicating an increased mitochondrial content in CLPP deficient liver during HFD-feeding. This finding was confirmed by ultrastructural analysis of liver tissue from control and $Clpp^{-/-}$ mice. Mitochondrial morphology and number were not different between control and $Clpp^{-/-}$ mice on NCD. A strong difference in mitochondrial number was apparent for HFD fed control and $Clpp^{-/-}$ mice (Figure 3.33 G). Thus, it is possible that due to the increased mitochondrial biogenesis/mass the mitochondrial protein synthesis is not able to meet the requirements. Hence, loss of CLPP during metabolic challenging conditions like HFD induces mitochondrial biogenesis to compensate the energy deficiency due to the mitochondrial dysfunction.

Mitochondrial dynamics are implicated to play a role in adaptations to different energy states. Mitochondrial fusion is supposed to function as a repair mechanism, by allowing content mixing and preventing mitophagy (Gomes et al., 2011). Thus, it was analyzed whether altered mitochondrial fusion is contributing to the observed phenotype. No significant differences were observed for the abundance of OPA1, MFN1 and MFN2 in between control and CLPP depleted liver mitochondria of NCD or HFD fed mice (Figure 3.33 E, F). Notably, all fusion proteins were increased in HFD fed control and $Clpp^{-/-}$ mice, indicating an increased need for fusion mediated quality control.

Taken together, these data demonstrate that decreased mitochondrial complex subunits in $Clpp^{-/-}$ mice upon HFD-feeding are not resulting from increased turnover, however, are possibly influenced by increased biogenesis.

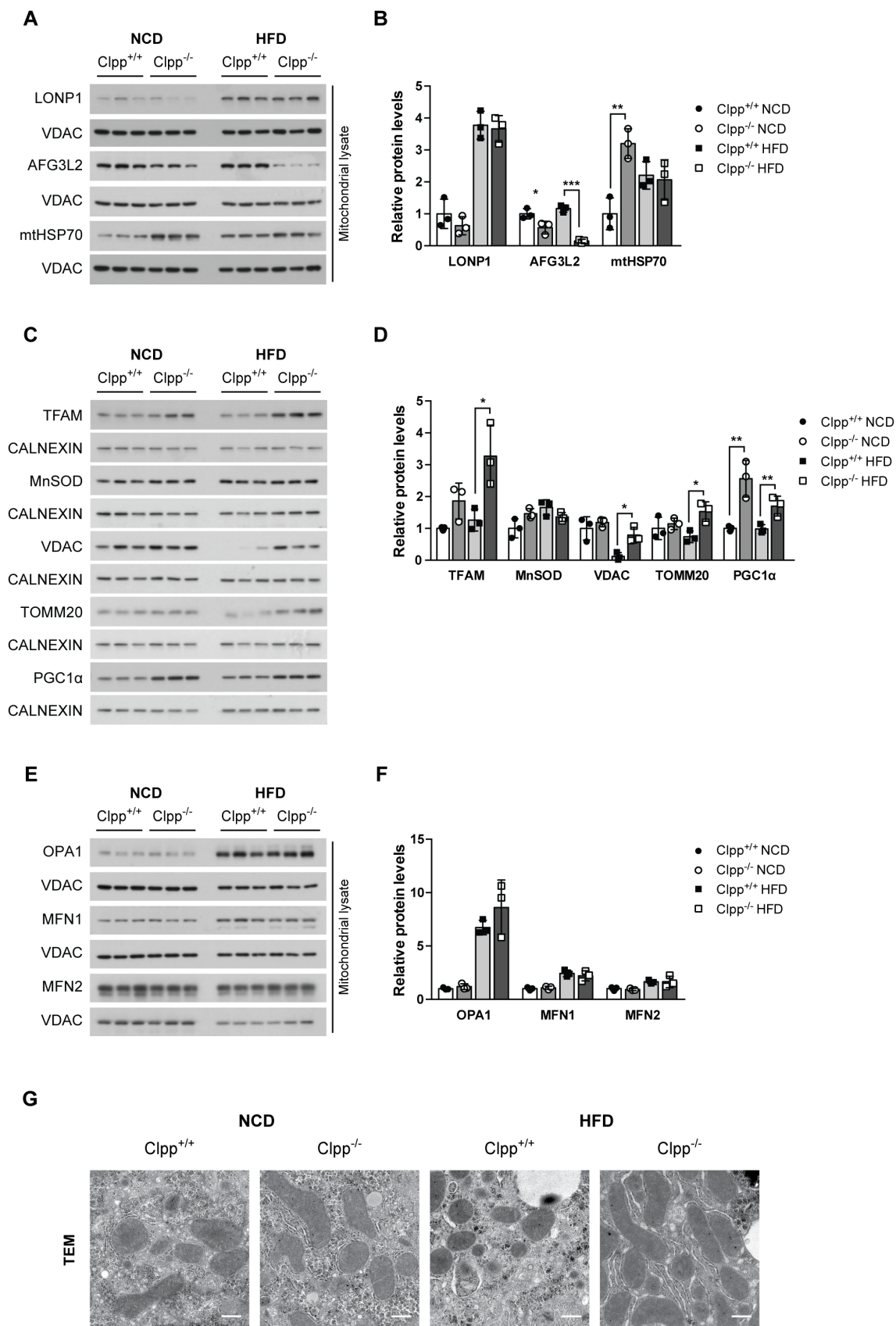


Figure 3.33 Decreased mitochondrial complex subunits in liver do not result from increased turnover or altered fusion events rather from increased biogenesis.

Figure 3.33 Decreased mitochondrial complex subunits in liver do not result from increased turnover or altered fusion events rather from increased biogenesis.

(A) Western blot analysis and (B) relative quantification of mitochondrial proteases and mtHSP70 in liver mitochondrial lysates of control and CLPP deficient mice fed NCD or HFD (n=3). VDAC is used as loading control. (C) Western blot analysis and (D) relative quantification of mitochondrial proteins indicative for mitochondrial biogenesis in liver extracts of control and Clpp^{-/-} mice (n=6). CALNEXIN is used as loading control. Data are presented as mean ± SD (*P<0.05, **P<0.01, ***P<0.001; one-way ANOVA, Tukey's post hoc test). (E) Western blot analysis of mitochondrial fusion proteins in isolated liver mitochondria of control and CLPP deficient mice fed NCD or HFD (n=3). VDAC serves as loading control. (F) Quantification of relative protein levels of blots shown in (E). (G) Transmission electron micrographs of liver tissue of control and Clpp^{-/-} mice fed NCD or HFD (Scale bar 0.5 μm) (n=3).

3.4.5 Loss of CLPP causes increased mitochondrial mRNA levels and reduced *de novo* protein synthesis with an aggravating effect of HFD

To decipher whether mitochondrial protein synthesis is accounting for the decreased levels of mitochondrial-encoded complex subunits in liver of Clpp^{-/-} mice during HDF-feeding, first mitochondrial transcription was assessed by determining levels of mitochondrial rRNAs and mRNAs using Northern blot. In agreement with previously reported increased mitochondrial mRNAs and rRNAs in CLPP deficient hearts (Szczeponowska et al., 2016), an increased level of ND1 was observed for NCD CLPP deficient liver and HFD was found to even have an additive effect on ND1 mRNA levels. Moreover, 16S rRNA was mildly increased in the absence of CLPP during NCD and HDF-feeding, whereas the levels of 12S rRNA were not different between both genotypes and diets (Figure 3.34 A, B). Proteomic data revealed increased levels of LRPPRC in liver of NCD and HFD fed Clpp^{-/-} mice, which relates to the increased steady state levels of the mitochondrial mRNA, since LRPPRC is required for mitochondrial mRNA stability (Ruzzenente et al., 2012). Although *de novo* mitochondrial transcription was not assessed, it can be assumed not to be impaired but rather enhanced similar to the heart (Szczeponowska et al., 2016).

Since not only mitochondrial-encoded complex subunits were decreased in HFD fed Clpp^{-/-} mice, relative transcript levels of nuclear-encoded complex subunits were determined by qPCR. None of the analyzed mitochondrial complex subunits differed in their relative expression between control and Clpp^{-/-} mice fed either NCD or HFD (Figure 3.34 C). Hence, mitochondrial and nuclear transcripts of mitochondrial complex subunits are not changed or increased by the loss of CLPP.

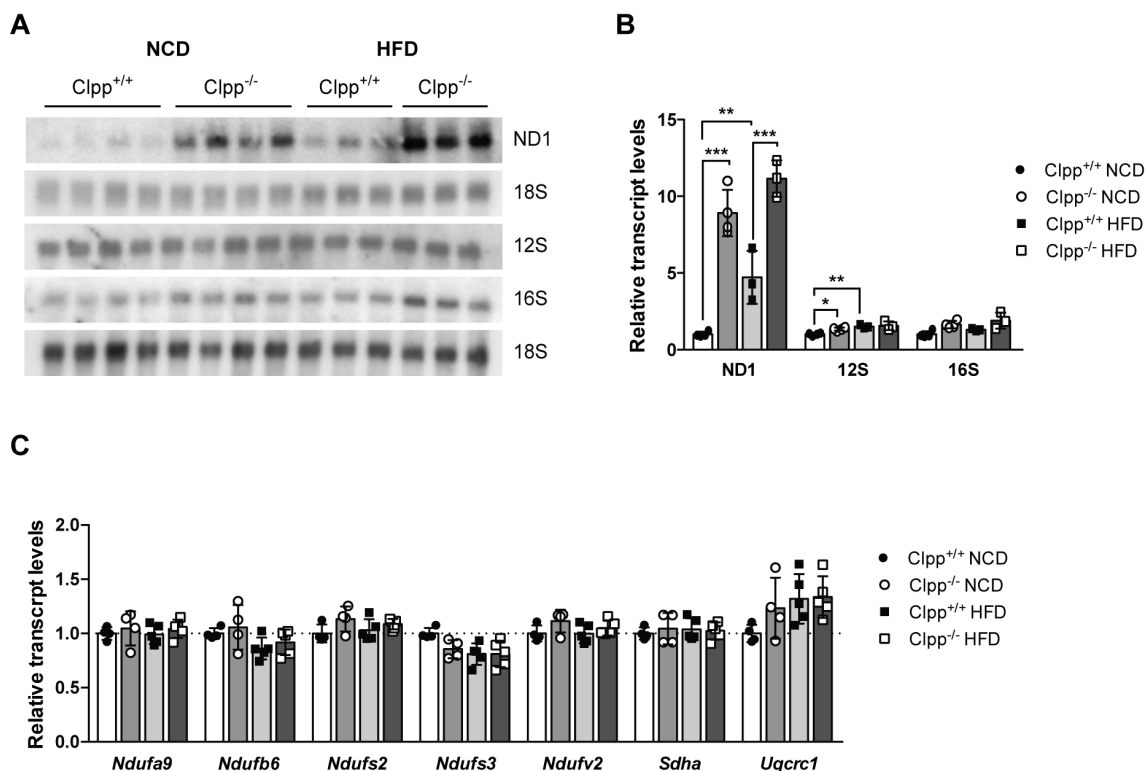


Figure 3.34 Mitochondrial transcript levels are increased in liver of CLPP deficient mice.

(A) Northern blot analysis and (B) and relative quantification of mitochondrial transcript levels in liver of control and CLPP deficient mice (n=3-4). (C) Relative expression levels of nuclear-encoded mitochondrial complex subunits in liver of control and Clpp^{-/-} mice (n=4-5). Data are presented as mean \pm SD (*P<0.05, **P<0.01, ***P<0.001; one-way ANOVA, Tukey's post hoc test).

To test whether a dietary intervention like HDF-feeding could have an impact on the hepatic mitochondrial translation upon loss of CLPP, *de novo* protein synthesis and degradation were analyzed in isolated liver mitochondria of NCD and HFD fed mice. During an *in organello* translation assay newly synthesized mitochondrial proteins were radiolabeled with ³⁵S-methionine (pulse) and their degradation was followed over time (chase). The protein synthesis was only mildly reduced in CLPP deficient mice fed NCD, whereas mitochondrial translation was significantly reduced by 40% in liver of CLPP deficient mice fed HFD (Figure 3.35 A, B). While the dietary conditions had a strong impact on the overall protein synthesis in CLPP deficient mitochondria, no difference was observed for the turnover of mitochondrial proteins (Figure 3.35 A, B). Thus, it can be concluded that metabolic stress as induced by HDF-feeding impairs protein translation in the absence of CLPP. Therefore, it seems reasonable to conclude that due to the decreased availability of mitochondrial-encoded complex subunits, the levels of nuclear-encoded subunits are adapted since proteins from both origins need to be assembled in correct stoichiometry (Edgar et al. 2009).

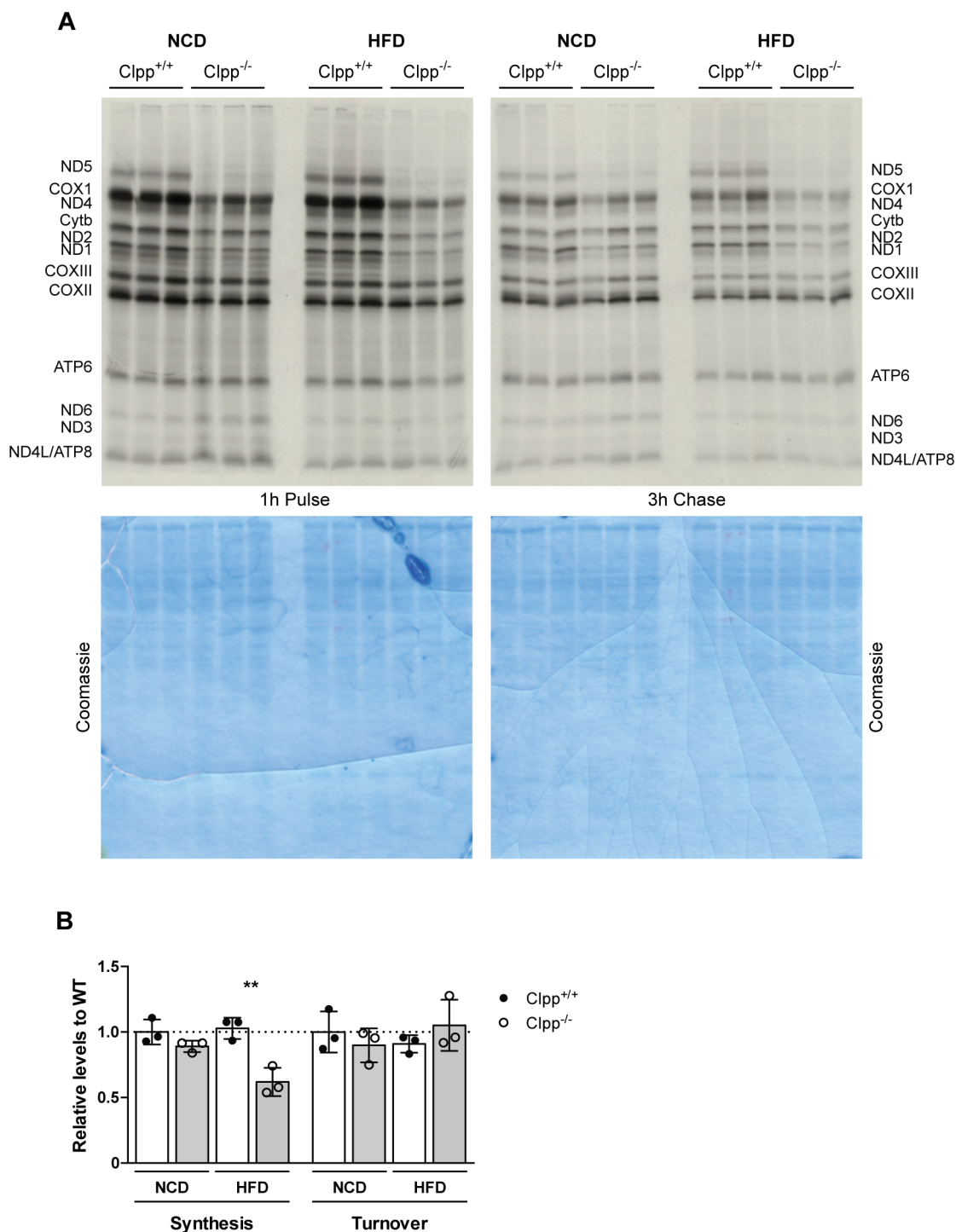


Figure 3.35 High fat feeding exacerbates the mitochondrial translation defect in liver in the absence of CLPP.

(A) Result of the *in organello* translation analysis of liver mitochondria of CLPP deficient mice fed either NCD or HFD. Proteins were isolated after pulse labeling with ³⁵S-methionine for 1 h to assess *de novo* mitochondrial protein synthesis or after 3 h cold chase to analyze mitochondrial protein turnover. Position of individual proteins is indicated on the left and right. Coomassie brilliant blue stained gel serves as loading control. (n=3) (B) Relative mitochondrial protein synthesis and turnover rate. (*P<0.05, **P<0.01, ***P<0.001; one-way ANOVA, Tukey's post hoc test). *In organello* translation analysis was performed together with Dr. Alexandra Kukat.

To further investigate whether the lactation period during the first three weeks of life is sufficient to impact mitochondrial translation in the absence of CLPP to the same extent than HFD, *de novo* protein synthesis was assessed in liver mitochondria of 5-week-old CLPP deficient and control mice. To note, pups rely for the first 15 days fully on the maternal lactation, afterwards they begin to ingest also solid food, while the nursing still continues. Upon 21 days they are weaned and feed on the NCD (Silver, 1995). Interestingly, the protein synthesis in liver mitochondria from 5-week-old *Clpp*^{-/-} mice was strongly reduced as compared to control mice, whereas the turnover of mitochondrial proteins was not different (Figure 3.36 A, B). The translation reduction in 5-week-old *Clpp*^{-/-} mice was comparable to HFD fed CLPP deficient mice.

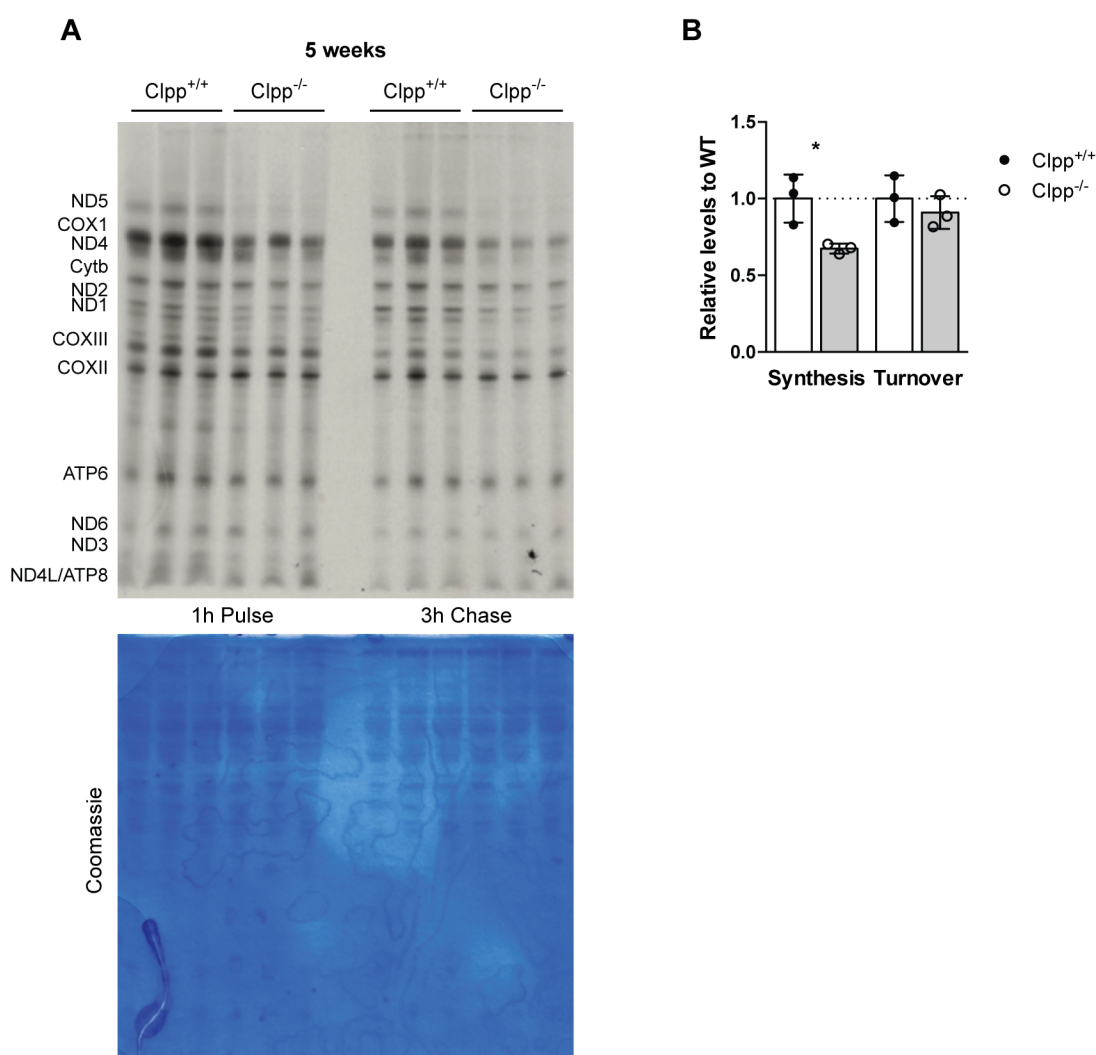


Figure 3.36 Mitochondrial translation defect in 5-week-old CLPP deficient liver is comparable to HFD fed *Clpp*^{-/-} mice.

(A) Result of the *in organello* translation analysis of liver mitochondria of 5-week-old CLPP deficient mice. Proteins were isolated after pulse labeling with ³⁵S-methionine for 1 h to assess *de novo* mitochondrial protein synthesis or after 3 h cold chase to analyze mitochondrial protein turnover. Position of individual proteins is indicated on the left and right. Coomassie brilliant blue stained gel serves as loading control (n=3). Data are presented as mean ± SD (*P<0.05, **P<0.01, ***P<0.001; unpaired two-tailed t-test).

3.4.6 Loss of CLPP does not impair hepatic mitoribosome assembly

To further address the observed translation defect in HFD CLPP deficient liver, first the abundance of mitochondrial ribosomal proteins was analyzed. No significant differences were observed for the steady state levels of mitoribosomal proteins of the small (MRPS18B, MRPS35) and large (MRPL37) ribosomal subunits between control and CLPP deficient mice fed NCD or HFD (Figure 3.37 A, B). This is in line with comparable levels of 12S and slightly increased levels of 16S rRNA, indicating no increase in ribosomal biogenesis despite the strong translation defect. To examine which step of hepatic mitochondrial translation might be affected, the assembly of mitoribosomes was assessed next. Mitochondrial lysates were subjected to sucrose gradient centrifugation for the separation of the 28S (small ribosomal subunit), 39S (large ribosomal subunit) and the fully assembled mitoribosome 55S (monosomes). As expected, MRPS35 and MRPS18B components of the small ribosome were present in the 28S and 55S fractions and MRPL37 a constituent of the large ribosome was located in the 39S and 55S fractions (Figure 3.37 C). Strikingly, there was no difference in the abundance of the small and large ribosomes and fully assembled mitoribosomes between control and CLPP deficient liver mitochondria, neither on NCD nor on HFD (Figure 3.37 C). In conclusion, CLPP deficiency in the liver does not affect mitoribosome assembly, indicating that the translation defect is not caused by defective mitoribosome assembly. This is in contrast to the phenotype observed in heart of CLPP deficient mice (Szczepanowska et al., 2016). In heart loss of CLPP was shown to cause accumulation of the 28S ribosome and to decrease mitoribosome assembly, due to enhanced association of the CLPP substrate ERAL1 with the small ribosomal subunit. The absence of the ribosomal phenotype in liver indicates a strong tissue specificity

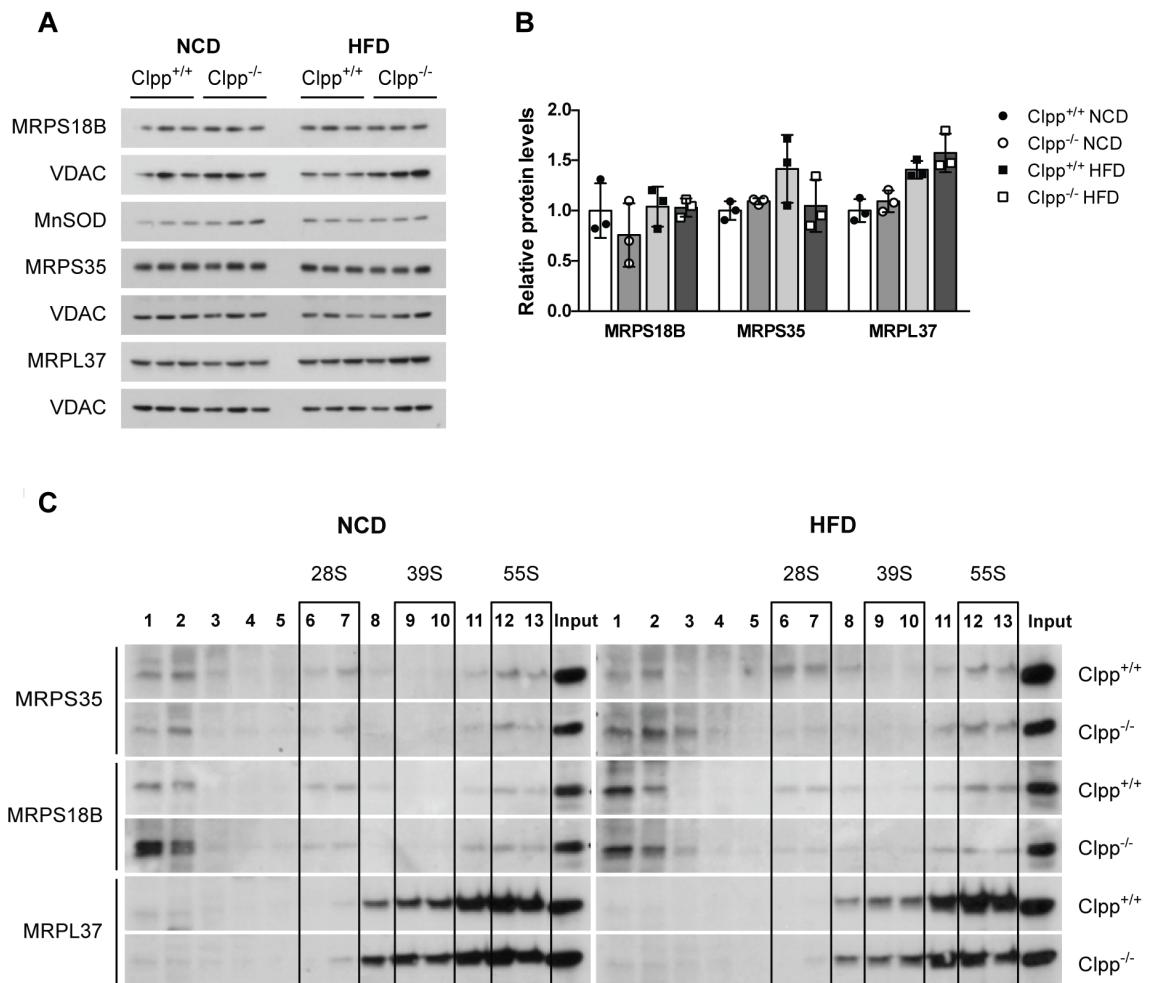


Figure 3.37 Loss of CLPP does not affect mitoribosomal protein levels of the small and large subunit and mitoribosome assembly in liver.

(A) Western blot analysis of mitochondrial ribosomal proteins in liver. VDAC serves as loading control. (n=3) (B) Quantification of Western blots shown in (A). (C) Analysis of mitoribosomal assembly by sucrose gradient density sedimentation in liver mitochondria of NCD and HFD fed control (n=3) and Clpp^{-/-} mice (n=3). The migration of small (28S) and large (39S) ribosomal subunits and monosomes (55S) was assessed by Western blot using antibodies against MRPS35, MRPS18B and MRPL37. Data are presented as mean \pm SD. Sucrose gradient analysis was performed by Dr. Karolina Szczepanowska.

3.4.7 Hepatic translation defect of CLPP deficient liver mitochondria is not caused by an increased association of ERAL1 with the 28S ribosomal subunit

In heart of CLPP deficient mice ERAL1 was demonstrated to associate with the 28S subunit due to insufficient removal by CLPP and thereby impair mitoribosome assembly (Szczepanowska et al., 2016). Although no assembly defect of mitoribosomes was detected for CLPP deficient liver of mice fed NCD or HFD (Figure 3.37 C), an increased association of ERAL1 with the 28S subunit could still affect the small ribosomal subunit assembly. Therefore, the migration of the CLPP substrates CLPX, EFG1 and ERAL1 with the 28S and 39S ribosomal subunits and 55S mitoribosomes were analyzed by sucrose gradient centrifugation followed by Western

blot analysis with the respective antibodies. The migration of ribosomal subunits and mitoribosomes were determined as formerly done by following the migration of MRPS35 and MRPL37 for simplicity reasons blots are not shown. In the absence of CLPP, CLPX was found to associate with the 28S subunit in NCD conditions, whereas this association was not observed for HFD CLPP ablated mitochondria (Figure 3.39). Whether this effect is dependent on diet or is due to experimental variation needs to be determined with additional repetitions of the experiment. EFG1 was only found in the free fractions and not associated with any ribosomal subunits, despite its higher abundance in the absence of CLPP, which is in contrast to previous studies reporting EFG1 to associate with the 28S subunit. This discrepancy might be explained by different experimental settings. For ERAL1, a mildly increased association with the 28S subunit was observed in the absence of CLPP for mice fed NCD and HFD (Figure 3.39), although this interaction was weak, indicating that this mechanism is conserved between heart and liver.

Taken together, a mildly increased association of ERAL1 with 28S in the absence of CLPP was found in liver of NCD and HFD fed mice and it might be the cause for the mild decrease in mitochondrial translation in liver of NCD fed mice. Since this association is comparable for NCD and HFD, the strong translation defect in CLPP deficient liver of HFD fed mice is caused by distinct factors.

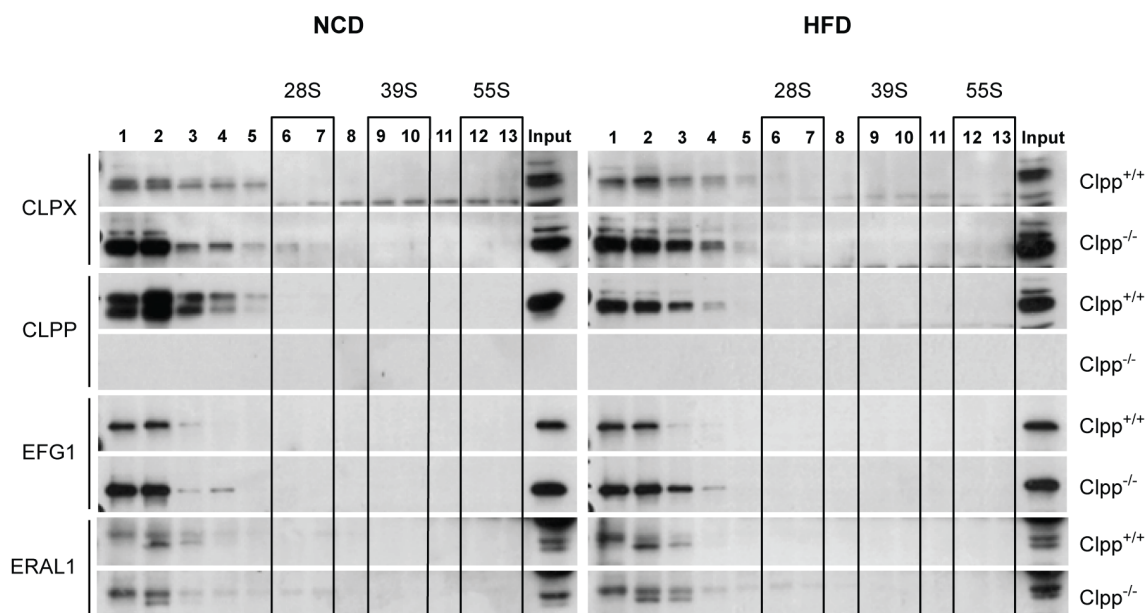


Figure 3.38 Mild comigration of the CLPP substrate ERAL1 with the small ribosomal subunit in liver irrespective of diet.

Sucrose gradient density sedimentation analysis of CLPX, EFG1 and ERAL1 in liver mitochondria of NCD and HFD fed control (n=3) and *Clpp*^{-/-} mice (n=3). The migration of the small (28S) and large (39S) ribosomal subunits and monosomes (55S) is indicated. Sucrose gradient analysis was performed by Dr. Karolina Szczepanowska.

Since loss of CLPP in liver had a different impact on mitoribosome assembly than in heart, protein expression of important parameters involved in this process was compared between heart and liver of control and *Clpp*^{-/-} mice fed NCD. To control for differences in mitochondrial mass, the analysis was performed in isolated mitochondria. Interestingly, the basal levels of CLPP differed between control heart and liver and was 2-fold greater in liver. The identified causative factor of the heart mitochondrial translation defect ERAL1 was 8-fold increased in CLPP deficient heart mitochondria, whereas in liver the difference was only 3-fold between control and *Clpp*^{-/-} mice, owing to the fact that the basal expression in liver was greater than in heart. Another CLPP substrate EFG1 was increased to the same extent in CLPP ablated mitochondria from heart and liver. In addition, analysis of MRPS35 revealed the previously mentioned increase in small ribosomal subunits in heart of *Clpp*^{-/-} mice and no significant difference in liver, however, the basal levels of MRPS35 was greater in liver. In contrast, VDAC was increased in heart as compared to liver in control and *Clpp*^{-/-} mice, emphasizing the general tissue-specific traits of mitochondria (Figure 3.38 A). Taken together, tissue-specific differences in the levels of ERAL1 and ribosomal protein in heart and liver might account for the observed differences in mitochondrial translation and mitoribosome assembly in the absence of CLPP on NCD.

In line with these observations, no significant difference in ERAL1 levels was observed in liver of NCD and HFD *Clpp*^{-/-} mice (Figure 3.38 C, D). Accordingly, basal CLPP expression was not altered between control mice fed NCD or HFD. Furthermore, CLPX was upregulated to the same extent in *Clpp*^{-/-} mice fed NCD or HFD. CLPX was shown to be itself a substrate of the ClpXP protease (Graham et al., 2013). Thus, differences in hepatic mitochondrial translation between NCD and HFD fed *Clpp*^{-/-} mice cannot be traced back to ERAL1.

Next, mitochondrial translation factors were analyzed to screen for possible differences in protein abundance between NCD and HFD *Clpp*^{-/-} mitochondria that could account for the altered mitochondrial protein synthesis. First the translation initiation factors MTIF2 and MTIF3 were analyzed. The levels of MTIF2 were not changed between control and *Clpp*^{-/-} mice fed NCD or HFD, yet its expression was induced by HFD-feeding. MTIF3 levels were decreased in CLPP deficient liver mitochondria irrespective of diet and MTIF3 expression was again induced upon HFD in control mice. The CLPP substrate EFG1 has been shown by proteomic analysis to be increased in the absence of CLPP on NCD and HFD and this was confirmed by Western blot analysis (Figure 3.38 E, F). Strikingly, no significant difference was observed for EFTU between control

and $Clpp^{-/-}$ mice on NCD, however, on HFD EFTU levels were elevated for control mice, whereas they were decreased in CLPP deficient mitochondria (Figure 3.38 E, F). EFTU is an elongation factor responsible for the delivery of aminoacyl-tRNAs to the ribosome, thus reduced levels of EFTU in liver of HFD fed $Clpp^{-/-}$ mice could slow down mitochondrial translation. These data indicate that HFD-feeding stimulates expression of mitochondrial translation factors in wildtype mice and proposes EFTU as a factor facilitating the translation defect in liver of HFD fed $Clpp^{-/-}$ mice. Correct ratios of translation factors have been shown to be essential for the mitochondrial translation process and ratios were further suggested to differ between different tissues (Coenen et al., 2004), which could explain the observed tissue-specific differences between heart, SkM and liver. Taken together, mitochondrial translation in liver is not regulated through the same mechanism as in heart and CLPP is specifically required for hepatic mitochondrial translation during metabolic stress conditions like HFD-feeding or lactation.

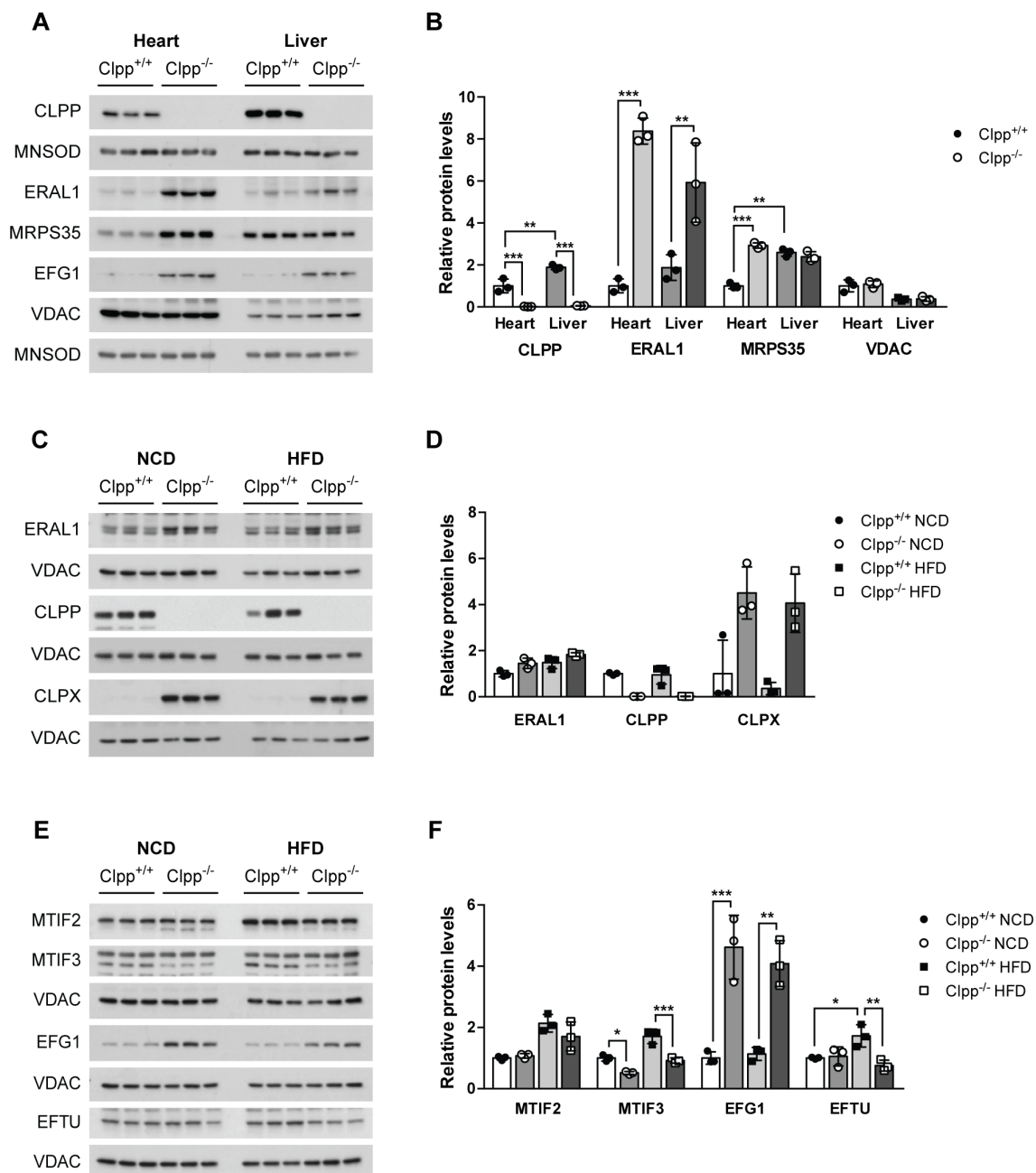


Figure 3.39 Difference in hepatic mitochondrial translation of NCD and HFD fed CLPP deficient mice might be affected by altered ratios of mitochondrial translation factors.

(A) Western blot analysis and (B) relative quantification of CLPP substrates and mitochondrial protein in heart and liver mitochondria of control and CLPP deficient mice. MNSOD is used as loading control.

(C) Protein levels of mitochondrial translation factors were assessed by Western blot analysis in liver mitochondria of control and Clpp^{-/-} mice fed NCD or HFD. VDAC serves as loading control. (D) Quantification of Western blots shown in (C).

(E) Western blot analysis ERAL1, CLPP and CLPX in liver mitochondria of control and Clpp^{-/-} mice. VDAC is used as loading control. Data are presented as mean \pm SD (*P<0.05, **P<0.01, ***P<0.001; one-way ANOVA, Tukey's post hoc test).

4 Discussion

The study of mitochondrial function has received broad interest in the last decades due to the large impact of mitochondrial dysfunction on the ageing process and human diseases. Mitochondria are the central core for energy production in the cell and many metabolic pathways converge in them at different levels. Defects in mitochondrial function could therefore affect several parts of the metabolic network and have broad cellular and physiological consequences. This points to the critical role of mitochondria for cellular homeostasis and explains why metabolic defects underlie a broad range of human diseases. The emergence of metabolic disorders, likely due to changes in lifestyle has further focused on studies of metabolism and its regulation.

Mitochondrial function and form is closely connected to the metabolic state and vice versa (Liesa and Shirihai, 2013). Therefore, it is essential to study how mitochondria regulate and maintain their function to understand defects observed in several metabolic diseases. Many components of the mitochondrial quality control machinery have been identified so far, however, the physiological function of several of these proteins, including mitochondrial proteases remains largely unknown.

This study aimed at deciphering the role of the mitochondrial matrix protease CLPP in mammalian metabolism. For this purpose different mouse models lacking CLPP were generated. First, a whole body CLPP deficient mouse model was analyzed to determine CLPP function under basal conditions and during high metabolic stress by feeding high fat diet. Second, CLPP function was investigated in distinct highly metabolically active tissues to determine the impact of disturbed mitochondrial proteostasis in individual organs on whole body metabolism. Finally, it was investigated whether the mitokine FGF21 is an essential metabolic mediator of the phenotype and the metabolic adaptations observed in CLPP deficient mice.

4.1 Loss of CLPP alters whole body metabolism

This study demonstrates that loss of CLPP under normal dietary condition has different tissue-specific consequences with an overall favorable metabolic phenotype. In humans, mutations in *C/pps* cause Perrault Syndrome, which is characterized by growth retardation, sensorineural hearing loss and ovarian failure (Jenkinson et al., 2013). CLPP deficient mice represent a faithful model of the Perrault syndrome displaying reduced growth and body weight, sterility and deafness (Gispert et al., 2013). Growth defects are a common feature of mitochondrial mutants, suggesting a similar underlying mechanism (Leong et al., 2012; Levéen et al., 2011; Wells et al., 2012). In many studies the growth defect was triggered by alterations in the GH/IGF1 axis. In growth restricted UCP1 transgenic mice, for example, decreased IGF1 levels were determined in serum (Keipert et al., 2014). Interestingly, we did not observe a decrease in *Igf1* transcript levels in liver, thus serum analysis might be another possibility to ascertain whether the GH/IGF1 axis is determining the growth restriction in the absence of CLPP.

Remarkably, in our study loss of CLPP does not have an impact on longevity, which is in contrast to another study performed in a different *C/pps* knockout mouse model. Here, an increased postnatal mortality was reported (Gispert et al., 2013), however, other observed phenotypes for both mouse models are similar. Possible reasons that might account for the discrepancy could be the different techniques used to generate the CLPP deficient mice (gene trapping or gene targeting) or differences in the hygienic status of the animal facilities. Moreover, the influence of CLPP absence on lifespan is also species dependent, since loss of CLPP in the fungus *P. anserina* leads to an increased lifespan (Fischer et al., 2015).

On the metabolic level, the loss of CLPP leads to enhanced glucose metabolism, as evidenced by increased insulin stimulated glucose disposal, reduced basal blood glucose levels and decreased hepatic and muscular glycogen stores. An increased glucose uptake can be facilitated by either increased protein expression of GLUT1 or GLUT4 and an enhanced stress related translocation of the latter one. In SkM and EWAT increased levels of the insulin dependent GLUT4 was observed. This relates to an increased activation of the metabolic regulator AMPK in SkM. AMPK is suggested to enhance glucose uptake by facilitating GLUT4 translocation (Fulco and Sartorelli, 2008). Its activation by phosphorylation at the Threonine residue 172 is mediated by upstream kinases and an allosteric interaction with AMP, indicating an increased AMP/ATP ratio in CLPP deficient SkM.

In general an enhanced glucose metabolism is commonly seen in mouse models with

OXPPOS dysfunction (Diaz et al., 2008a; Levéen et al., 2011; Wredenberg et al., 2006). A metabolic switch to increased glycolysis might be an alternative source of ATP, thereby reducing glycogen stores. Glycogen synthesis might be additionally decreased due to hormonal influence of increased glucagon levels, as it was shown for *Clpp*^{-/-} mice.

Several groups have implicated mitochondrial dysfunction in the etiology of type 2 diabetes as a cause of insulin resistance (Kim et al., 2000; Petersen et al., 2003; Ritov et al., 2004), which is in contrast to results obtained in this study. Different metabolic impacts of mitochondrial stress or dysfunction might be dependent on the degree and the localization of the mitochondrial defect. An interesting example is the deletion of TFAM specifically in β -cells or skeletal muscle. In beta-cells TFAM deletion leads to impaired mitochondrial function (Silva et al., 2000), deficient insulin secretion and glucose intolerance, whereas skeletal muscle-specific deletion of TFAM causes enhanced glucose tolerance (Wredenberg et al., 2006). The importance of the degree of mitochondrial dysfunction becomes evident by comparing homozygous and heterozygous PolG mutator mice. These mice accumulate somatic mitochondrial mtDNA mutations due to a proofreading-deficient polymerase gamma, leading to respiratory chain dysfunction and a premature ageing phenotype. Homozygous mice display resting hypoglycemia and enhanced glucose tolerance, whereas heterozygous mice are glucose intolerant and exhibit an obesity phenotype (Saleem et al., 2015; Wanagat and Hevener, 2016). Our model depicts a global deletion of CLPP with varying degrees of mitochondrial dysfunction in different tissues, yet glucose metabolism is not impaired but rather enhanced, questioning the causal role for OXPPOS dysfunction and insulin resistance.

Another interesting finding of this study is that loss of CLPP increases energy expenditure. The total energy expenditure is composed of the basal metabolic rate, cold-induced thermogenesis (at non thermoneutrality), thermic effect of food and physical activity (Speakman, 2013). The physical activity is decreased in CLPP mice, most likely due to reduced OXPPOS function and resulting energy deficiency in SkM. Since the food intake was not changed in CLPP mice it can be assumed that the thermic effect of food is neglectable, indicating that an increased thermogenesis or an increased basal metabolic rate could account for the increased energy expenditure in CLPP deficient mice. A possible contributing factor to enhanced energy expenditure is increased uncoupling of the mitochondrial electron transfer system from the ATP synthesis by UCP1. Unexpectedly, the loss of CLPP in BAT resulted in the dissociation of lipid storage from lipid use, despite comparable levels of UCP1 in male mice, leading to whitening of BAT. In contrast, EWAT exhibited a reduced mass and a transcript

profile associated with browning, suggesting an enhanced energy expenditure of EWAT. The reduction of CLPP deficient EWAT mass was due to a decrease in adipocyte number rather than adipocyte size. Similarly, a mouse model of Costeff syndrome $OPA3^{L122P}$ displays whitening of BAT, browning of EWAT and no effect on IWAT, proposing a similar tissue-specific response to the mitochondrial perturbation (Wells et al., 2012). The function of OPA3 has not been fully elucidated; it was reported to induce mitochondrial fragmentation and mutations in the *OPA3* gene have been linked to this metabolic syndrome.

Moreover, whitening of BAT was also observed in mouse models of FAO deficient adipose tissue (Lee et al., 2015) and a globally impaired supercomplex assembly due to lack of COX7RP (Ikeda et al., 2013), indicating that FAO as well supercomplex assembly is required for BAT homeostasis, both being affected or impaired in the absence of CLPP. The inability of CLPP deficient mice to maintain body temperature upon cold exposure, demonstrates a requirement of CLPP function specifically during metabolic stress conditions. During acute cold exposure there is an increased energy supply to BAT mitochondria with enhanced glucose uptake and increased FAO. Although under physiological conditions the FAO in CLPP ablated BAT was not affected, it can be speculated that in combination with the cold-stress induced OXPHOS dysfunction, the FAO was not functioning to the fullest capacity leading to the severe hypothermia. Additionally, the ability of UCP1 induction upon cold exposure was decreased by CLPP ablation.

The β -adrenergic stimulation upon cold exposure was reported to increase lipolysis (Chondronikola et al., 2016). Thus, the gender-specific phenotypes discovered in female $Clpp^{-/-}$ mice, increased lipolysis and decreased UCP1 levels in BAT, might be intimately linked. The decreased UCP1 abundance might cause a reduced body temperature and thereby induce β -adrenergic signaling leading to the activation of lipolysis. However, to affirm this hypothesis the body temperature of female $Clpp^{-/-}$ mice needs to be determined.

Unlike in *C.elegans*, where ClpXP was shown to degrade only misfolded proteins and thereby take part in the UPR^{mt}, a recent study in *P.anserina* suggested the involvement of CLPP in energy metabolism (Fischer et al., 2015; Haynes et al., 2007, 2011). Based on a CLPP substrate-trapping assay, using a catalytically inactive human CLPP version, many potential substrates have been identified in various metabolic pathways, including fatty acid metabolism (Fischer et al., 2015). Correspondingly, in this study VLCAD, which is involved in FAO of long chain fatty acids, is proposed as novel substrate of mammalian CLPP, further supporting a role for CLPP in lipid metabolism.

As one would assume for a potential substrate, the steady state levels of VLCAD were increased in the absence of CLPP, however, FAO rates were decreased in liver and SkM of *Clpp*^{-/-} mice on NCD. This decrease in FAO can be attributed to the reduced levels of CPT2, which is required for the uptake of long chain fatty acids, suggesting a countervailing response to limit fatty acid oxidation as a protective measure. Interestingly, CPT2 abundance was dependent on the dietary supply of lipids, since HDF-feeding induced CPT2 expression. A similar adaptation was reported for VLCAD depleted mice (Zhang et al., 2010). These mice are protected against HFD induced obesity due to a compensatory increase in LCAD in certain tissues, an enzyme with overlapping fatty acid chain length specificity. Tissue-specific adaptations in response to FAO disorders are most likely dependent on their reliance on FAO. Impaired FAO in liver due to loss of CPT2 leads to hepatosteatosis upon fasting (Lee et al., 2016a) and loss of CPT2 in adipose tissue triggers lipid accumulation in BAT, whereas WAT is unaffected by loss of CPT2 and is even protected from HFD induced oxidative stress and inflammation (Lee et al., 2015, 2016b). These observations support our result of the absence of compensatory CPT2 downregulation in WAT of *Clpp*^{-/-} mice.

A question that remains unanswered is how CPT2 expression is regulated in response to the increased VLCAD stability upon loss of CLPP. Transcriptional regulation of the *Cpt2* gene can be excluded, since transcript levels were not changed and additionally *Ppara* levels were not altered. PPAR α is an important transcriptional regulator of genes involved in fatty acid oxidation, including *Cpt2* (Barrero et al., 2003; Rakhshandehroo et al., 2009). Hence, either mRNA stability of *Cpt2* might be decreased or the turnover of the CPT2 protein increased.

Taken together, the presented data indicate that in the absence of CLPP, VLCAD is stabilized most likely due to decreased turnover, which leads to different compensatory regulations of CPT2 thereby reducing FAO under NCD conditions or increasing it under HFD conditions. Thus, the reduced body fat may be a result of robust carbohydrate usage that reduces fatty acid synthesis, since increased fatty acid oxidation can be excluded under NCD conditions. However, under HFD conditions FAO is most likely increased in *Clpp*^{-/-} mice. A limiting factor for mitochondrial FAO is the recovery of the cofactor NAD⁺, which is required by the 3-hydroxyacyl-CoA dehydrogenase. Especially, mitochondrial OXPHOS dysfunctions were reported to limit FAO due to the inability to recover NAD⁺ from NADH and thereby favoring glycolysis (Levéen et al., 2011). The profound decrease in CoI in CLPP deficient liver upon HDF-feeding might also imply an inhibition of FAO due to reduced recovery of NAD⁺. However, unpublished data from our lab reveal the presence of a functional N-module with NADH oxidative activity that is probably not associated with CoI in mitochondria lacking CLPP, suggesting a potent

NAD⁺ recovery in the absence of CLPP. Thus, FAO might be increased in conditions of high dietary burden upon loss of CLPP and contributes to the resistance of HFD induced obesity.

4.2 FGF21 is not a metabolic regulator of the CLPP phenotype

The fibroblast growth factor 21 (FGF21) is an endocrine hormone induced and secreted upon starvation from the liver to elicit adaptive responses in glucose and lipid metabolism (Potthoff et al., 2009). Its beneficial metabolic actions raised the interest in FGF21 as possible anti-diabetic drug candidate (Kharitonov and Adams, 2014). Recently, FGF21 was also shown to be induced and secreted from heart and SkM in response to different kinds of mitochondrial perturbations and integrated stress response activation (Dogan et al., 2014; Keipert et al., 2014; Tynismaa et al., 2010; Vandanmagsar et al., 2016), suggesting an adaptive mitochondrial stress-related starvation response. In line with these reports, a general induction of *Fgf21* was observed in all analyzed tissues of CLPP ablated mice and an increase in FGF21 serum levels. Interestingly, the degree of mitochondrial dysfunction in the different tissues correlates with the levels of *Fgf21* expression. An increase in *Fgf21* expression by age with increasing levels of mitochondrial dysfunction has been previously reported for the 'deletor mouse'. This mouse model expresses a mutant mitochondrial helicase Twinkle, leading to the accumulation of mtDNA deletions, which mimics late-onset mitochondrial myopathy (Tynismaa et al., 2010).

Since liver mitochondria are only very mildly affected by the absence of CLPP under NCD conditions, one could argue that the increase in hepatic *Fgf21* expression is induced by the fasting-like phenotype of CLPP deficient mice. However, in CLPP deficient liver no increase in *Ppara* was detected, the transcription factor found to induce *Fgf21* upon starvation (Inagaki et al., 2007). ATF4 is another transcription factor known to induce *Fgf21*, yet no concurrent increase in expression was detected in the analyzed tissues in the absence of CLPP. Due to the concordant increase of *Atf5* in all CLPP deficient tissues with increased *Fgf21* expression, ATF5 is suggested as an additional transcriptional regulator of *Fgf21* expression. Further investigations are required to understand whether ATF5 is involved in the transcriptional activation of *Fgf21*.

As the proposed function of FGF21 suggests, systemic metabolic adaptations were observed in CLPP deficient animals, including reduced body weight and fat mass as well as growth retardation and increased insulin sensitivity. Many previous studies speculated on the beneficial functions of FGF21, however, only very few studies

provide proof of principle experiments using genetic ablation of FGF21 to show its causal role. In contrast to a previous study on muscle autophagy deficient mice (Kim et al., 2013), our study on *Clpp/Fgf21* DKO mice clearly shows that the mitochondrial stress induced leanness and reduced body fat content is independent of FGF21. Notably, autophagy is involved in many cellular processes and the metabolic response induced by the obstruction of autophagy might not ascend from mitochondrial stress, but rather from a generally impaired cellular homeostasis demanding FGF21 action.

In accordance with our results, the depletion of FGF21 in a mouse model with increased mitochondrial uncoupling in SkM did not lead to the attenuation of the decreased body weight, reduced fat mass and reduced body length (Ost et al., 2016). This study further presented that the glycolytic control in UCP1 transgenic mice was independent of FGF21. In addition, they demonstrate that the browning of WAT was clearly dependent on FGF21 (Ost et al., 2016). Currently, we are analyzing the browning of WAT in our DKO mice, however, this could indicate that the browning of WAT is not contributing significantly to the whole body energy expenditure in CLPP depleted mice. This assumption awaits further experimental evidence. Impaired FAO in SkM was also shown to induce FGF21 with metabolic adaptations similar to the *Clpp*^{-/-} mice (Vandanmagsar et al., 2016). Likewise to our results, the growth defect and fat mass were not corrected by the absence of FGF21, whereas the decreased body weight and the increased glucose uptake were attenuated by the lack of FGF21 in their model (Vandanmagsar et al., 2016). The preceding observations, together with our data, demonstrate that growth defects induced by mitochondrial dysfunction are the only consistent phenotype not to be rescued by *Fgf21* knockout. Hence, they seem not to be mediated by FGF21 induced growth hormone insensitivity, as suggested for *Fgf21* knockout mice (Inagaki et al., 2008). Moreover, whether or not FGF21 is involved in metabolic adaptations like changes in body weight or fat mass, browning of white adipose tissue and adjustment in insulin sensitivity depends on the primary affected mitochondrial/cellular process responsible for the FGF21 induction. Another explanation for different outcomes with regard to the mitigation of metabolic phenotypes in the absence of FGF21 in mitochondrial mutant mice is the possibility of a compensatory substitution of FGF21 by other myokines/mitokines.

Therefore, FGF21 could be used as indicator of mitochondrial dysfunction in *Clpp*^{-/-} mice, however, the adaptive metabolic responses due to the absence of CLPP are mostly occurring independent of FGF21.

4.3 Tissue-specific CLPP deletion does not have systemic implications

The whole body ablation of CLPP has a profound metabolic phenotype as evidenced in this and previous studies (Gispert et al., 2013). However, the systemic consequences of CLPP deficiency in distinct tissues are not known. Therefore, we generated liver- and SkM/heart- specific *Clpp* knockout mouse models. Liver and muscle are both important tissues involved in the regulation of whole body metabolism by regulating glucose and lipid metabolism. Nonetheless, loss of CLPP in either tissue has no significant impact on the whole body metabolism. Both models present a normal body weight development and no difference in the glucose metabolism at the age of 15 weeks, indicating that loss of CLPP in distinct tissues does not elicit systemic alterations as early as for the full body knockout. The complete loss of CLPP was confirmed at 15 weeks of age, however, depending on the turnover of the protein, the complete loss might be achieved rather late, thus delaying the phenotype development. For example MTERF3 was still detectable in heart at 12 weeks of age upon *Ckmm-Cre* deletion and fully absent only at 16 weeks of age (Park et al., 2007). Recently, CLPP has been ascribed to have a role in mitochondrial translation (Szczepanowska et al., 2016). In the tissue-specific *Clpp* knockout mice, the translation defect manifests in decreased supercomplex levels. Interestingly, the decrease in supercomplex levels in the tissue-specific CLPP mice is more pronounced than in the whole body CLPP deficient mice in the respective tissues of the same age, indicating that different adaptive responses might be activated depending on a restricted or systemic mitochondrial defect.

These observations are different from other studies using *Ckmm-Cre* mediated deletion of mitochondrial transcription/translation genes like *Tfam* (Hansson et al., 2004), *Tfb1m* (Metodieiev et al., 2009), *Mterf4* (Cámara et al., 2011). The systemic effects of these mitochondrial perturbations are detectable as early as 2 weeks of age for *Tfam*, 15 weeks for *Tfb1m* and 5 weeks of age for *Mterf4*. The different phenotypes of these mice as compared to the *Clpp*^{MKO} mice can be explained by the much more severe mitochondrial dysfunction of these mutants, owing to the fact that those are essential genes as their full body deletion is lethal. All mouse models displayed a severe cardiomyopathy, whereas SkM was only mildly affected. Moreover, TFAM has also been deleted exclusively in SkM using the *Mlc1f-Cre* recombinase (Wredenberg et al., 2002, 2006). Interestingly, these mice are healthy till 4 months of age and display an increased glucose tolerance only upon two 2 months of age.

The role of hepatic mitochondrial dysfunction did not receive as much attention as the heart or brain, most likely because most mitochondrial pathologies are related to these

energy demanding tissues. To date, no Afp-Cre mediated hepatic mitochondrial mouse model has been published to our knowledge. Another common liver-specific Cre line is exploiting the albumin promoter (Alb-Cre), which was reported to result in incomplete recombination (Diaz et al., 2008b). Nevertheless, studies with moderate and severe OXPHOS dysfunction in liver induced by depletion of the AIF (Pospisilik et al., 2007) or COX10 (Diaz et al., 2008b) with the Alb-Cre are in part supporting and in part contrasting our results. Similar to loss of CLPP, AIF depletion mostly affects Col and these mice also exhibit an unchanged body weight yet increased insulin sensitivity. Thus, depending on the degree of mitochondrial dysfunction, the tissue is able to cope with the defect before systemic alterations are visible. To determine how liver or SkM are able to cope with CLPP deficiency a longer follow-up of these mice is required. Furthermore, it would be interesting to determine whether tissue-specific CLPP deletion is sufficient to protect against HFD induced obesity.

4.4 CLPP is required for hepatic mitochondrial translation in metabolic stress conditions

The current study shows that ubiquitous loss of CLPP protects against HFD induced obesity and insulin resistance. Another key finding is that in the absence of CLPP, dietary food with high fat content has a negative impact on mitochondrial translation explicitly in liver. HFD-feeding was demonstrated to decrease hepatic mitochondrial translation, which resulted in decreased supercomplex levels in CLPP deficient liver mitochondria. Moreover, the observed translation defect was distinct from the former translation mechanism described for CLPP deficient hearts (Szczepanowska et al., 2016).

Our results are consistent with HFD studies performed in other mitochondrial mutants, which are also protected against diet induced obesity (Kim et al., 2013; Quintens et al., 2013; Vernochet et al., 2012; Zhang et al., 2010). The protection from diet induced obesity in *Clpp*^{-/-} mice is linked to the enhancement of a fasting-like phenotype as described for the NCD that is evidenced by reduced blood glucose levels and favorable hormone levels (reduced leptin and insulin levels, increased glucagon and ghrelin levels). Evidence for enhanced lipid catabolism or decreased lipid synthesis are reduced EWAT hypertrophy and generally reduced body fat content despite the increased dietary fat content.

Results of HFD studies are hard to compare and interpret due to different experimental schemes, different diet compositions and sources of fat, lard (saturated fatty acids) vs. fish oil (poly-unsaturated fatty acids). In this study, HFD rich in lard was used

containing mainly saturated fatty acids, which is known to induce obesity related complications like diabetes and inflammation (Buettner et al., 2006). In control mice insulin-mediated AKT phosphorylation is blunted after 7 weeks on HFD, leading to insulin resistance, whereas loss of CLPP is protective.

On the molecular level, loss of CLPP during HDF-feeding leads to a severe OXPHOS defect exclusively in liver (not in SkM and heart), as revealed by reduced Col containing supercomplexes and reduced steady state levels of complex subunits. This finding is on the one hand in line with data obtained for heart mitochondria (NCD) (Szczepanowska et al., 2016) and on the other hand contradicting them, since the deregulated OXPHOS subunits in liver were only observed for HFD, whereas on NCD loss of CLPP had no effect on hepatic complexes yet in heart complex levels are decreased, indicating tissue-specific functions or requirements for CLPP during different metabolic burdens.

The question arises why predominantly Col is affected in *Clpp*^{-/-} mice and also in many other mitochondrial mutants or mitochondrial pathologies. One can only speculate on the mechanism: firstly the majority of mitochondrial-encoded subunits are Col subunits; secondly Col contains more subunits and redox groups than the other complexes; thirdly there might be distinct requirements for turnover due to different susceptibilities to cellular insults or environmental factors (Mimaki et al., 2012).

This is along the line with the tissue specificity observed for mitochondrial diseases and also for the absence of CLPP. The mitochondrial dysfunction observed for heart and SkM deficient in CLPP is affected to the same extent by NCD or HDF-feeding, however, in liver only on HFD mitochondrial dysfunction is evident. Proposed mechanisms are tissue-specific differences in mitochondrial proteome composition and quantities that lead to different capacities to remodel mitochondrial complexes, different energy demands or the reliance on glycolysis or fatty acid oxidation as primary source of ATP (Mootha et al., 2003; Pagliarini et al., 2008; Rossignol et al., 1999). Hence, CLPP might be required in liver for the maintenance of OXPHOS and mitochondrial translation only during condition of metabolic stress.

Interestingly, hepatic respiratory complex levels in control mice are not altered upon 8 weeks HDF-feeding, however, a loss of mitochondrial mass becomes apparent, indicating that HFD does not induce mitochondrial dysfunction per se, yet energy production/expenditure might be limited due to reduced mitochondrial number.

The hepatic mitochondrial dysfunction in *Clpp*^{-/-} mice triggered a compensatory activation in biogenesis, accompanied by an increase in mitochondrial transcripts as compensation for the decreased mitochondrial translation. This is in accordance with other mouse models of impaired protein synthesis like *Mterf3*, *Mterf4*, *Nsun4* (Cámara

et al., 2011; Metodiev et al., 2014; Park et al., 2007) and results obtained for CLPP deficient heart, despite the tissue-specific susceptibility to the HFD (Szczepanowska et al., 2016).

The striking decrease in hepatic mitochondrial translation in the absence of CLPP upon high dietary lipid content either after HFD or lactation, suggests a novel role for CLPP in conditions of high metabolic stress in liver. The translation defect in CLPP deficient liver seems to be distinctive from the mechanism recently described in heart, where an increased association of ERAL1 to the small ribosomal subunit leads to an impaired mitoribosome assembly (Szczepanowska et al., 2016). Here, no evidence was found for an impaired mitoribosome assembly, additionally the steady state levels of mitoribosomal proteins, as well as the small and large subunit levels were unchanged. Most importantly, the association of ERAL1 with the small ribosomal subunit was not different on NCD or HFD in the absence of CLPP, implying an alternative mechanism for the translation defect in liver.

The ratio of mitochondrial translation factors was reported to be very essential and although excess of EFG1 or EFG2 has no effect on mitochondrial translation, excess of EFTU or EFTS impairs it (Coenen et al., 2004), suggesting that also a decrease in EFTU could reduce translation velocity. This assumption is strengthened by the finding that knockdown of EFTU decreases tumor cell growth by reducing mitochondrial-encoded complex subunits (Škrtić et al., 2011). In CLPP deficient liver, decreased levels of MTIF3 and increased levels of EFG1 were detected on NCD and HFD, whereas EFTU was only decreased on HFD. Furthermore, a recent study demonstrated that CLPP slows down translation velocity (Dominic Seiferling, PhD thesis). In combination with the imbalance in translation factors particularly in CLPP deficient liver on HFD, this might be a factor contributing to the translation defect.

So far there are no reports on defective mitochondrial translation due to high loads of dietary lipids. The observation that hepatic mitochondrial translation is impaired to the same extent in liver of HFD fed *Clpp*^{-/-} mice and in young *Clpp*^{-/-} mice, which have already been without lactation for 2 weeks at the time of analysis, suggested a more enduring alteration of CLPP deficient liver mitochondria like changes in the lipid composition of the mitochondrial membrane. Depletion of the *PGS1* gene in *S.cerevisiae* results in a decrease of phosphatidylglycerol the precursor of cardiolipin and cardiolipin itself and was accompanied by a selective decrease in mitochondrial translation products (Chang et al., 1998; Ostrander et al., 2001). Interestingly, CLPP might be involved in the turnover of SLP-2, a protein implicated in the regulation of cardiolipin synthesis, since it was enriched in label-free quantification and CLPP

trapping experiments (unpublished data from Dr. Karolina Szczepanowska) (Christie et al., 2011). However, whether loss of CLPP has an impact on cardiolipin content or remodeling and this might in turn affect mitochondrial translation needs to be experimentally addressed.

Taken together, loss of CLPP protects against HFD induced obesity and insulin resistance. Moreover, CLPP function is required for hepatic mitochondrial translation in conditions with high lipid burden.

4.5 Summary

Our results demonstrate that ubiquitous deletion of CLPP results in a lean phenotype with enhanced glucose metabolism, owing to increased energy expenditure in part by WAT browning, despite decreased physical activity. Moreover, CLPP was shown to be involved in fatty acid oxidation by the regulation of its putative substrate VLCAD. In addition, CLPP has a critical role in BAT homeostasis and thermogenesis.

Furthermore, FGF21 was shown to be induced by the mild to moderate mitochondrial dysfunction caused by the loss of CLPP, yet FGF21 is not mediating the metabolic changes observed in *Clpp*^{-/-} mice.

The tissue-specific depletion of CLPP revealed a dispensable role for CLPP with regard to whole body metabolism, although tissue restricted mitochondrial dysfunction was present. Finally, ablation of CLPP protects against HFD induced obesity and insulin resistance and it was shown for the first time that hepatic mitochondrial translation is compromised by metabolic stress in the absence of CLPP.

Therefore, this study is contributing to the basic understanding of the CLPP protease function and its regulated metabolic pathways, which may help to understand pathologies with deregulated CLPP expression.

References

- Abizaid, A., Liu, Z.W., Andrews, Z.B., Shanabrough, M., Borok, E., Elsworth, J.D., Roth, R.H., Sleeman, M.W., Picciotto, M.R., Tschöp, M.H., et al. (2006). Ghrelin modulates the activity and synaptic input organization of midbrain dopamine neurons while promoting appetite. *J. Clin. Invest.*
- Ahmadian, M., Suh, J.M., Hah, N., Liddle, C., Atkins, A.R., Downes, M., and Evans, R.M. (2013). PPARgamma signaling and metabolism: the good, the bad and the future. *Nat Med* 19, 557–566.
- Akram, M. (2014). Citric Acid Cycle and Role of its Intermediates in Metabolism. *Cell Biochem. Biophys.* 68, 475–478.
- Atamna, H. (2004). Heme, iron, and the mitochondrial decay of ageing. *Ageing Res. Rev.* 3, 303–318.
- Badman, M.K., Pissios, P., Kennedy, A.R., Koukos, G., Flier, J.S., and Maratos-Flier, E. (2007). Hepatic fibroblast growth factor 21 is regulated by PPARalpha and is a key mediator of hepatic lipid metabolism in ketotic states. *Cell Metab.* 5, 426–437.
- Baggio, L.L., and Drucker, D.J. (2007). Biology of Incretins: GLP-1 and GIP. *Gastroenterology* 132, 2131–2157.
- Baker, T.A., and Sauer, R.T. (2012). ClpXP, an ATP-powered unfolding and protein-degradation machine. *Biochim. Biophys. Acta* 1823, 15–28.
- Barrero, M.J., Camarero, N., Marrero, P.F., and Haro, D. (2003). Control of human carnitine palmitoyltransferase II gene transcription by peroxisome proliferator-activated receptor through a partially conserved peroxisome proliferator-responsive element. *Biochem. J.* 369, 721–729.
- Barrientos, A., Barros, M.H., Valnot, I., Rötig, A., Rustin, P., and Tzagoloff, A. (2002). Cytochrome oxidase in health and disease. In *Gene*, pp. 53–63.
- Becker, G., Klauck, E., and Hengge-Aronis, R. (2000). The response regulator RssB, a recognition factor for *s*. *Mol. Microbiol.* 35, 657–666.
- Bender, T., Lewrenz, I., Franken, S., Baitzel, C., and Voos, W. (2011). Mitochondrial enzymes are protected from stress-induced aggregation by mitochondrial chaperones and the Pim1/LON protease. *Mol. Biol. Cell* 22, 541–554.
- Berg, J.M., Tymoczko, J.L., and Stryer, L. (2002). *Biochemistry* (W. H. Freeman and Company New York).
- Boesch, P., Ibrahim, N., Dietrich, A., and Lightowlers, R.N. (2009). Membrane association of mitochondrial DNA facilitates base excision repair in mammalian mitochondria. *Nucleic Acids Res.* 38, 1478–1488.
- Bollen, M., Keppens, S., and Stalmans, W. (1998). Specific features of glycogen metabolism in the liver. *Biochem. J* 336, 19–31.
- Bonnard, C., Durand, D., Peyrol, S., Chanseaux, E., Chauvin, M. a, Morio, B., Vidal, H., and Rieusset, J. (2008). Mitochondrial dysfunction results from oxidative stress in the skeletal muscle of diet-induced insulin resistant mice. *J Clin Invest* 118, 789–800.
- Brown, P.J.B., Hardy, G.G., Trimble, M.J., and Brun, Y. V (2009). Complex regulatory pathways coordinate cell-cycle progression and development in *Caulobacter crescentus*. *Adv. Microb. Physiol.* 54, 1–101.
- Brownsey, R.W., Boone, A.N., Elliott, J.E., Kulpa, J.E., and Lee, W.M. (2006).

- Regulation of acetyl-CoA carboxylase. *Biochem. Soc. Trans.* **34**, 223–227.
- Buettner, R., Parhofer, K.G., Woenckhaus, M., Wrede, C.E., Kunz-Schughart, L.A., Schölmerich, J., and Bollheimer, L.C. (2006). Defining high-fat-diet rat models: Metabolic and molecular effects of different fat types. *J. Mol. Endocrinol.* **36**, 485–501.
- Cairns, R., Harris, I., and Mak, T. (2011). Regulation of cancer cell metabolism. *Nat. Rev. Cancer* **11**, 85–95.
- Cámara, Y., Asin-Cayueta, J., Park, C.B., Metodiev, M.D., Shi, Y., Ruzzenente, B., Kukat, C., Habermann, B., Wibom, R., Hultenby, K., et al. (2011). MTERF4 Regulates Translation by Targeting the Methyltransferase NSUN4 to the Mammalian Mitochondrial Ribosome. *Cell Metab.* **13**, 527–539.
- Campbell, J.E., and Drucker, D.J. (2015). Islet [alpha] cells and glucagon-critical regulators of energy homeostasis. *Nat Rev Endocrinol* **11**, 329–338.
- Cannon, B., and Nedergaard, J. (2004). Brown adipose tissue: function and physiological significance. *Physiol. Rev.* **84**, 277–359.
- Cannon, B., and Nedergaard, J. (2010). Nonshivering thermogenesis and its adequate measurement in metabolic studies. *J. Exp. Biol.* **214**.
- Chaban, Y., Boekema, E.J., and Dudkina, N. V (2014). Structures of mitochondrial oxidative phosphorylation supercomplexes and mechanisms for their stabilisation. *Biochim. Biophys. Acta - Bioenerg.* **1837**, 418–426.
- Chae, Y.C., Caino, M.C., Lisanti, S., Ghosh, J.C., Dohi, T., Danial, N.N., Villanueva, J., Ferrero, S., Vaira, V., Santambrogio, L., et al. (2012). Control of Tumor Bioenergetics and Survival Stress Signaling by Mitochondrial HSP90s. *Cancer Cell* **22**, 331–344.
- Chan, D.C. (2006). Mitochondria: Dynamic Organelles in Disease, Aging, and Development. *Cell* **125**, 1241–1252.
- Chang, S.C., Heacock, P.N., Clancey, C.J., and Dowhan, W. (1998). The PEL1 gene (renamed PGS1) encodes the phosphatidylglycerophosphate synthase of *Saccharomyces cerevisiae*. *J. Biol. Chem.* **273**, 9829–9836.
- Cheng, C.-W., Kuo, C.-Y., Fan, C.-C., Fang, W.-C., Jiang, S., Lo, Y.-K., Wang, T.-Y., Kao, M.-C., and Lee, A.-L. (2013). Overexpression of Lon contributes to survival and aggressive phenotype of cancer cells through mitochondrial complex I-mediated generation of reactive oxygen species. *Cell Death Dis.* **4**.
- Choi, K.H., and Licht, S. (2005). Control of peptide product sizes by the energy-dependent protease ClpAP. *Biochemistry* **44**, 13921–13931.
- Chondronikola, M., Volpi, E., Børshheim, E., Porter, C., Saraf, M.K., Annamalai, P., Yfanti, C., Chao, T., Wong, D., Shinoda, K., et al. (2016). Brown Adipose Tissue Activation Is Linked to Distinct Systemic Effects on Lipid Metabolism in Humans. *Cell Metab.* **23**, 1200–1206.
- Christie, D.A., Lemke, C.D., Elias, I.M., Chau, L.A., Kirchhof, M.G., Li, B., Ball, E.H., Dunn, S.D., Hatch, G.M., and Madrenas, J. (2011). Stomatin-like protein 2 binds cardiolipin and regulates mitochondrial biogenesis and function. *Mol. Cell. Biol.* **31**, 3845–3856.
- Civitaresse, A.E., MacLean, P.S., Carling, S., Kerr-Bayles, L., McMillan, R.P., Pierce, A., Becker, T.C., Moro, C., Finlayson, J., Lefort, N., et al. (2010). Regulation of skeletal muscle oxidative capacity and insulin signaling by the mitochondrial rhomboid protease PARL. *Cell Metab.* **11**, 412–426.
- Coenen, M.J., Antonicka, H., Ugalde, C., Sasarman, F., Rossi, R., Heister, J.G.A.M.A., Newbold, R.F., Trijbels, F.J.M.F., van den Heuvel, L.P., Shoubridge, E.A., et al. (2004).

- Mutant Mitochondrial Elongation Factor G1 and Combined Oxidative Phosphorylation Deficiency. *N. Engl. J. Med.* 351, 2080–2086.
- Cole, A., Wang, Z., Coyaud, E., Voisin, V., Gronda, M., Jitkova, Y., Mattson, R., Hurren, R., Babovic, S., Maclean, N., et al. (2015). Inhibition of the Mitochondrial Protease ClpP as a Therapeutic Strategy for Human Acute Myeloid Leukemia. *Cancer Cell* 27, 864–876.
- Dennerlein, S., Rozanska, A., Wydro, M., Chrzanowska-Lightowlers, Z.M.A., and Lightowlers, R.N. (2010). Human ERAL1 is a mitochondrial RNA chaperone involved in the assembly of the 28S small mitochondrial ribosomal subunit. *Biochem. J* 430, 551–558.
- Diaz, F., Fukui, H., Garcia, S., and Moraes, C.T. (2006). Cytochrome c Oxidase Is Required for the Assembly/Stability of Respiratory Complex I in Mouse Fibroblasts. *Mol. Cell. Biol.* 26, 4872–4881.
- Diaz, F., Garcia, S., Hernandez, D., Regev, A., Rebelo, A., Oca-Cossio, J., and Moraes, C.T. (2008a). Pathophysiology and fate of hepatocytes in a mouse model of mitochondrial hepatopathies. *Gut* 57, 232–242.
- Diaz, F., Garcia, S., Hernandez, D., Regev, A., Rebelo, A., Oca-Cossio, J., and Moraes, C.T. (2008b). Pathophysiology and fate of hepatocytes in a mouse model of mitochondrial hepatopathies. *Gut* 57, 232–242.
- Doenst, T., Nguyen, T.D., and Abel, E.D. (2013). Cardiac metabolism in heart failure: Implications beyond atp production. *Circ. Res.* 113, 709–724.
- Dogan, S.A., Pujol, C., Maiti, P., Kukat, A., Wang, S., Hermans, S., Senft, K., Wibom, R., Rugarli, E.I., and Trifunovic, A. (2014). Tissue-specific loss of DARS2 activates stress responses independently of respiratory chain deficiency in the heart. *Cell Metab.* 19, 458–469.
- Dudkina, N. V., Kouřil, R., Peters, K., Braun, H.-P., and Boekema, E.J. (2010). Structure and function of mitochondrial supercomplexes. *Biochim. Biophys. Acta - Bioenerg.* 1797, 664–670.
- Eaton, S., Bartlett, K., and Pourfarzam, M. (1996). Mammalian mitochondrial β -oxidation. *Biochem. J* 320, 345–357.
- Edgar, D., Shabalina, I., Camara, Y., Wredenberg, A., Calvaruso, M.A., Nijtmans, L., Nedergaard, J., Cannon, B., Larsson, N.G., and Trifunovic, A. (2009). Random Point Mutations with Major Effects on Protein-Coding Genes Are the Driving Force behind Premature Aging in mtDNA Mutator Mice. *Cell Metab.* 10, 131–138.
- Fillmore, N., Mori, J., and Lopaschuk, G.D. (2014). Mitochondrial fatty acid oxidation alterations in heart failure , ischaemic heart disease and diabetic cardiomyopathy. *Br. J. Pharmacol. Themed* 171, 2080–2090.
- Fischer, F., Weil, A., Hamann, A., Osiewacz, H.D., Tatsuta, T., Langer, T., Baker, B.M., Haynes, C.M., Fischer, F., Hamann, A., et al. (2013). Human CLPP reverts the longevity phenotype of a fungal ClpP deletion strain. *Nat. Commun.* 4, 1397.
- Fischer, F., Langer, J.D., and Osiewacz, H.D. (2015). Identification of potential mitochondrial CLPXP protease interactors and substrates suggests its central role in energy metabolism. *Sci. Rep.* 5, 18375.
- Flynn, J.M., Levchenko, I., Seidel, M., Wickner, S.H., Sauer, R.T., and Baker, T.A. (2001). Overlapping recognition determinants within the *ssrA* degradation tag allow modulation of proteolysis. *Proc. Natl. Acad. Sci. U. S. A.* 98, 10584–10589.
- Flynn, J.M., Neher, S.B., Kim, Y.-I., Sauer, R.T., and Baker, T.A. (2003). Proteomic Discovery of Cellular Substrates of the ClpXP Protease Reveals Five Classes of ClpX-

Recognition Signals. *Mol. Cell* 11, 671–683.

Flynn, J.M., Levchenko, I., Sauer, R.T., and Baker, T.A. (2004). Modulating substrate choice: the SspB adaptor delivers a regulator of the extracytoplasmic-stress response to the AAA+ protease ClpXP for degradation. *Genes Dev.* 18, 2292–2301.

Fontanesi, F., Soto, I.C., Horn, D., and Barrientos, A. (2006). Assembly of mitochondrial cytochrome c-oxidase, a complicated and highly regulated cellular process. *Am. J. Physiol. Cell Physiol.* 291, C1129–C1147.

Forner, F., Foster, L.J., Campanaro, S., Valle, G., and Mann, M. (2006). Quantitative proteomic comparison of rat mitochondria from muscle, heart, and liver. *Mol. Cell. Proteomics* 5, 608–619.

Fothergill-Gilmore, L.A. (1986). The evolution of the glycolytic pathway. *Trends Biochem. Sci.* 11, 47–51.

Frees, D., Qazi, S.N.A., Hill, P.J., and Ingmer, H. (2003). Alternative roles of ClpX and ClpP in *Staphylococcus aureus* stress tolerance and virulence. *Mol. Microbiol.* 48, 1565–1578.

Frey, T., Renken, C., and Perkins, G. (2002). Insight into mitochondrial structure and function from electron tomography. *Biochim. Biophys. Acta - Bioenerg.* 1555, 196–203.

Fulco, M., and Sartorelli, V. (2008). Comparing and contrasting the roles of AMPK and SIRT1 in metabolic tissues. *Cell Cycle* 7, 3669–3679.

Gaillot, O., Pellegrini, E., Bregenholt, S., Nair, S., and Berche, P. (2000). The ClpP serine protease is essential for the intracellular parasitism and virulence of *Listeria monocytogenes*. *Mol. Microbiol.* 35, 1286–1294.

Genova, M.L., Baracca, A., Biondi, A., Casalena, G., Faccioli, M., Falasca, A.I., Formiggini, G., Sgarbi, G., Solaini, G., and Lenaz, G. (2008). Is supercomplex organization of the respiratory chain required for optimal electron transfer activity? *Biochim. Biophys. Acta - Bioenerg.* 1777, 740–746.

Gerdes, F., Tatsuta, T., and Langer, T. (2012). Mitochondrial AAA proteases - Towards a molecular understanding of membrane-bound proteolytic machines. *Biochim. Biophys. Acta - Mol. Cell Res.* 1823, 49–55.

Gilkerson, R.W., Selker, J.M.L., and Capaldi, R.A. (2003). The cristal membrane of mitochondria is the principal site of oxidative phosphorylation. *FEBS Lett.* 546, 355–358.

Gispert, S., Parganlija, D., Klinkenberg, M., Dröse, S., Wittig, I., Mittelbronn, M., Grzmil, P., Koob, S., Hamann, A., Walter, M., et al. (2013). Loss of mitochondrial peptidase Clpp leads to infertility, hearing loss plus growth retardation via accumulation of CLPX, mtDNA and inflammatory factors. *Hum. Mol. Genet.* 22, 4871–4887.

Glynn, S.E., Martin, A., Nager, A.R., Baker, T.A., and Sauer, R.T. (2009). Structures of Asymmetric ClpX Hexamers Reveal Nucleotide-Dependent Motions in a AAA+ Protein-Unfolding Machine. *Cell* 139, 744–756.

Gomes, L.C., Benedetto, G. Di, and Scorrano, L. (2011). During autophagy mitochondria elongate, are spared from degradation and sustain cell viability. *Nat. Cell Biol.* 13, 589–598.

Görs, S., Kucia, M., Langhammer, M., Junghans, P., Metges, C.C., Bünger, L., Laidlaw, A., Bulfield, G., Eisen, E.J., Medrano, J.F., et al. (2009). Technical note: Milk composition in mice--methodological aspects and effects of mouse strain and lactation day. *J. Dairy Sci.* 92, 632–637.

Gottesman, S., Roche, E., Zhou, Y., and Sauer, R.T. (1998). The ClpXP and ClpAP

- proteases degrade proteins with carboxy-terminal peptide tails added by the SsrA-tagging system. *Genes Dev.* *12*, 1338–1347.
- Graham, J.W., Lei, M.G., and Lee, C.Y. (2013). Trapping and identification of cellular substrates of the *Staphylococcus aureus* ClpC chaperone. *J. Bacteriol.* *195*, 4506–4516.
- Greene, A.W., Grenier, K., Aguilera, M.A., Muise, S., Farazifard, R., Haque, M.E., McBride, H.M., Park, D.S., and Fon, E.A. (2012). Mitochondrial processing peptidase regulates PINK1 processing, import and Parkin recruitment. *EMBO Rep.* *13*, 378–385.
- Grevengoed, T.J., Klett, E.L., and Coleman, R.A. (2014). Acyl-CoA Metabolism and Partitioning. *Annu. Rev. Nutr.* *34*, 1–30.
- Hansson, A., Hance, N., Dufour, E., Rantanen, A., Hultenby, K., Clayton, D.A., Wibom, R., and Larsson, N.-Go. (2004). A switch in metabolism precedes increased mitochondrial biogenesis in respiratory chain-deficient mouse hearts. *Proc. Natl. Acad. Sci.* *101*, 3136–3141.
- Haynes, C.M., Petrova, K., Benedetti, C., Yang, Y., and Ron, D. (2007). ClpP mediates activation of a mitochondrial unfolded protein response in *C. elegans*. *Dev. Cell* *13*, 467–480.
- Haynes, C.M., Yang, Y., Blais, S.P., Neubert, T.A., and Ron, D. (2010). The Matrix Peptide Exporter HAF-1 Signals a Mitochondrial UPR by Activating the Transcription Factor ZC376.7 in *C. elegans*. *Mol. Cell* *37*, 529–540.
- Haynes, C.M., Yang, Y., Blais, S.P., and Neubert, T.A. (2011). NIH Public Access. *37*, 529–540.
- Hengge, R. (2009). Proteolysis of σ^S (RpoS) and the general stress response in *Escherichia coli*. *Res. Microbiol.* *160*, 667–676.
- Hillgartner, F.B., Salati, L.M., and Goodridge, A.G. (1995). Physiological and Molecular Mechanisms Involved in Nutritional Regulation of Fatty Acid Synthesis. *PHYSIOLOGICAL Rev.* *75*.
- Holt, I.J., and Reyes, A. (2012). Human mitochondrial DNA replication. *Cold Spring Harb. Perspect. Biol.* *4*, a012971.
- Hornig-Do, H.-T., Tatsuta, T., Buckermann, A., Bust, M., Kollberg, G., Rötig, A., Hellmich, M., Nijtmans, L., Wiesner, R.J., Acin-Perez, R., et al. (2012). Nonsense mutations in the COX1 subunit impair the stability of respiratory chain complexes rather than their assembly. *EMBO J.* *31*, 1293–1307.
- Hou, X.H., Zhang, J.Q., Song, X.Y., Ma, X.B., and Zhang, S.Y. (2014). Contribution of ClpP to stress tolerance and virulence properties of *Streptococcus mutans*. *J. Basic Microbiol.* *54*, 1222–1232.
- Houtkooper, R.H., Mouchiroud, L., Ryu, D., Moullan, N., Katsyuba, E., Knott, G., Williams, R.W., and Auwerx, J. (2013). Mitonuclear protein imbalance as a conserved longevity mechanism. *Nature* *497*, 451–457.
- Huang, J., Wang, X., Cao, Q., Feng, F., Xu, X., and Cai, X. (2016). ClpP participates in stress tolerance and negatively regulates biofilm formation in *Haemophilus parasuis*. *Vet. Microbiol.* *182*, 141–149.
- Hue, H.G., and Hers, L. (1983). GLUCONEOGENESIS AND RELATED ASPECTS OF GLYCOLYSIS. *Annu. Rev. Biochem.* *52*, 617–653.
- Huynh, F.K., Green, M.F., Koves, T.R., and Hirschey, M.D. (2014). Measurement of fatty acid oxidation rates in animal tissues and cell lines. *Methods Enzymol.* *542*, 391–405.

- Ikeda, K., Shiba, S., Horie-Inoue, K., Shimokata, K., Inoue, S., Schägger, H., Pfeiffer, K., Schägger, H., Pfeiffer, K., Acín-Pérez, R., et al. (2013). A stabilizing factor for mitochondrial respiratory supercomplex assembly regulates energy metabolism in muscle. *Nat. Commun.* 4, 1777–1783.
- Inagaki, T., Dutchak, P., Zhao, G., Ding, X., Gautron, L., Parameswara, V., Li, Y., Goetz, R., Mohammadi, M., Esser, V., et al. (2007). Endocrine regulation of the fasting response by PPAR α -mediated induction of fibroblast growth factor 21. *Cell Metab.* 5, 415–425.
- Inagaki, T., Lin, V.Y., Goetz, R., Mohammadi, M., Mangelsdorf, D.J., and Kliewer, S.A. (2008). Inhibition of growth hormone signaling by the fasting-induced hormone FGF21. *Cell Metab.* 8, 77–83.
- Jenkinson, E.M., Rehman, A.U., Walsh, T., Clayton-Smith, J., Lee, K., Morell, R.J., Drummond, M.C., Khan, S.N., Naeem, M.A., Rauf, B., et al. (2013). Perrault syndrome is caused by recessive mutations in CLPP, encoding a mitochondrial ATP-dependent chambered protease. *Am. J. Hum. Genet.* 92, 605–613.
- Ji, K., Zheng, J., Lv, J., Xu, J., Ji, X., Luo, Y.B., Li, W., Zhao, Y., and Yan, C. (2015). Skeletal muscle increases FGF21 expression in mitochondrial disorders to compensate for energy metabolic insufficiency by activating the mTOR-YY1-PGC1 α pathway. *Free Radic. Biol. Med.* 84, 161–170.
- Jitrapakdee, S. (2012). Transcription factors and coactivators controlling nutrient and hormonal regulation of hepatic gluconeogenesis. *Int. J. Biochem. Cell Biol.* 44, 33–45.
- Jonckheere, A.I., Smeitink, J.A.M., and Rodenburg, R.J.T. (2012). Mitochondrial ATP synthase: Architecture, function and pathology. *J. Inherit. Metab. Dis.* 35, 211–225.
- Kang, S.G., Maurizi, M.R., Thompson, M., Mueser, T., and Ahvazi, B. (2004). Crystallography and mutagenesis point to an essential role for the N-terminus of human mitochondrial ClpP. *J. Struct. Biol.* 148, 338–352.
- Kang, S.G., Dimitrova, M.N., Ortega, J., Ginsburg, A., and Maurizi, M.R. (2005). Human mitochondrial ClpP is a stable heptamer that assembles into a tetradecamer in the presence of ClpX. *J. Biol. Chem.* 280, 35424–35432.
- Keiler, K.C., Waller, P.R., and Sauer, R.T. (1996). Role of a peptide tagging system in degradation of proteins synthesized from damaged messenger RNA. *Science* 271, 990–993.
- Keipert, S., Ost, M., Johann, K., Imber, F., Jastroch, M., van Schothorst, E.M., Keijer, J., and Klaus, S. (2014). Skeletal muscle mitochondrial uncoupling drives endocrine cross-talk through the induction of FGF21 as a myokine. *Am. J. Physiol. Endocrinol. Metab.* 306, E469–82.
- Kellendonk, C., Opherck, C., Anlag, K., Schütz, G., and Tronche, F. (2000). Hepatocyte-specific expression of Cre recombinase. *Genesis* 26, 151–153.
- Kelley, D.E., He, J., Menshikova, E. V., and Ritov, V.B. (2002). Dysfunction of mitochondria in human skeletal muscle in type 2 diabetes. *Diabetes* 51, 2944–2950.
- Kharitonov, A., and Adams, A.C. (2014). Inventing new medicines: The FGF21 story. *Mol. Metab.* 3, 221–229.
- Kim, K.H. (1997). Regulation of mammalian acetyl-coenzyme A carboxylase. *Annu. Rev. Nutr.* 17, 77–99.
- Kim, J.-Y., Hickner, R.C., Cortright, R.L., Dohm, G.L., and Houmard, J.A. (2000). Lipid oxidation is reduced in obese human skeletal muscle. *Am. J. Physiol. - Endocrinol. Metab.* 279.

- Kim, K.H., Jeong, Y.T., Oh, H., Kim, S.H., Cho, J.M., Kim, Y.-N., Kim, S.S., Kim, D.H., Hur, K.Y., Kim, H.K., et al. (2013). Autophagy deficiency leads to protection from obesity and insulin resistance by inducing Fgf21 as a mitokine. *Nat. Med.* *19*, 83–92.
- Kishida, T., Ejima, A., Yamamoto, K., Tanaka, S., Yamamoto, T., and Mazda, O. (2015). Reprogrammed Functional Brown Adipocytes Ameliorate Insulin Resistance and Dyslipidemia in Diet-Induced Obesity and Type 2 Diabetes. *Stem Cell Reports* *5*, 569–581.
- Klip, A., and Pâquet, M.R. (1990). Glucose transport and glucose transporters in muscle and their metabolic regulation. *Diabetes Care* *13*, 228–243.
- Koves, T.R., Ussher, J.R., Noland, R.C., Slentz, D., Mosedale, M., Ilkayeva, O., Bain, J., Stevens, R., Dyck, J.R.B., Newgard, C.B., et al. (2008). Mitochondrial Overload and Incomplete Fatty Acid Oxidation Contribute to Skeletal Muscle Insulin Resistance. *Cell Metab.* *7*, 45–56.
- Kurland, C.G., and Andersson, S.G.E. (2000). Origin and Evolution of the Mitochondrial Proteome. *Microbiol. Mol. Biol. Rev.* *64*, 786–820.
- Kurland, C.G., Andersson, S.G.E., Zomorodipour, A., Andersson, J.O., Sicheritz-Pontén, T., Alsmark, U.C.M., Podowski, R.M., Näslund, A.K., Eriksson, A.-S., and Winkler, H.H. (1998). The genome sequence of *Rickettsia prowazekii* and the origin of mitochondria. *Nature* *396*, 133–140.
- Kusminski, C.M., and Scherer, P.E. (2012). Mitochondrial dysfunction in white adipose tissue. *Trends Endocrinol. Metab.* *23*, 435–443.
- Kusminski, C.M., Park, J., Scherer, P.E., Zimmet, P., Alberti, K.G., Shaw, J., Axen, K. V., Dikeakos, A., Sclafani, A., Bessesen, D.H., et al. (2014). MitoNEET-mediated effects on browning of white adipose tissue. *Nat. Commun.* *5*, 782–787.
- Laemmli, U.K. (1970). Cleavage of structural proteins during the assembly of the head of bacteriophage T4. *Nature* *227*, 680–685.
- Laron, Z. (2001). Insulin-like growth factor 1 (IGF-1): a growth hormone. *Mol. Pathol.* *54*, 311–316.
- Larsson, N.-O. (2010). Somatic Mitochondrial DNA Mutations in Mammalian Aging. *Annu. Rev. Biochem* *79*, 683–706.
- Larsson, N.G., Wang, J., Wilhelmsson, H., Oldfors, A., Rustin, P., Lewandoski, M., Barsh, G.S., and Clayton, D.A. (1998). Mitochondrial transcription factor A is necessary for mtDNA maintenance and embryogenesis in mice. *Nat. Genet.* *18*, 231–236.
- Lazarou, M., McKenzie, M., Ohtake, A., Thorburn, D.R., and Ryan, M.T. (2007). Analysis of the Assembly Profiles for Mitochondrial- and Nuclear-DNA-Encoded Subunits into Complex I. *Mol. Cell. Biol.* *27*, 4228–4237.
- Lee, J., Ellis, J.M., and Wolfgang, M.J. (2015). Adipose fatty acid oxidation is required for thermogenesis and potentiates oxidative stress-induced inflammation. *Cell Rep.* *10*, 266–279.
- Lee, J., Choi, J., Scafidi, S., and Wolfgang, M.J. (2016a). Hepatic Fatty Acid Oxidation Restrains Systemic Catabolism during Starvation. *Cell Rep.* *16*, 1–12.
- Lee, J., Choi, J., Aja, S., Scafidi, S., and Wolfgang, M.J.J. (2016b). Loss of Adipose Fatty Acid Oxidation Does Not Potentiate Obesity at Thermoneutrality. *Cell Rep.* *14*, 1308–1316.
- Leong, D.W., Komen, J.C., Hewitt, C.A., Arnaud, E., McKenzie, M., Phipson, B., Bahlo, M., Laskowski, A., Kinkel, S.A., Davey, G.M., et al. (2012). Proteomic and metabolomic analyses of mitochondrial complex I-deficient mouse model generated by spontaneous

- B2 short interspersed nuclear element (SINE) insertion into NADH dehydrogenase (ubiquinone) Fe-S protein 4 (Ndufs4) gene. *J. Biol. Chem.* 287, 20652–20663.
- Levéen, P., Kotarsky, H., Mörgelin, M., Karikoski, R., Elmér, E., and Fellman, V. (2011). The GRACILE mutation introduced into Bcs1l causes postnatal complex III deficiency: A viable mouse model for mitochondrial hepatopathy. *Hepatology* 53, 437–447.
- Liesa, M., and Shirihai, O.S. (2013). Mitochondrial dynamics in the regulation of nutrient utilization and energy expenditure. *Cell Metab.* 17, 491–506.
- Lill, R., and Mühlenhoff, U. (2005). Iron–sulfur-protein biogenesis in eukaryotes. *Trends Biochem. Sci.* 30, 133–141.
- Lin, J., Wu, P.-H., Tarr, P.T., Lindenberg, K.S., St-Pierre, J., Zhang, C.-Y., Mootha, V.K., Jäger, S., Vianna, C.R., Reznick, R.M., et al. (2004). Defects in adaptive energy metabolism with CNS-linked hyperactivity in PGC-1alpha null mice. *Cell* 119, 121–135.
- Lippe, G., Sorgato, M.C., and Harris, D. a (1988). Structure and dynamics of the mitochondrial inner membrane cristae. *Biochim. Biophys. Acta* 1763, 542–548.
- Liu, Q., Krzewska, J., Liberek, K., and Craig, E.A. (2001). Mitochondrial Hsp70 Ssc1: role in protein folding. *J. Biol. Chem.* 276, 6112–6118.
- Lyons, G.E., Mühlebach, S., Moser, A., Masood, R., Paterson, B.M., Buckingham, M.E., and Perriard, J.C. (1991). Developmental regulation of creatine kinase gene expression by myogenic factors in embryonic mouse and chick skeletal muscle. *Development* 113, 1017–1029.
- Marcinek, D.J., Schenkman, K.A., Ciesielski, W.A., and Conley, K.E. (2004). Mitochondrial coupling in vivo in mouse skeletal muscle. *Am. J. Physiol. Cell Physiol.* 286, C457–63.
- Margulis, L. (1975). Symbiotic theory of the origin of eukaryotic organelles; criteria for proof. *Symp. Soc. Exp. Biol.* 21–38.
- Marques, I., Dencher, N.A., Videira, A., and Krause, F. (2007). Supramolecular organization of the respiratory chain in *Neurospora crassa* mitochondria. *Eukaryot. Cell* 6, 2391–2405.
- Maruyama, R., Shimizu, M., Li, J., Inoue, J., and Sato, R. (2016). Fibroblast growth factor 21 induction by activating transcription factor 4 is regulated through three amino acid response elements in its promoter region. *Biosci. Biotechnol. Biochem.* ISSN 80, 929–934.
- McBride, H.M., Neuspiel, M., and Wasiak, S. (2006). Mitochondria: More Than Just a Powerhouse. *Curr. Biol.* 16, R551–R560.
- Metallo, C.M., and Vander Heiden, M.G. (2013). Understanding Metabolic Regulation and Its Influence on Cell Physiology. *Mol. Cell* 49, 388–398.
- Metodiev, M.D., Lesko, N., Park, C.B., Cámara, Y., Shi, Y., Wibom, R., Hultenby, K., Gustafsson, C.M., and Larsson, N.-G. (2009). Methylation of 12S rRNA Is Necessary for In Vivo Stability of the Small Subunit of the Mammalian Mitochondrial Ribosome. *Cell Metab.* 9, 386–397.
- Metodiev, M.D., Spåhr, H., Loguercio Polosa, P., Meharg, C., Becker, C., Altmueller, J., Habermann, B., Larsson, N.G., and Ruzzenente, B. (2014). NSUN4 Is a Dual Function Mitochondrial Protein Required for Both Methylation of 12S rRNA and Coordination of Mitoribosomal Assembly. *PLoS Genet.* 10, 1–11.
- Mimaki, M., Wang, X., McKenzie, M., Thorburn, D.R., and Ryan, M.T. (2012). Understanding mitochondrial complex I assembly in health and disease. *Biochim.*

- Biophys. Acta-Bioenergetics 1817, 851–862.
- Minokoshi, Y., Kim, Y.-B., Peroni, O.D., Fryer, L.G.D., Müller, C., Carling, D., and Kahn, B.B. (2002). Leptin stimulates fatty-acid oxidation by activating AMP-activated protein kinase. *Nature* 415, 339–343.
- Mootha, V.K., Bunkenborg, J., Olsen, J. V., Hjerrild, M., Wisniewski, J.R., Stahl, E., Bolouri, M.S., Ray, H.N., Sihag, S., Kamal, M., et al. (2003). Integrated analysis of protein composition, tissue diversity, and gene regulation in mouse mitochondria. *Cell* 115, 629–640.
- Mullis, K.B., and Faloona, F.A. (1987). [21] Specific synthesis of DNA in vitro via a polymerase-catalyzed chain reaction. *Methods Enzymol.* 155, 335–350.
- Mytinger, J.R., Rao Passi, G., Newman, W., M Smeets, H.J., van der Knaap, M.S., M de Coo, I.F., M, H.J., Tej, T., Dmei, H., Hartog ENM, M.-D., et al. (2016). Specific MRI Abnormalities Reveal Severe Perrault Syndrome due to CLPP Defects. *Front. Neurol.* 7.
- Nargund, A.M., Pellegrino, M.W., Fiorese, C.J., Baker, B.M., and Haynes, C.M. (2012). Mitochondrial import efficiency of ATFS-1 regulates mitochondrial UPR activation. *Science* 337, 587–590.
- Neher, S.B., Villé, J., Oakes, E.C., Bakalarski, C.E., Sauer, R.T., Gygi, S.P., and Baker, T.A. (2006). Proteomic Profiling of ClpXP Substrates after DNA Damage Reveals Extensive Instability within SOS Regulon. *Mol. Cell* 22, 193–204.
- Neupert, W., and Herrmann, J.M. (2007). Translocation of Proteins into Mitochondria. *Annu. Rev. Biochem.* 76, 723–749.
- Ngo, J.K., and Davies, K.J. (2007). Importance of the Lon protease in mitochondrial maintenance and the significance of declining Lon in aging. *Ann. N. Y. Acad. Sci.* 1119, 78–87.
- Nunnari, J., and Suomalainen, A. (2012). Mitochondria: In Sickness and in Health. *Cell* 148, 1145–1159.
- Ojuka, E., Andrew, B., Bezuidenhout, N., George, S., Maarman, G., Madlala, H.P., Mendham, A., and Osiki, P.O. (2016). Measurement of beta-oxidation capacity of biological samples by respirometry: A review of principles and substrates. *Am. J. Physiol. - Endocrinol. Metab.* ajpendo.00475.2015.
- Ortega, J., Singh, S.K., Ishikawa, T., Maurizi, M.R., and Steven, A.C. (2000). Visualization of Substrate Binding and Translocation by the ATP-Dependent Protease, ClpXP. *Mol. Cell* 6, 1515–1521.
- Ost, M., Coleman, V., Voigt, A., van Schothorst, E.M., Keipert, S., van der Stelt, I., Ringel, S., Graja, A., Ambrosi, T., Kipp, A.P., et al. (2016). Muscle mitochondrial stress adaptation operates independently of endogenous FGF21 action. *Mol. Metab.* 5, 79–90.
- Ostermann, J., Horwich, A.L., Neupert, W., and Hartl, F.-U. (1989). Protein folding in mitochondria requires complex formation with hsp60 and ATP hydrolysis. *Nature* 341, 125–130.
- Ostrander, D.B., Zhang, M., Mileykovskaya, E., Rho, M., and Dowhan, W. (2001). Lack of mitochondrial anionic phospholipids causes an inhibition of translation of protein components of the electron transport chain. A yeast genetic model system for the study of anionic phospholipid function in mitochondria. *J. Biol. Chem.* 276, 25262–25272.
- Owen, O.E., Kalhan, S.C., and Hanson, R.W. (2002). The key role of anaplerosis and cataplerosis for citric acid cycle function. *J. Biol. Chem.* 277, 30409–30412.

- Pagliarini, D.J., Calvo, S.E., Chang, B., Sheth, S.A., Vafai, S.B., Ong, S.E., Walford, G.A., Sugiana, C., Boneh, A., Chen, W.K., et al. (2008). A Mitochondrial Protein Compendium Elucidates Complex I Disease Biology. *Cell* 134, 112–123.
- Park, C.B., Asin-Cayuela, J., Cámara, Y., Shi, Y., Pellegrini, M., Gaspari, M., Wibom, R., Hultenby, K., Erdjument-Bromage, H., Tempst, P., et al. (2007). MTERF3 Is a Negative Regulator of Mammalian mtDNA Transcription. *Cell* 130, 273–285.
- Patti, M.-E., and Corvera, S. (2010). The role of mitochondria in the pathogenesis of type 2 diabetes. *Endocr. Rev.* 31, 364–395.
- Pelleymounter, M.A., Cullen, M.J., Baker, M.B., Hecht, R., Winters, D., Boone, T., and Collins, F. (1995). Effects of the obese gene product on body weight regulation in ob/ob mice. *Science* 269, 540–543.
- Petersen, K.F., Befroy, D., Dufour, S., Dziura, J., Ariyan, C., Rothman, D.L., DiPietro, L., Cline, G.W., and Shulman, G.I. (2003). Mitochondrial dysfunction in the elderly: possible role in insulin resistance. *Science* 300, 1140–1142.
- Phillips, F.C., and Ainsworth, S. (1977). Allosteric properties of rabbit muscle pyruvate kinase. *Int. J. Biochem.* 8, 729–735.
- Pospisilik, J.A., Knauf, C., Joza, N., Benit, P., Orthofer, M., Cani, P.D., Ebersberger, I., Nakashima, T., Sarao, R., Neely, G., et al. (2007). Targeted Deletion of AIF Decreases Mitochondrial Oxidative Phosphorylation and Protects from Obesity and Diabetes. *Cell* 131, 476–491.
- Potthoff, M.J., Inagaki, T., Satapati, S., Ding, X., He, T., Goetz, R., Mohammadi, M., Finck, B.N., Mangelsdorf, D.J., Kliewer, S.A., et al. (2009). FGF21 induces PGC-1 α and regulates carbohydrate and fatty acid metabolism during the adaptive starvation response. *Proc. Natl. Acad. Sci. U. S. A.* 106, 10853–10858.
- Quintens, R., Singh, S., Lemaire, K., De Bock, K., Granvik, M., Schraenen, A., Vroegrijk, I.O.C.M., Costa, V., Van Noten, P., Lambrechts, D., et al. (2013). Mice deficient in the respiratory chain gene *Cox6a2* are protected against high-fat diet-induced obesity and insulin resistance. *PLoS One* 8, e56719.
- Quiró S, P.M., Ramsay, A.J., Sala, D., Ferná Ndez-Vizarrá, E., Rodríguez, F., Peinado, J.R., Soledad Ferná Ndez-García, M., Vega, J.A., Enríquez, J.A., Zorzano, A., et al. (2012). Loss of mitochondrial protease OMA1 alters processing of the GTPase OPA1 and causes obesity and defective thermogenesis in mice. *EMBO J.* 31, 2117–2133.
- Quirós, P.M., Español, Y., Acín-Pérez, R., Rodríguez, F., Bárcena, C., Watanabe, K., Calvo, E., Loureiro, M., Fernández-García, M.S., Fueyo, A., et al. (2014). ATP-dependent Lon protease controls tumor bioenergetics by reprogramming mitochondrial activity. *Cell Rep.* 8, 542–556.
- Rakhshandehroo, M., Hooiveld, G., Müller, M., and Kersten, S. (2009). Comparative analysis of gene regulation by the transcription factor PPAR α between mouse and human. *PLoS One* 4, e6796.
- Randle, P.J. (1963). Endocrine control of metabolism. *Annu. Rev. Physiol.* 25, 291–324.
- Rappsilber, J., Ishihama, Y., and Mann, M. (2002). Stop and Go Extraction Tips for Matrix-Assisted Laser Desorption/Ionization, Nano-electrospray, and LC/MS Sample Pretreatment in Proteomics. *Anal. Chem.* 75, 663–670.
- Al Rawi, S., Louvet-Vallée, S., Djeddi, A., Sachse, M., Culetto, E., Hajjar, C., Boyd, L., Legouis, R., Galy, V., Birky, C.W., et al. (2011). Postfertilization autophagy of sperm organelles prevents paternal mitochondrial DNA transmission. *Science* 334, 1144–1147.

- Ritov, V.B., Menshikova, E. V., He, J., Ferrell, R.E., Goodpaster, B.H., and Kelley, D.E. (2004). Deficiency of Subsarcolemmal Mitochondria in Obesity and Type 2 Diabetes. *Diabetes* 54.
- Rizza, R.A., Mandarino, L.J., and Gerich, J.E. (1981). Dose-response characteristics for effects of insulin on production and utilization of glucose in man. *Am. J. Physiol.* 240, E630–E639.
- Rodríguez, E., Monjo, M., Rodríguez-Cuenca, S., Pujol, E., Amengual, B., Roca, P., and Palou, A. (2001). Sexual dimorphism in the adrenergic control of rat brown adipose tissue response to overfeeding. *Pflügers Arch.* 442, 396–403.
- Rodríguez-Cuenca, S., Pujol, E., Justo, R., Frontera, M., Oliver, J., Gianotti, M., and Roca, P. (2002). Sex-dependent thermogenesis, differences in mitochondrial morphology and function, and adrenergic response in brown adipose tissue. *J. Biol. Chem.* 277, 42958–42963.
- Rosignol, R., Malgat, M., Mazat, J.-P., and Letellier, T. (1999). Threshold Effect and Tissue Specificity. *J Biol. Chem.* 274, 33426–33432.
- Rugarli, E.I., and Langer, T. (2012). Focus Review Mitochondrial quality control: a matter of life and death for neurons. *EMBO J.* 31, 1336–1349.
- Rui, L. (2014). Energy metabolism in the liver. *Compr. Physiol.* 4, 177–197.
- Rustan, A.C. (2009). Fatty Acids: Structures and Properties. *Encycl. Life Sci.* 1–7.
- Rutter, J., Winge, D.R., and Schiffman, J.D. (2010). Succinate dehydrogenase – Assembly, regulation and role in human disease. *Mitochondrion* 10, 393–401.
- Ruzzenente, B., Metodiev, M.D., Wredenberg, A., Bratic, A., Park, C.B., Cámara, Y., Milenkovic, D., Zickermann, V., Wibom, R., Hulthenby, K., et al. (2012). LRPPRC is necessary for polyadenylation and coordination of translation of mitochondrial mRNAs. *EMBO J.* 31, 443–456.
- Saiki, R.K., Gelfand, D.H., Stoffel, S., Scharf, S.J., Higuchi, R., Horn, G.T., Mullis, K.B., and Erlich, H.A. (1988). Primer-directed enzymatic amplification of DNA with a thermostable DNA polymerase. *Science* 239, 487–491.
- S J Pilkis, and, and Granner, D.K. (1992). Molecular Physiology of the Regulation of Hepatic Gluconeogenesis and Glycolysis. *Annu. Rev. Physiol.* 54, 885–909.
- Saleem, A., Safdar, A., Kitaoka, Y., Ma, X., Marquez, O.S., Akhtar, M., Nazli, A., Suri, R., Turnbull, J., and Tamopolsky, M.A. (2015). Polymerase gamma mutator mice rely on increased glycolytic flux for energy production. *Mitochondrion* 21, 19–26.
- Saltiel, A.R., and Kahn, C.R. (2001). Insulin signalling and the regulation of glucose and lipid metabolism. *Nature* 414, 799–806.
- Sauer, R.T., and Baker, T.A. (2011). AAA+ proteases: ATP-fueled machines of protein destruction. *Annu. Rev. Biochem.* 80, 587–612.
- Schägger, H., and Pfeiffer, K. (2000). Supercomplexes in the respiratory chains of yeast and mammalian mitochondria. *EMBO J.* 19, 1777–1783.
- Schägger, H., de Coo, R., Bauer, M.F., Hofmann, S., Godinot, C., and Brandt, U. (2004). Significance of respirasomes for the assembly/stability of human respiratory chain complex I. *J. Biol. Chem.* 279, 36349–36353.
- Schon, E.A., DiMauro, S., and Hirano, M. (2012). Human mitochondrial DNA: roles of inherited and somatic mutations. *Nat Rev Genet* 13, 878–890.
- Schwartz, M.W., Woods, S.C., Porte, D., Seeley, R.J., and Baskin, D.G. (2000). Central nervous system control of food intake. *Nature* 404, 661–671.

- Sebastián, D., Hernández-Alvarez, M.I., Segalés, J., Sorianello, E., Muñoz, J.P., Sala, D., Waget, A., Liesa, M., Paz, J.C., Gopalacharyulu, P., et al. (2012). Mitofusin 2 (Mfn2) links mitochondrial and endoplasmic reticulum function with insulin signaling and is essential for normal glucose homeostasis. *Proc. Natl. Acad. Sci. U. S. A.* *109*, 5523–5528.
- Seiferling, D., Szczepanowska, K., Becker, C., Senft, K., Hermans, S., Maiti, P., König, T., Kukat, A., and Trifunovic, A. (2016). Loss of CLPP alleviates mitochondrial cardiomyopathy without affecting the mammalian UPRmt. *EMBO Rep.* *17*, 1–12.
- Shimizu, I., and Walsh, K. (2015). The Whitening of Brown Fat and Its Implications for Weight Management in Obesity. *Curr. Obes. Rep.* *4*, 224–229.
- Silva, J.P., Köhler, M., Graff, C., Oldfors, A., Magnuson, M.A., Berggren, P.O., and Larsson, N.G. (2000). Impaired insulin secretion and beta-cell loss in tissue-specific knockout mice with mitochondrial diabetes. *Nat. Genet.* *26*, 336–340.
- Silver, L.M. (1995). *Mouse Genetics Concepts and Applications* (New York: Oxford University Press).
- Škrtić, M., Sriskanthadevan, S., and Jhas, B. (2011). Inhibition of mitochondrial translation as a therapeutic strategy for human acute myeloid leukemia. *Cancer Cell* *20*, 674–688.
- Slavin, B.G., Ong, J.M., and Kern, P.A. (1994). Hormonal regulation of hormone-sensitive lipase activity and mRNA levels in isolated rat adipocytes. *J. Lipid Res.* *35*, 1535–1541.
- Solon-Biet, S.M., Cogger, V.C., Pulpitel, T., Heblinski, M., Wahl, D., McMahon, A.C., Warren, A., Durrant-Whyte, J., Walters, K.A., Krycer, J.R., et al. (2016). Defining the Nutritional and Metabolic Context of FGF21 Using the Geometric Framework. *Cell Metab.* *24*, 555–565.
- Speakman, J.R. (2013). Measuring energy metabolism in the mouse - theoretical, practical, and analytical considerations. *Front. Physiol.* *4* MAR, 34.
- Stein, L.R., and Imai, S.I. (2012). The dynamic regulation of NAD metabolism in mitochondria. *Trends Endocrinol. Metab.* *23*, 420–428.
- Steppan, C.M., Bailey, S.T., Bhat, S., Brown, E.J., Banerjee, R.R., Wright, C.M., Patel, H.R., Ahima, R.S., and Lazar, M.A. (2001). The hormone resistin links obesity to diabetes. *Nature* *409*, 307–312.
- Stewart, J.B., and Chinnery, P.F. (2015). The dynamics of mitochondrial DNA heteroplasmy: Implications for human health and disease. *Nat. Rev. Genet.* *16*, 530–542.
- Strauss, M., Hofhaus, G., Schröder, R.R., and Kühlbrandt, W. (2008). Dimer ribbons of ATP synthase shape the inner mitochondrial membrane. *EMBO J.* *27*, 1154–1160.
- Szczepanowska, K., Maiti, P., Kukat, A., Hofsetz, E., Nolte, H., Senft, K., Becker, C., Ruzzenente, B., Hornig-Do, H.-T., Wibom, R., et al. (2016). CLPP coordinates mitoribosomal assembly through the regulation of ERAL1 levels. *EMBO J.* *35*, 2566–2583.
- Thompson, M.W., Singh, S.K., and Maurizi, M.R. (1994). Processive degradation of proteins by the ATP-dependent Clp protease from *Escherichia coli*: Requirement for the multiple array of active sites in ClpP but not ATP hydrolysis. *J. Biol. Chem.* *269*, 18209–18215.
- Thor Johnson, D., Harris, R.A., French, S., Blair, P. V, You, J., Bemis, K.G., Wang, M., and Balaban, R.S. (2007). Tissue heterogeneity of the mammalian mitochondrial proteome. *Am J Physiol Cell Physiol* *292*, 689–697.

- Timmis, J.N., Ayliffe, M.A., Huang, C.Y., and Martin, W. (2004). Endosymbiotic gene transfer: organelle genomes forge eukaryotic chromosomes. *Nat. Rev. Genet.* 5, 123–135.
- Torchon, E., Ray, R., Hulver, M.W., McMillan, R.P., and Voy, B.H. (2017). Fasting rapidly increases fatty acid oxidation in white adipose tissue of young broiler chickens. *Adipocyte* 6, 33–39.
- Tschöp, M., Smiley, D.L., and Heiman, M.L. (2000). Ghrelin induces adiposity in rodents. *Nature* 407, 908–913.
- Tyynismaa, H., Carroll, C.J., Raimundo, N., Ahola-Erkkilä, S., Wenz, T., Ruhanen, H., Guse, K., Hemminki, A., Peltola-Mjøsund, K.E., Tulkki, V., et al. (2010). Mitochondrial myopathy induces a starvation-like response. *Hum. Mol. Genet.* 19, 3948–3958.
- Vandanmagsar, B., Warfel, J.D., Wicks, S.E., Ghosh, S., Salbaum, J.M., Burk, D., Dubuisson, O.S., Mendoza, T.M., Zhang, J., Noland, R.C., et al. (2016). Impaired Mitochondrial Fat Oxidation Induces FGF21 in Muscle. *Cell Rep.* 15, 1686–1699.
- Vernochet, C., Mourier, A., Bezy, O., Macotela, Y., Boucher, J., Rardin, M.J., An, D., Lee, K.Y., Ilkayeva, O.R., Zingaretti, C.M., et al. (2012). Adipose-Specific Deletion of TFAM Increases Mitochondrial Oxidation and Protects Mice against Obesity and Insulin Resistance. *Cell Metab.* 16, 765–776.
- Vogel, F., Bornhövd, C., Neupert, W., and Reichert, A.S. (2006). Dynamic subcompartmentalization of the mitochondrial inner membrane. *J. Cell Biol.* 175.
- Wagner, I., Arit, H., Dyck, L. Van, Langer, T., and Neupert, W. (1994). Molecular chaperones cooperate with PIM1 protease in the degradation of misfolded proteins in mitochondria. *EMBO J.* 13, 5135–5145.
- Wai, T., García-Prieto, J., Baker, M.J., Merkwirth, C., Benit, P., Rustin, P., Rupérez, F.J., Barbas, C., Ibañez, B., and Langer, T. (2015). Imbalanced OPA1 processing and mitochondrial fragmentation cause heart failure in mice. *Science* (80-.). 350.
- Wakil, S.J. (1989). Fatty acid synthase, a proficient multifunctional enzyme. *Biochemistry* 28, 4523–4530.
- Wallace, D.C. (2005). A Mitochondrial Paradigm of Metabolic and Degenerative Diseases, Aging, and Cancer: A Dawn for Evolutionary Medicine. *Annu. Rev. Genet.* 39, 359–407.
- Wallace, D.C. (2007). Why Do We Still Have a Maternally Inherited Mitochondrial DNA? Insights from Evolutionary Medicine. *Annu. Rev. Biochem.* 76, 781–821.
- Wallace, D.C. (2013). A mitochondrial bioenergetic etiology of disease. *J. Clin. Invest.* 123, 1405–1412.
- Wanagat, J., and Hevener, A.L. (2016). Mitochondrial quality control in insulin resistance and diabetes. *Curr. Opin. Genet. Dev.* 38, 118–126.
- Wang, J., Hartling, J.A., and Flanagan, J.M. (1997). The Structure of ClpP at 2.3 Å Resolution Suggests a Model for ATP-Dependent Proteolysis. *Cell* 91, 447–456.
- Wells, T., Davies, J.R., Guschina, I.A., Ball, D.J., Davies, J.S., Davies, V.J., Evans, B.A.J., and Votruba, M. (2012). Opa3, a novel regulator of mitochondrial function, controls thermogenesis and abdominal fat mass in a mouse model for Costeff syndrome. *Hum. Mol. Genet.* 21, 4836–4844.
- Wittig, I., and Schägger, H. (2009). Supramolecular organization of ATP synthase and respiratory chain in mitochondrial membranes. *Biochim. Biophys. Acta* 1787, 672–680.
- Wong, L.-J.C. (2007). Diagnostic challenges of mitochondrial DNA disorders. *Mitochondrion* 7, 45–52.

- Wredenberg, A., Wibom, R., Wilhelmsson, H., Graff, C., Wiener, H.H., Burden, S.J., Oldfors, A., Westerblad, H., and Larsson, N.-G. (2002). Increased mitochondrial mass in mitochondrial myopathy mice. *Proc. Natl. Acad. Sci. U. S. A.* *99*, 15066–15071.
- Wredenberg, A., Freyer, C., Sandström, M.E., Katz, A., Wibom, R., Westerblad, H., and Larsson, N.-G. (2006). Respiratory chain dysfunction in skeletal muscle does not cause insulin resistance. *Biochem. Biophys. Res. Commun.* *350*, 202–207.
- Wu, S., Grunwald, T., Kharitonov, A., Dam, J., Jockers, R., and De Luca, F. (2013). Increased expression of fibroblast growth factor 21 (FGF21) during chronic undernutrition causes growth hormone insensitivity in chondrocytes by inducing leptin receptor overlapping transcript (LEPROT) and leptin receptor overlapping transcript-like 1 (LE. *J. Biol. Chem.* *288*, 27375–27383.
- Yakar, S., Rosen, C.J., Beamer, W.G., Ackert-Bicknell, C.L., Wu, Y., Liu, J.-L., Ooi, G.T., Setser, J., Frystyk, J., Boisclair, Y.R., et al. (2002). Circulating levels of IGF-1 directly regulate bone growth and density. *J. Clin. Invest.* *110*, 771–781.
- Yamamoto, T., Sashinami, H., Takaya, A., Tomoyasu, T., Matsui, H., Kikuchi, Y., Hanawa, T., Kamiya, S., and Nakane, A. (2001). Disruption of the genes for ClpXP protease in *Salmonella enterica* serovar Typhimurium results in persistent infection in mice, and development of persistence requires endogenous gamma interferon and tumor necrosis factor alpha. *Infect. Immun.* *69*, 3164–3174.
- Yan, H., Parsons, D.W., Jin, G., McLendon, R., Rasheed, B.A., Yuan, W., Kos, I., Batinic-Haberle, I., Jones, S., Riggins, G.J., et al. (2009). IDH1 and IDH2 Mutations in Gliomas. *N. Engl. J. Med.* *360*, 765–773.
- Yang, C.G., Liao, Z.F., Qiu, W.C., Yan, J., and Wang, Z.G. (2014). Function of ghrelin and ghrelin receptors in the network regulation of gastric motility. *Mol. Med. Rep.* *10*, 2453–2458.
- Yin, X., Li, Y., Xu, G., An, W., and Zhang, W. (2009). Ghrelin fluctuation, what determines its production? *Acta Biochim. Biophys. Sin. (Shanghai)*. *41*, 188–197.
- Yu, A.Y.H., and Houry, W.A. (2007). ClpP: A distinctive family of cylindrical energy-dependent serine proteases. *FEBS Lett.* *581*, 3749–3757.
- Yuan, H.-X., Xiong, Y., and Guan, K.-L. (2013). Nutrient Sensing, Metabolism, and Cell Growth Control. *Mol. Cell* *49*, 379–387.
- Zhang, D., Christianson, J., Liu, Z.-X., Tian, L., Choi, C.S., Neschen, S., Dong, J., Wood, P.A., and Shulman, G.I. (2010). Resistance to high-fat diet-induced obesity and insulin resistance in mice with very long-chain acyl-CoA dehydrogenase deficiency. *Cell Metab.* *11*, 402–411.
- Zhang, W.C., Ng, S.C., Yang, H., Rai, A., Umashankar, S., Ma, S., Soh, B.S., Sun, L.L., Tai, B.C., Nga, M.E., et al. (2012a). Glycine decarboxylase activity drives non-small cell lung cancer tumor-initiating cells and tumorigenesis. *Cell* *148*, 259–272.
- Zhang, Y., Xie, Y., Berglund, E.D., Coate, K.C., He, T.T., Katafuchi, T., Xiao, G., Potthoff, M.J., Wei, W., Wan, Y., et al. (2012b). The starvation hormone, fibroblast growth factor-21, extends lifespan in mice. *Elife* *1*, e00065.
- Zhao, Q., Wang, J., Levichkin, I. V., Stasinopoulos, S., Ryan, M.T., and Hoogenraad, N.J. (2002). A mitochondrial specific stress response in mammalian cells. *EMBO J.*
- Zhao, S., Xu, W., Jiang, W., Yu, W., Lin, Y., Zhang, T., Yao, J., Zhou, L., Zeng, Y., Li, H., et al. (2010). Regulation of Cellular Metabolism by Protein Lysine Acetylation. *Science (80-.)*. *327*.
- Zhou, Y., Gottesman, S., Hoskins, J.R., Maurizi, M.R., and Wickner, S. (2001). The RssB response regulator directly targets sigmaS for degradation by ClpXP. *GENES*

Dev. 15, 627–637.

Acknowledgment

This PhD thesis would not have been possible without the help and support of many wonderful people at the scientific and the personal level for that I am very grateful.

First of all *Thank you* Sandra (Prof. Dr. Aleksandra Trifunovic) for the opportunity to be part of the lab and for your support, patience and encouragement over the years. Of course *Thank you* for the delicious cooking during the lab events.

Prof. Dr. Elena Rugarli *Thank you* for being member of my thesis committee.

Prof. Dr. Jan Riemer *Thank you* for being chair of my thesis committee.

Thank you to the Cologne Graduate School of Ageing Research for financial support.

Alexandra Kukat, Alex *Thank you* for your support in so many different ways: your great and irreplaceable help during many experiments, your scientific know-how, extensive proofreading of this thesis, comforting in stressful times, spirit-lifting coffee breaks, your empathy and being there in case of need and for becoming a friend.

Katharina Senft, Katha *Thank you* for your excellent technical assistance, all the hours spent in the mouse house together and taking over genotypings not only during the writing period. *Thank you* for supporting me and being there inside and outside the lab, sharing moments of tears and laughter.

Linda Baumann, Lindi *Thank you* for always being supportive and taking care for everything. *Thank you* for your singing in the lab, daily lunch breaks, coffee breaks, the time spent outside the lab and our trip to Antwerp.

Karolina Szczepanowska, *Thank you* for the nice scientific discussions about CLPP.

Thank you to all other present and former members of the Trifunovic Lab for help and expertise, coffee breaks, chocolates, cakes and a great time: Steffen Hermans, Sophie Kaspar, Eduard Hofsetz, Marijana Aradjanski, Estela Cepeda Cores, Marija Herholz, Dominic Seiferling, Sarah Maciej, Christoph Brandscheid, Anastasia Rumyantseva, Triinu Siibak, Elke Mainz, Victor Pavlenko, Priyanka Maiti, Anil Dogan, Claire Pujol and Rozina Kardakaris.

Danke an meine Freunde, ganz besonders an Sarah, für die nötige Ablenkung und dafür, dass ich immer auf euch zählen kann.

Mama und Papa, ich bin euch unendlich dankbar für eure Unterstützung. *Danke*, dass ihr immer für mich da seid.

Und natürlich Ludwig...*Danke* für deine unglaubliche Geduld mit mir, deine Unterstützung über all die Zeit, deine Liebe und für so vieles mehr...

Erklärung

Ich versichere, dass ich die von mir vorgelegte Dissertation selbständig angefertigt, die benutzten Quellen und Hilfsmittel vollständig angegeben und die Stellen der Arbeit - einschließlich Tabellen, Karten und Abbildungen -, die anderen Werken im Wortlaut oder dem Sinn nach entnommen sind, in jedem Einzelfall als Entlehnung kenntlich gemacht habe; dass diese Dissertation noch keiner anderen Fakultät oder Universität zur Prüfung vorgelegen hat; dass sie - abgesehen von unten angegebenen Teilpublikationen - noch nicht veröffentlicht worden ist sowie, dass ich eine solche Veröffentlichung vor Abschluss des Promotionsverfahrens nicht vornehmen werde.

Die Bestimmungen der Promotionsordnung sind mir bekannt. Die von mir vorgelegte Dissertation ist von Prof. Dr. Aleksandra Trifunovic betreut worden.

Köln, März 2017

(Christina Becker)

Curriculum vitae

Christina Becker, MSc

Persönliche Daten

Geburtstag	13. Oktober 1987
Geburtsort	Werl
Adresse	Thebäerstraße 15, 50823 Köln
Email	becker.christina@uni-koeln.de
Nationalität	deutsch

Ausbildung

10/2012- 04/2017	Doktorarbeit in Genetik , Universität zu Köln Cologne Cluster of Excellence on Cellular Stress Responses in Aging-associated Diseases (CECAD) Prof. Dr. Aleksandra Trifunovic
09/2010- 07/2012	Master of Science in Clinical Molecular Life Sciences Universität Maastricht, Maastricht, Niederlande
09/2007- 08/2010	Bachelor of Science in Applied Biology Hochschule Bonn-Rhein-Sieg, Rheinbach
08/2004 - 01/2005	Airport Highschool, Michigan, USA
07/1998 - 06/2007	Ursulinengymnasium Werl

Stipendien

10/2012 – 09/2015	Cologne Graduate School of Ageing Research Doktorandenstipendium, Universität zu Köln
-------------------	---

Publikationen

Szczepanowska, K., Maiti, P., Kukat, A., Hofsetz, E., Nolte, H., Senft, K., Becker, C., Ruzzenente, B., Hornig-Do, H.-T., Wibom, R., et al. (2016). CLPP coordinates mitoribosomal assembly through the regulation of ERAL1 levels. EMBO J. 35, 2566-2583.

Seiferling, D., Szczepanowska K., Becker C., Senft K., Hermans S., Kukat A., and Trifunovic A. (2016) Loss of CLPP alleviates mitochondrial cardiomyopathy without affecting the mammalian mitochondrial unfolded protein response. EMBO reports. 17, 953-964.

Kukat, A., Dogan, S.A., Edgar, D., Mourier, A., Jacoby, C., Maiti, P., Mauer, J., Becker, C., Senft, K., Wibom, R., et al. (2014). Loss of UCP2 attenuates mitochondrial dysfunction without altering ROS production and uncoupling activity. PLoS Genet. 10, e1004385.

Salpini, R., Colagrossi, L., Bellocchi, M.C., Surdo, M., Becker, C., Alteri, C., Aragri, M., Ricciardi, A., Armenia, D., Pollicita, M., et al. (2014). HBsAg genetic elements critical for immune escape correlate with HBV-reactivation upon immunosuppression. Hepatology. 61, 823-833.

Internationale Konferenzteilnahmen

Keystone Symposium

Obesity and the Metabolic Syndrome: Mitochondria and Energy Expenditure

Whistler, Kanada, März 2015

Euromit 2014 International Meeting on Mitochondrial Pathology

Tampere, Finnland, Juni 2014

Köln, März 2017